



**COMPARISON OF RAY TRACING  
THROUGH IONOSPHERIC MODELS**

THESIS

Shayne C. Aune, Second Lieutenant, USAF  
AFIT/GE/ENG/06-04

**DEPARTMENT OF THE AIR FORCE  
AIR UNIVERSITY**

***AIR FORCE INSTITUTE OF TECHNOLOGY***

---

**Wright-Patterson Air Force Base, Ohio**

APPROVED FOR PUBLIC RELEASE; DISTRIBUTION UNLIMITED

The views expressed in this thesis are those of the author and do not reflect the official policy or position of the United States Air Force, Department of Defense, or the United States Government.

AFIT/GE/ENG/06-04

COMPARISON OF RAY TRACING THROUGH IONOSPHERIC MODELS

THESIS

Presented to the Faculty

Department of Systems and Engineering Management

Graduate School of Engineering and Management

Air Force Institute of Technology

Air University

Air Education and Training Command

In Partial Fulfillment of the Requirements for the  
Degree of Master of Science in Electrical Engineering

Shayne C. Aune, B.S.E.E.

Second Lieutenant, USAF

March 2006

APPROVED FOR PUBLIC RELEASE; DISTRIBUTION UNLIMITED.

COMPARISON OF RAY TRACING THROUGH IONOSPHERIC MODELS

Shayne C. Aune, B.S.E.E.  
Second Lieutenant, USAF

Approved:

                    /signed/                      
Lt Col Matthew E. Goda, PhD (Chairman)

          3 Mar 06            
date

                    /signed/                      
Dr. William S. Borer (Member)

          3 Mar 06            
date

                    /signed/                      
Dr. Ronald F. Tuttle (Member)

          6 Mar 06            
date

                    /signed/                      
Maj Christopher G. Smithtro, PhD (Member)

          6 Mar 06            
date

**Abstract**

A comparison of ray tracing predictions for transionospheric electromagnetic wave refraction and group delays through ionospheric models is presented. Impacted applications include over-the-horizon RADAR, high frequency communications, direction finding, and satellite communications. The ionospheric models used are version 2.1 of Utah State University's Global Assimilation of Ionospheric Measurements (USU GAIM) model and the 2001 version of the International Reference Ionosphere (IRI) model. In order to provide ray tracing results applicable to satellite communications for satellites at geosynchronous orbit (GEO), a third ionospheric model is used to extend the sub-2000-km USU GAIM and IRI ionospheric specifications to 36540 km in altitude. The third model is based on an assumption of diffusive equilibrium for ion species above 2000 km. The ray-tracing code used is an updated implementation of the Jones-Stephenson ray-tracing algorithm provided by L. J. Nickisch and Mark A. Hausman. Ray-tracing predictions of signal refraction and group delay are given for paths between Goldstone Deep Space Observatory near Barstow, California, and the PanAmSat Galaxy 1R satellite. Results are given for varying frequency between 11MHz to 1GHz, varying time of day between 0600 and 1700 Pacific Standard Time on 1 November 2004, and varying signal transmission elevation angle. Ray tracing predicts minimal ionospheric effects on signals at or above approximately 100 MHz. Ray-tracing predictions of signal refraction and group delay differ dependent upon the model used for ray-tracing. Ray tracing in diffusive equilibrium extended (DEE) USU GAIM (DEE GAIM) predicts as much as 500 km less group path length than DEE IRI. This is most likely due to the DEE model propagating high electron densities found in the upper altitudes of IRI-2001 specifications. USU GAIM ray tracing predicts higher frequencies are necessary to penetrate the F<sub>2</sub> region during the period of interest than IRI-2001.

AFIT/GE/ENG/06-04

*To My True Love*

## Acknowledgments

GOD REIGNS. I stand beside the believers who acknowledge a thesis is accomplished by love, persistence, and sacrifice, not only from self, but by all those whom love the author most dearly. This work is first and foremost accomplished by GOD's intervention. FATHER, I pray YOUR hands continue to lift up all who seek YOUR enlightenment through lifelong study and devotion to understanding YOUR creation.

Second only to God is my family. To my True Love, to our Lord's most wonderful gifts, our children, and to my mother, father, brothers, and sisters: I devote this work to all of you. There are no words to express my gratitude for the love you have given and sacrifices you have made allowing me to become a Master. I will always love you and seek to empower you as you have empowered me to achieve this milestone.

I would also like to express my deep appreciation to the many people who went out of their way to assist in my development, guiding this research. To my advisor and sponsor, Dr. William Borer, for your patience and support from afar; it is no easy task taking on a master's student with an already completely full schedule. I have no idea how you did it, but I realize you went way out on a limb to help me achieve beyond my own wildest research expectations. Thank You. To my AFIT advisor, Lt Col Matt Goda, thank you, sir, for your enduring support, for your MATLAB coding expertise, and for keeping the pressure to a minimum while keeping me on task to accomplish something rarely (if ever) done here before: a "stand-alone" AND an addendum. Thank you, Dr. Ronald Tuttle, for agreeing at practically the last minute to help with this effort, and for always being the first to read and provide feedback on my many thesis drafts. And, Thank you, Maj Christopher Smithtro, for your ionospheric expertise and always being ready to provide immediate feedback and recommendations on how to proceed into this churning, mysterious, and amazing medium!

I am also indebted to the many professionals who spent their valuable time carefully instructing me in the science of ionospheric modeling and ray tracing. Thank you, Dr. L. J. Nickisch, for introducing me to the theory and history of ray tracing. Thank you, Dr. Mark Hausman, for your expertise and recommendations in implementing and displaying ray tracing results using numerous computer applications. Thank you, Maj Herbert Keyser and Capt Craig Baker for providing the multitude of USU GAIM specifications required. Thank you, Dr. Don Thompson, for your USU GAIM model expertise, and thank you, Dr. Dieter Bilitza, for your IRI model expertise.

Thank you, Craig Miller, Don Soulliere, Anthony Virgilio, and Pat Dolan, for getting operations going on both sides of the wall so I could explore a new frontier! Your good humor and patience kept me sane when it came down to the wire. Thank you, my fellow AFIT masters students, especially Lt Jared Herweg, Capt Drew Hyatt, Capt Evan James, Maj Chris Lemanski, Lt John MacDonald, Lt Becky Eckert, Capt Neil Paris, Lt Steve Mawhorter, Lt Willie Mims, and all the rest. We made it together! May God continue to bless us!

Thank you, John Hando, Dr. Tom Brehm, Lt Col Kevin Allen, Capt William Sacovitch, Capt Michael Pratt, Dr. William Frix, and Will Sturgis for your support from NASIC. Thank you also, Dr. Andrew Terzuoli, Dr. John Raquet, and Lt Col Stewart DeVilbiss at AFIT, for your help and guidance along this winding path. Thank you, Mr. Al Gifford and Lt Col James Bolles, for your approval and support of this research effort. And, finally, THANK YOU, Lt Col Eric Claunch, for leading, mentoring, and providing me with the network to help pave the road for future students at AFIT. You passed the torch and ensured my success from the beginning. MISSION ACCOMPLISHED, SIR!

/signed/  
Shayne Christopher Aune



## Table of Contents

	Page
Abstract .....	v
Dedication .....	vi
Acknowledgements .....	vii
Table of Contents .....	ix
List of Figures .....	xi
List of Tables .....	xii
 I. Introduction .....	 1
General Issue .....	1
Overview .....	2
Results Preview .....	4
 II. Background.....	 5
The Ionosphere .....	5
Signal Propagation in the Ionosphere .....	9
Raytracing .....	16
Ionospheric Models .....	20
 III. Methodology .....	 25
Overview .....	25
The Models.....	27
The Raytracing Algorithm.....	33
MATLAB® .....	34
 IV. Results.....	 35
Overview .....	35
TEC Maps .....	36
Ray Refraction.....	45
Angular Deviation .....	49
Signal Group Path .....	56
 V. Conclusion.....	 59
Summary .....	59
Future Research.....	61
 Appendix A. IRI Model Specification Input and Output Example .....	 63
 Appendix B. MATLAB m-Files.....	 64
FullTECPlot.m .....	64

GAIM4mat_extend.m.....	66
RayOutput.m.....	68
RaytraceOut.m.....	70
Appendix C. Ray Tracing Algorithm Input and Output Examples .....	72
Appendix D. Variable DEE IRI Grid-Spacing Effects on Ray-Tracing Predictions .....	76
Appendix E. Attempted USU GAIM Model Specification Extrapolation.....	78
Bibliography.....	79
Vita.....	81

## List of Figures

Figure	Page
2.1. Ionospheric Electron Density Profile Showing Regions .....	6
2.2. Ionospheric TEC Variability .....	8
2.3. Snell's Law.....	11
2.4. Frequency- and Electron Density-Dependence of Index of Refraction.....	11
2.5. A Real-Time Ionogram .....	13
2.6. Comparison of Ray-Traced Ionospheric Path versus Straight-Line Path .....	14
2.7. 10_MHz Signal Ionospheric Refraction as a Function of Angle of Incidence .....	15
2.8. Spherical Polar Coordinates Relative to Cartesian Coordinates.....	19
3.1. Methodology Process .....	26
3.2. Diffusive Equilibrium Extended (DEE) IRI Ionospheric Profile .....	29
3.3. DEE GAIM Ionospheric Profile.....	31
3.4. Comparison of DEE IRI and DEE GAIM Ionospheric Profiles .....	32
4.1. IRI-2001 TEC Map at 0600 PST.....	38
4.2. USU GAIM 2.1 TEC Map at 0600 PST.....	38
4.3. IRI-2001 TEC Map at 1400 PST.....	40
4.4. USU GAIM 2.1 TEC Map at 1400 PST.....	40
4.5. IRI-GAIM TEC Difference Map at 1400 PST .....	41
4.6. DEE IRI TEC Map at 1400 PST .....	43
4.7. DEE GAIM TEC Map at 1400 PST .....	43
4.8. DEE IRI-DEE GAIM TEC Difference Map at 1400 PST.....	44
4.9. Varying Elevation Ray Refraction for 11-14 MHz thru DEE IRI at 1400 PST .....	46
4.10. Varying Elevation Ray Refraction for 11-14 MHz thru DEE GAIM at 1400 PST .....	46
4.11. Varying Elevation 11-14 MHz Crossrange Ray Refraction thru DEE IRI at 1400 PST.....	48
4.12. Varying Elevation 11-14 MHz Crossrange Ray Refraction thru DEE IRI at 1400 PST.....	48
4.13. Elevation Deviation vs Time of Day for 15-1000 MHz thru DEE IRI.....	50

4.14. Elevation Deviation vs Time of Day for 15-1000 MHz thru DEE GAIM .....	50
4.15. Target Miss Distance for Angle Deviation.....	51
4.16. Azimuth Deviation vs Time of Day for 15-1000 MHz thru DEE IRI .....	54
4.17. Azimuth Deviation vs Time of Day for 15-1000 MHz thru DEE GAIM.....	54
4.18. Azimuth Deviation from LOS Zero Crossing as a Function of Time of Day.....	55
4.19. Group Path vs Time of Day for 15-1000 MHz thru DEE IRI .....	57
4.20. Group Path vs Time of Day for 15-1000 MHz thru DEE GAIM .....	57
D.1. Ray-Tracing Predicted Azimuth Deviation for Varying DEE IRI Grid Spacing.....	76
D.2. Ray-Tracing Predicted Elevation Deviation for Varying DEE IRI Grid Spacing .....	77
D.3. Ray-Tracing Predicted Group Path Deviation for Varying DEE IRI Grid Spacing .....	77
E.1. Extrapolated GAIM TEC Map at 0600 PST .....	78

### List of Tables

Table	Page
1. Ray-Tracing Equation Symbols .....	18

# **COMPARISON OF RAY TRACING THROUGH IONOSPHERIC MODELS**

## **I. Introduction**

### **General Issue**

Various United States national defense activities are affected by the ionosphere in the accomplishment of their missions. Satellite communications (SATCOMM) relies on signals which must propagate through the ionosphere, while over-the-horizon RADAR (OTHR), high frequency (HF) communications, and target direction finding (DF) require predictable signal reflection from the ionosphere for effective operations. These activities use signal frequencies below 1 gigahertz (GHz) and they all benefit by knowledge of the ionospheric state and its impacts on their signals. Predictions of the ionosphere's state are typically made using ionospheric models, which sometimes provide inaccurate estimates resulting in errors to the above activities. Two of the ionospheric signal effects that cause errors in these activities are refraction and group path delay (increases to signal group path length). Unpredicted ionospheric refraction results in deficient antenna aim in SATCOMM and HF leading to sub-optimal communications. Poor compensation for refraction and group path delays may result in erroneous target identification and coordinate estimation by OTHR and DF, placing friendly forces at greater risk of failure to identify, locate, and engage adversaries.

Signal propagation prediction methods, such as three-dimensional ray-tracing algorithms applied to ionospheric models are used by some national defense activities to estimate and

mitigate ionospheric effects on signals. Advancing ionospheric modeling technology may hold the potential to further reduce errors in activities by providing for more accurate ray-tracing predictions. However, there are numerous models available, many being updated as technology improves, and each may be based on differing assumptions, inputs, calculations, and result in differing outputs.

Very little research has been done to compare ionospheric models and their appropriateness for obtaining ray-tracing predictions in order to mitigate effects on various activities' signals. For instance, ray-tracing prediction for SATCOMM requires the use of ionospheric model specifications up to geosynchronous orbit (GEO) altitude: where many communications satellites reside. This thesis will focus on the SATCOMM application and seek to compare two ionospheric models, extended to GEO by a third ionospheric model, to highlight the differences in refraction and group path predictions obtained by ray tracing through the models for transionospheric signals below 1 GHz. The results of this thesis examine some differences between the models and the differences in predictions obtained by ray tracing through the models.

## **Overview**

This thesis includes a comparison of vertical total electron content (TEC) maps created using Utah State University's Global Assimilation of Ionospheric Measurements (USU GAIM or GAIM) model, version 2.1, and the 2001 version of the International Reference Ionosphere (IRI-2001 or IRI) model. This thesis also presents ray-tracing predictions of ionospheric effects on

signals below 1 GHz. However, it is critical to highlight before continuing that many of the results obtained in this thesis are *not* solely due to IRI and GAIM ionospheric specifications. Because IRI and GAIM model specifications only extend to 2000 km and 1380 km in altitude respectively and this thesis seeks to include ray-tracing predictions to GEO in order to be useful to SATCOMM, most of the model specifications used for ray-tracing in this thesis include a *third* ionospheric model, referred to as the diffusive equilibrium extension (DEE) model. Therefore, many of the ray-tracing predictions shown in this thesis are accomplished by ray tracing signal paths through DEE IRI and DEE GAIM specifications. DEE IRI and DEE GAIM ray-tracing predictions are *not* the results of ray tracing through the IRI and GAIM models. Only the results obtained by ray tracing through the specifications to altitudes less than the IRI and GAIM maximum altitudes can be attributed to those models.

Chapter two of this thesis discusses background: the ionosphere, how it theoretically affects signal propagation, the Jones-Stephenson ray-tracing algorithm, and finally, the ionospheric models used. Chapter three covers methodology, which is primarily the process of integrating the major components of this research: the models, the ray-tracing algorithm, and MATLAB®. Chapter four presents results to include a comparison of model-predicted TEC maps and ray-tracing predictions of ionospheric signal refraction, angular deviation from line of sight (LOS) to a target, and group path. Finally, chapter five gives a summary and recommendations for future research. The next section provides a preview of the results obtained by this research.

## Results Preview

GAIM results show more concentrated ionospheric electron density layers during the period of interest, while IRI predicts lower electron densities, spread over greater volume. GAIM and IRI TEC maps are on the same order of magnitude, with GAIM maps showing more intense gradients than IRI. GAIM ray-tracing predictions show higher frequencies are necessary to penetrate the lower ionosphere than frequencies predicted by ray tracing in IRI. However, IRI typically predicts higher electron densities than GAIM in the upper altitudes of corresponding specifications. As a consequence of this and due to the DEE model and extension method used, the resulting DEE IRI TEC map is an order of magnitude higher than the DEE GAIM TEC map. Ray tracing through DEE IRI predicts higher angular deviation from the LOS elevation and azimuth to a satellite receiver from the ground, and longer group path lengths than DEE GAIM. DEE IRI ray-tracing predictions also appear smoothly varying during the day of 1 November 2004, whereas DEE GAIM results have steeper gradients, i.e. a more “jagged” appearance in the results than DEE IRI. The differences seen in predictions from ray tracing through DEE IRI and DEE GAIM indicate an accurate topside ionospheric specification extension is critical to ray-tracing predictions. Yet, one important similarity found is ray tracing through both extended model specifications predicts the ionosphere causes minimal refraction and group path effects on signals at frequencies above approximately 100 MHz. Refer to chapter four for the details of these results.



## II. Background

### The Ionosphere

The ionosphere is an ionized, highly non-linear, and dynamic medium, formed mainly by solar energy. It is affected by space and terrestrial weather, and by the Earth's magnetosphere. The "boundaries" of the ionosphere depend on the reference consulted, but most seem to agree it begins at no less than 50 kilometers (km) in altitude and extends into the plasmasphere, the edge of which is 4-8 Earth radii distance (depending on solar activity). The ionosphere is primarily formed by the Sun's extreme ultraviolet (EUV) and soft x-ray radiation breaking atmospheric molecules into ions and free electrons, known as the photoionization process. This thesis will focus on the daytime, mid-latitude ionosphere. This segment of the ionosphere may be subdivided into several regions, or layers: D, E, F1, F2, the *topside ionosphere*, and the *protonosphere* (Schunk, 2000). An illustration of these regions is provided in figure 2.1, which is generated using a combination of ionospheric models. A detailed description for each region is beyond the scope of this report, but a summary of each will be given next.

Each ionospheric region is characterized by a peak density typically in a certain altitude range, each corresponds to a different dominating ion composition, and each is subject to different processes and rates of ion production and loss. The D region (60 to 100 km) is the most difficult to observe and describe. It is a complex mixture of both positive and negative ions,

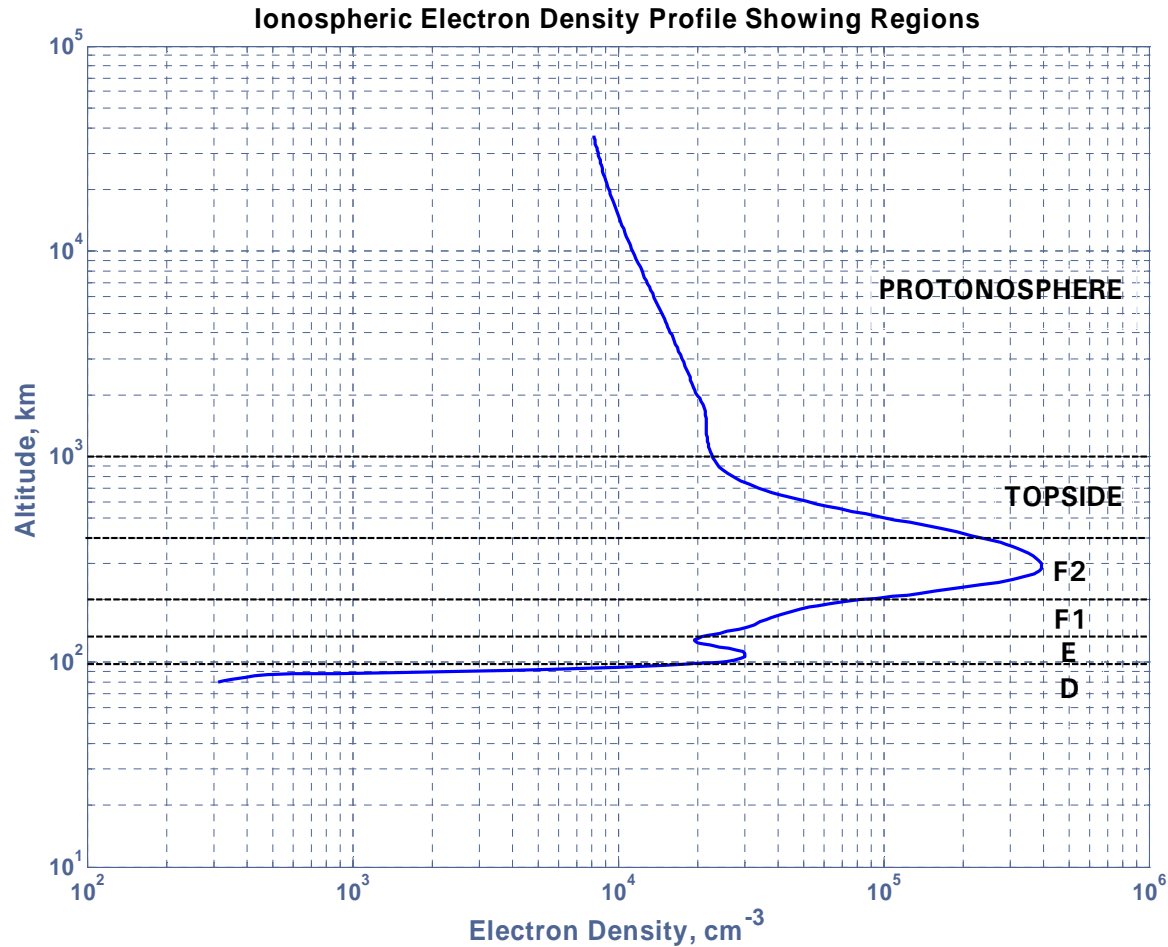


Figure 2.1. A log-log ionospheric electron density versus altitude profile displaying the main regions of the ionosphere, D, E, F<sub>1</sub>, F<sub>2</sub>, *topside*, and the *protonosphere*. The peak densities will vary in altitude. This figure was generated using the International Reference Ionosphere (IRI) ionospheric model, and extended above 2000 km using a diffusive equilibrium model.

numerous neutral species, and water cluster ions. The E region (100 to 150 km) provides the first ion density peak, and was the first region detected. The major ion species in the E region are NO<sup>+</sup>, O<sub>2</sub><sup>+</sup>, and N<sub>2</sub><sup>+</sup>. The F<sub>1</sub> region (150 to 250 km) is primarily another transition region, in which O<sup>+</sup> becomes the major ion. O<sup>+</sup> remains the major ion throughout the F<sub>2</sub> region (250 to 400 km) and in the *topside ionosphere* (300 to 1000 km). Ion-atom interchange and transport processes start to become important in F<sub>1</sub>, and the ionosphere's peak ion density, which occurs in

F<sub>2</sub>, is the result of a balance between plasma transport and chemical loss processes. The peak density in F<sub>2</sub> is approximately an order of magnitude greater than the peak in the E region. Beyond this peak is the region called the *topside ionosphere*, in which the density decays with increasing altitude. The *protonosphere* (above 1000 km) is the region where H<sup>+</sup> and He<sup>+</sup> replace O<sup>+</sup> as the dominant ion. In these last two regions, plasma transport is the dominating process (Schunk and Nagy, 2000). This summary has revealed some of the complexities a physical description of the ionosphere requires. Further complicating this description are the cyclical and unpredictable variations described next.

Figure 2.2 displays one measure of the ionosphere's variability in the form of TEC. The figure shows TEC (1 TEC = 10<sup>16</sup> electrons per square meter) measured on a daily basis over Hamilton, Massachusetts, for the year of 1989. It provides the observer with a somewhat predictable pattern. Just before sunrise, TEC begins to increase and peaks between noon and 1400 local time. It then decreases as loss processes, such as chemical recombination, dominate over production processes, such as photoionization. During the night, ion and free electron losses continue versus minimal photoionization such that minimum TEC occurs a few hours before sunrise. Figure 2.2 also alludes to the ionosphere's seasonal variation, showing TEC peaks higher in winter than in summer. There are notable day-to-day differences, most likely due to solar and geomagnetic disturbances, or short-term effects and localized anomalies, such as traveling ionospheric disturbances (TID). Not apparent here is how the ionosphere also varies according to the 11-year long solar cycle (from solar maximum to minimum and back to maximum). All of these ongoing variations hold important consequences for transionospheric electromagnetic (EM) waves (Misra, 2001).

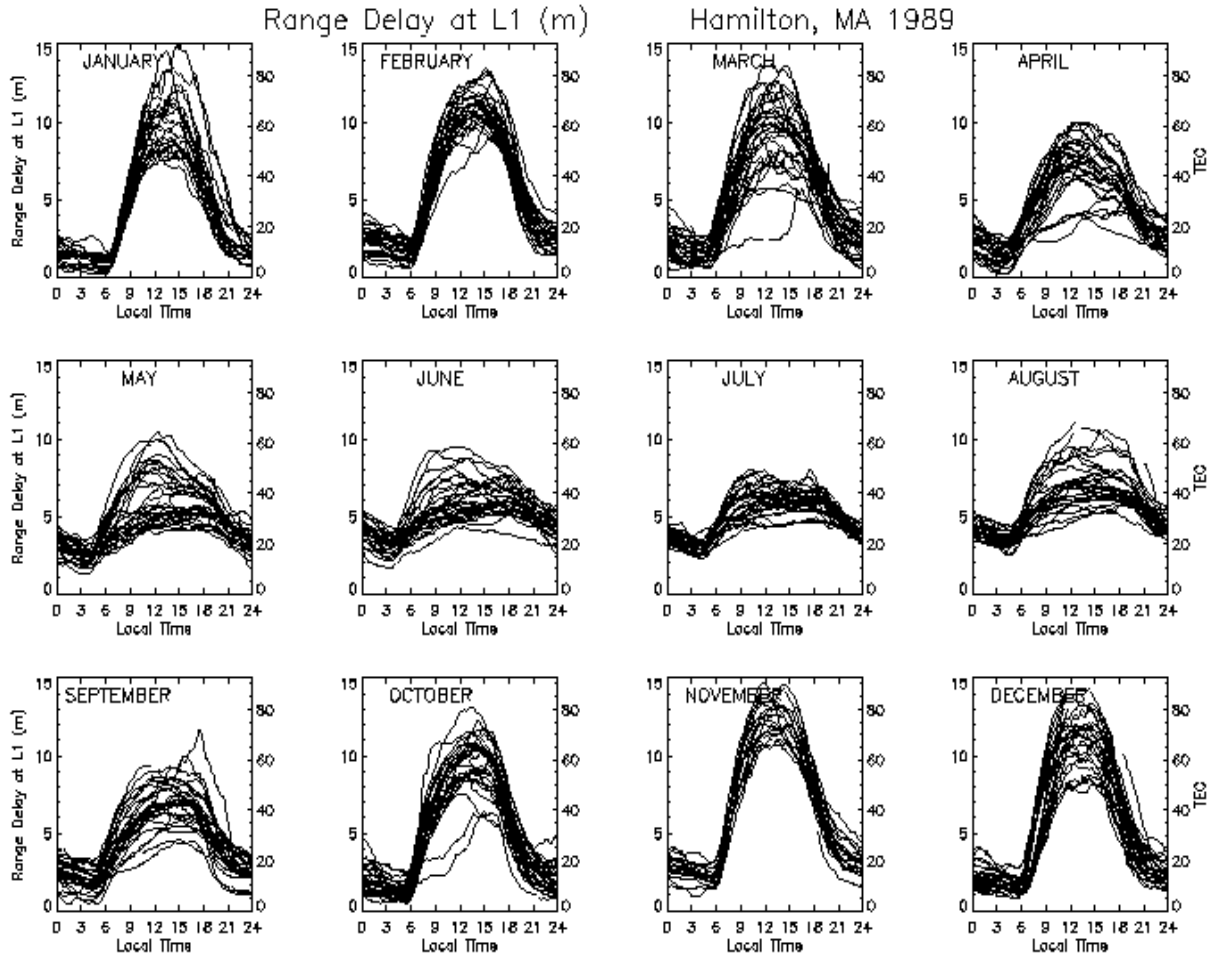


Figure 2.2. Ionospheric TEC variability provides a measure of how the ionosphere varies over Hamilton, Massachusetts during 1989. (One TEC is  $10^{16}$  electrons per square meter.) Note the day-to-day and seasonal variation (Borer, 2005).

## Signal Propagation in the Ionosphere

The most well-established ionospheric effects on transionospheric EM signals include absorption, refraction, phase and group delay, frequency shift, polarization shift, and Faraday rotation. This thesis focuses on characterizing and analyzing two of these effects: 1) signal refraction and 2) signal group delay. Both of these effects are related to the ionosphere's varying index of refraction which can be directly linked to the free electron content. A simple case is shown by an EM signal traveling in the vertical direction through a nonmagnetic, ionized medium. The waves' phase velocity,  $u$ , is related to the speed of light in a vacuum,  $c$ , by

$$u = \frac{c}{\sqrt{1 - \frac{n_e q^2}{\pi m_e f^2}}} \quad (2.1)$$

where  $n_e$  is the electron density in units of electron count per cubic centimeter,  $q$  is the magnitude of the electron charge,  $m_e$  is the mass of the electron in grams, and  $f$  is the frequency of the EM wave (Tascione, p. 113). The refractive index of the medium,  $\mu$ , is defined as

$$\mu = \frac{c}{u} = \sqrt{1 - \frac{n_e q^2}{\pi m_e f^2}} \quad (2.2)$$

Therefore, as a wave passes from lower to higher electron density regions, the refractive index affecting the wave decreases, and the wave phase accelerates. Alternatively, as the wave passes

from higher to lower electron density, the refractive index affecting the wave increases, and the wave phase decelerates.

Snell's Law is given mathematically as

$$\mu_1 \sin \theta_1 = \mu_2 \sin \theta_2 \quad (2.3)$$

where subscripts refer to two adjacent mediums through which an EM wave propagates, and  $\theta$  is the angle of propagation in the relevant medium. This law indicates that, as shown in Figure 2.3, a wave exiting a medium with index of refraction,  $\mu_1$ , at angle  $\theta_1$  relative to the boundary normal, is refracted upon entering a medium with index of refraction,  $\mu_2$ , at angle  $\theta_2$ , where  $\theta_2 > \theta_1$  when  $\mu_2 < \mu_1$ . According to equation 2.2, the index of refraction approaches unity (the point at which no refraction occurs) when either the wave frequency approaches infinity or when the medium's electron density goes to zero, since all other quantities in the relationship are constants. Figure 2.4 provides a visual representation of higher frequencies refracting less in the ionosphere. It further shows that as electron density decreases, signals also refract less. For the purposes of this thesis, signals above 1GHz are considered to have no appreciable signal refraction.

Additionally, the group delays of signals above 1GHz will not be studied here because, although the ionospheric-added group delays are not negligible for the purposes of SATCOMM, plenty of applicable research is already well-documented and compensation techniques are in common use by the Global Positioning Satellite (GPS) system (Misra, 2001). This thesis focuses on ionospheric refraction and group delay on signals at frequencies below 1GHz.

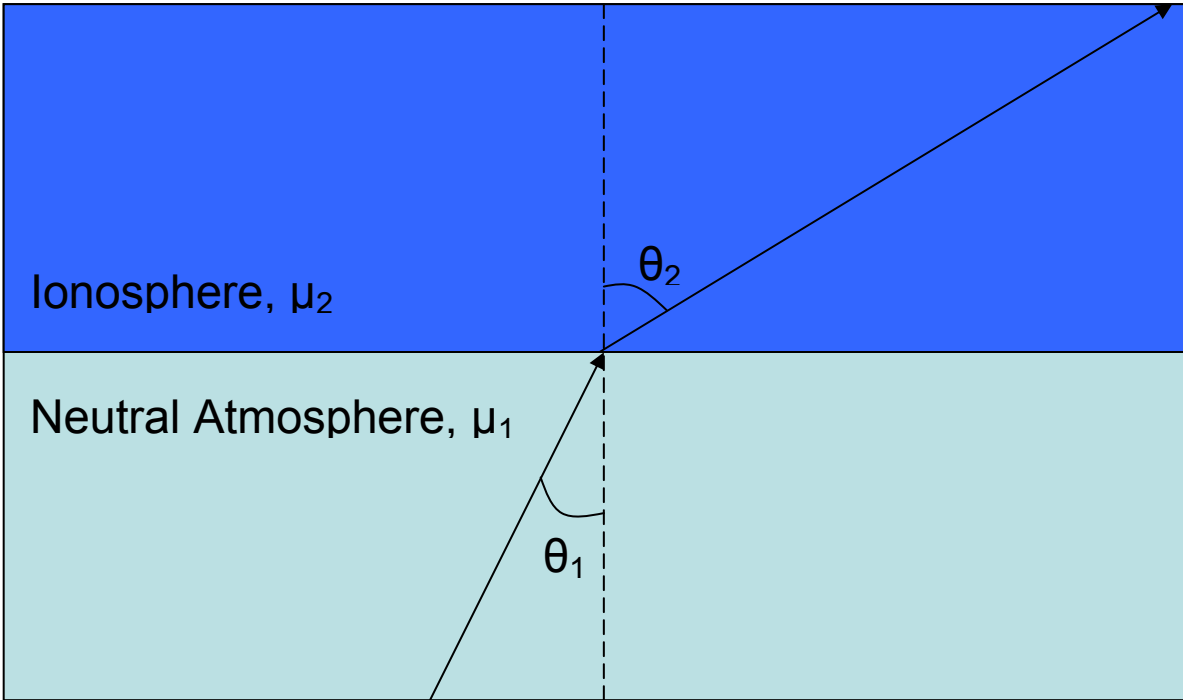


Figure 2.3. Snell's Law indicates that because the ionospheric index of refraction is greater than that of the neutral atmosphere, the signal direction will change to make a greater angle with the normal to the boundary,  $\theta_2 > \theta_1$ .

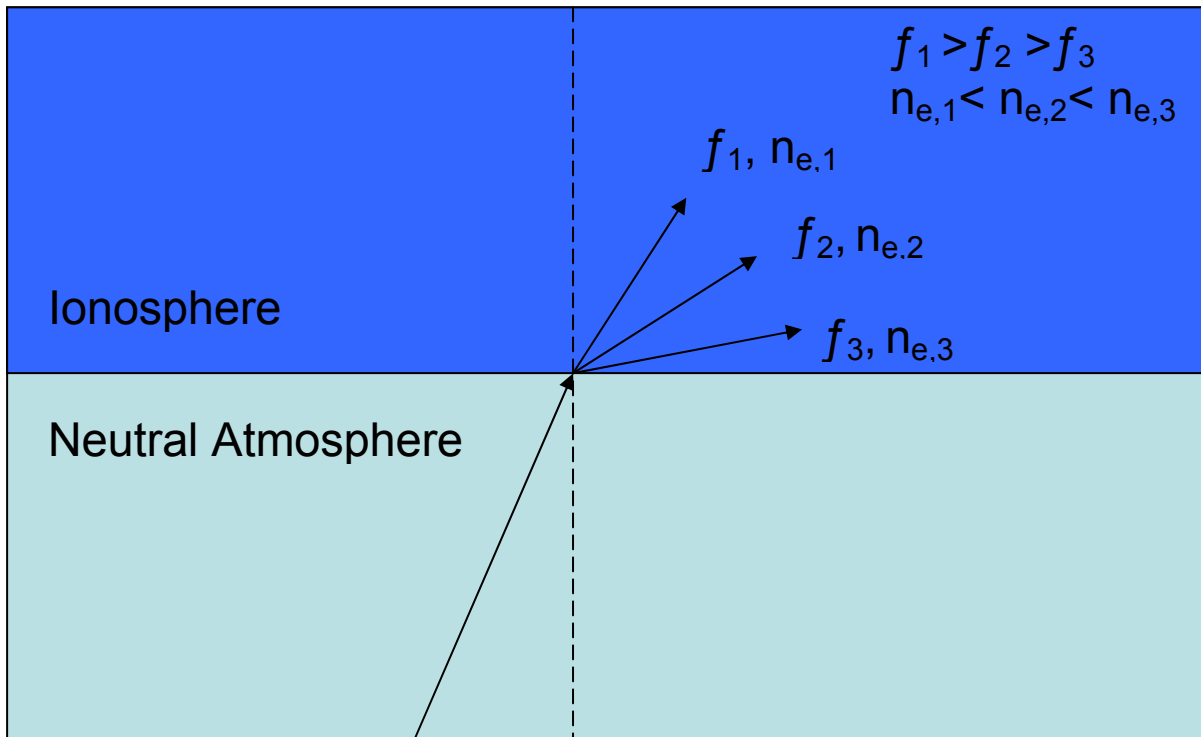


Figure 2.4. The index of refraction is frequency and/or electron density dependent such that as the signal frequency increases and/or electron density decreases, the signal is less refracted.

Another important relationship can be derived from equation 2.1 by noting that as  $n_e q^2$  approaches  $\pi m_e f^2$ , the phase velocity,  $u$ , approaches infinity, at which point the signal's forward progression is reversed and the signal is reflected. Substituting in for  $\pi$ , the electron charge magnitude, and the electron mass provides an equation for when reflection occurs, at the critical frequency for a known electron density:

$$f_r = 9 \times 10^{-3} \sqrt{n_e} \text{ Hz} \quad (2.4)$$

This relationship makes it possible to map the reflective or “bottomside” ionosphere from the ground, as shown in the ionogram in Figure 2.5.

An ionogram is generated by an ionosonde, which transmits and records the echoes from vertically-aimed, high frequency radio pulses reflected by the ionosphere. The ionosonde sweeps the pulses over a range of frequencies to detect varying electron densities, and determines their corresponding altitudes based upon the time difference between transmission and echo return. Equation 2.4 relates each frequency to the electron density that reflects it. Initially, altitudes are calculated by multiplying the assumed signal velocity (free-space propagation) by the time of signal propagation and dividing by two since the signal propagates up and back. However, because the signal velocity is not constant (not free-space propagation), it is necessary to rescale the real-time “virtual” altitude calculation. Computers handle true height scaling, correcting for lower atmospheric and ionospheric composition, which affects signal velocity prior to reflection (NGDC/STP, 2004). The scaled, “true” altitude versus



frequency is shown in figure 2.5 as the lowest curve spanning the ionogram and increasing from left to right.

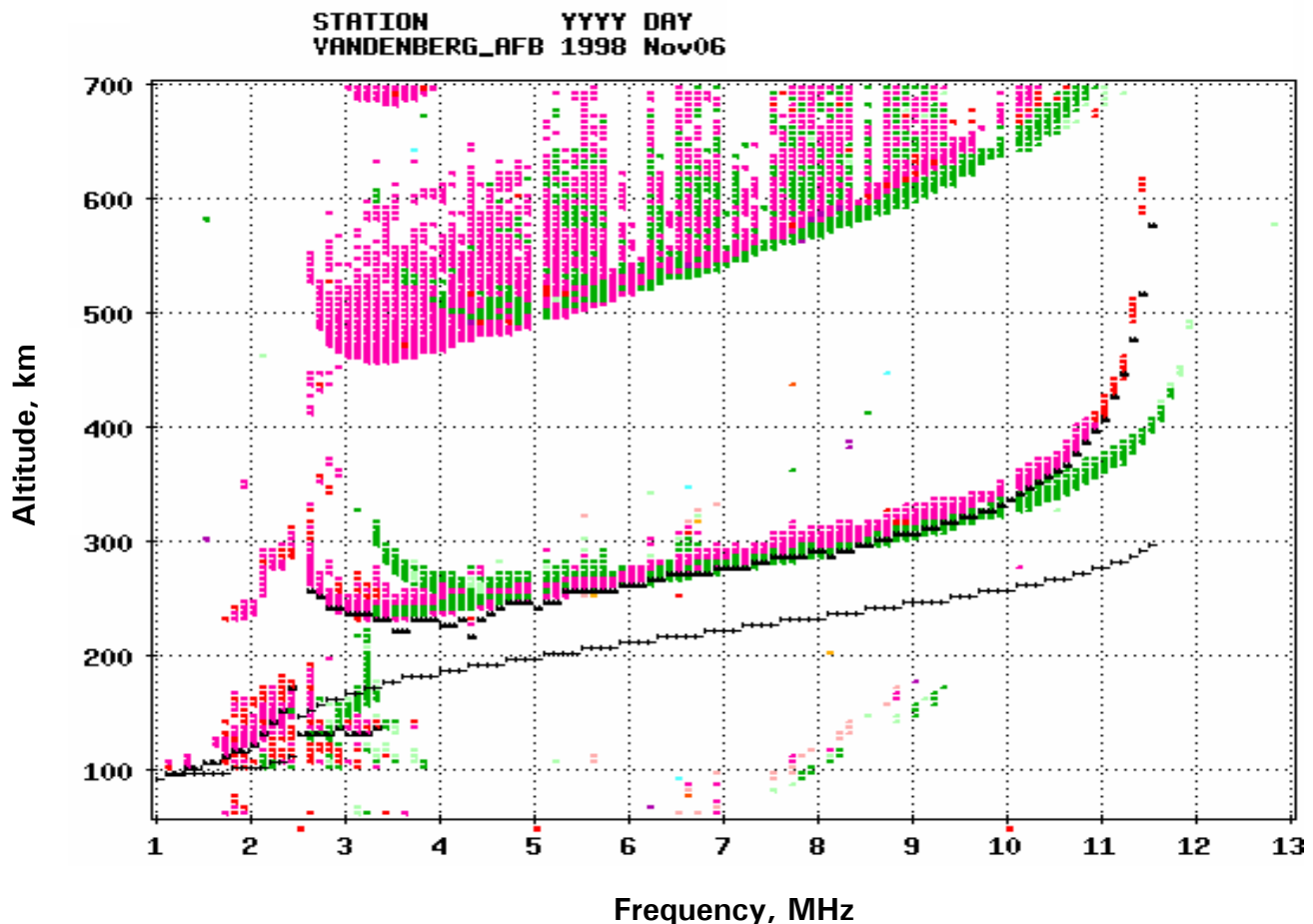


Figure 2.5. A real-time ionogram shows a bottomside ionospheric profile of altitude versus frequency. Ionograms are generated by ionosondes, which transmit varying-frequency, vertically aimed radio pulses and record the pulse echoes reflected by the ionosphere. Each echoed frequency identifies an electron density in the ionosphere; higher frequencies penetrate further before being reflected. The upper black curve is at “virtual” altitudes, determined by time difference between each pulse transmission and reception, and the lower black curve is the computer-scaled, true altitude, which takes into account non-linear pulse velocities. Note the highest-altitude returns are assumed to be secondary pulse echoes (NGDC/STP, 2004).

It is important to keep in mind the ionosphere is not a mirror-like shell enclosing the Earth. It is a dynamic medium through which signals are delayed and refracted prior to being

either reflected back towards the Earth, or propagating through the peak electron density into space. It is also important to remember that whether or not a signal is reflected or penetrates depends on the angle at which it strikes the ionosphere and the electron content in its path.

Figure 2.6 shows a signal path through an electron density model of the ionosphere versus a straight-line path. (Note: the LOS path is curved due to flattening of the Earth's surface to be the horizontal axis.) The raytraced signal refracts away from vertical propagation as the signal enters increasingly higher electron density layers, and then refracts back towards vertical propagation as the signal moves past the maximum density region.

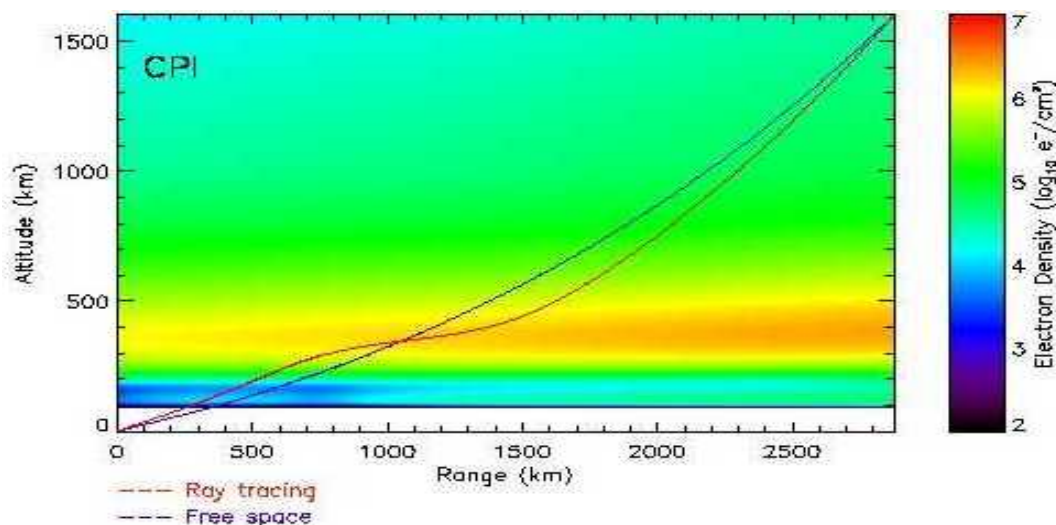


Figure 2.6. Comparison of a ray-traced ionospheric signal path versus a straight-line path. The straight-line path appears curved because it is relative to a flattened Earth (horizontal axis). The electron density refracts the transionospheric signal from what would otherwise be a straight path; first refracting it more towards the Earth's surface as the electron density increases, and then away as the signal moves into decreasing density (Borer, 2005).

Figure 2.7 shows a 10-MHz signal entering the ionosphere at increasing angles of incidence. The signal is initially propagated vertical linearly, but as the angle increases it is increasingly refracted, and then completed reflected by the ionosphere. Further, note that as the incident angle continues to increase beyond reflection, the signal penetrates to lesser altitudes.

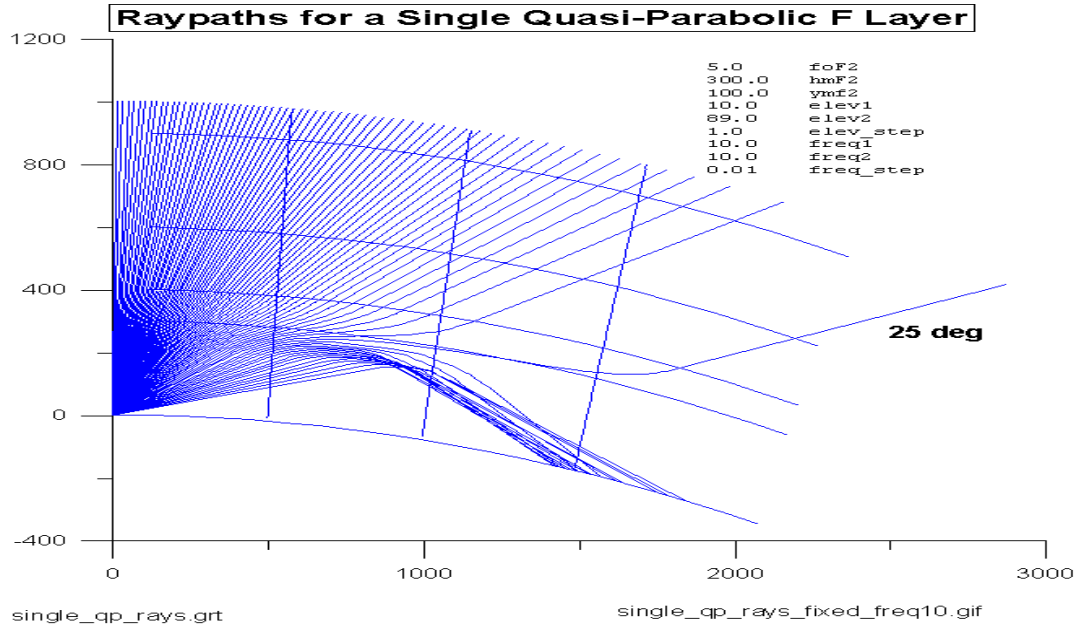


Figure 2.7. A 10-MHz signal transmitted from a single ground location at increasing angles of incidence is increasingly refracted, to the point of reflection by the ionosphere. As the incident angle increases further, the signal penetrates to lesser altitudes before being reflected. Also note the signal stays in the ionosphere over longer paths at medium transmission angles (Borer, 2005).

A first order approximation between a signal's group path length and the total electron content in the signal's path is given by

$$\text{Group Path Length} \approx \frac{40.3 \times \text{TEC}}{f^2} \text{ Hz} \quad (2.5)$$

This relationship indicates that signal path length is directly proportional to the path TEC (Misra, 2001). With this in mind and recalling the ionospheric TEC variability seen in figure 2.2, it is clearly not easy to predict precisely when and where transionospheric signals will end up. One approach to predicting a signal's refracted path and group delay through the ionosphere is signal ray tracing, the background of which is the focus of the following section.

## Ray Tracing

As shown in the previous section, signals in the frequency range of interest for this thesis, below 1GHz, are highly susceptible to ionospheric refraction and group delays versus free space paths due to the ionosphere's fluctuating index of refraction. Moreover, the induced refraction causes signals to remain in the ionosphere and subject to its delaying effects longer than if they traveled straight-line paths. The true transionospheric group delay a signal experiences can only be found after determining the actual three-dimensional path throughout which the signal is refracted, and the signal's velocity at every point in the path. Yet, due to the typical path length being on the order of thousands of kilometers, and considering the fluctuation of the ionospheric refractive index throughout the path, an exact determination of the signal path and hence, its group delay, is beyond existing capabilities. However, the potential does exist to estimate the most likely signal path and the corresponding delay using EM wave ray tracing theory.

Ray tracing theory is founded on geometrical optics, and provides a reliable method to estimate the dominant path of energy flow in propagating EM waves. In 1837, in the Third Supplement to his treatise on geometrical optics, William Rowan Hamilton introduced a system of differential equations describing ray paths through general anisotropic media (Hamilton, 1931). In 1954, Jenifer Haselgrove proposed Hamilton's equations were "suitable for numerical integration on a *high-speed* electronic computer," and "a new method for calculating ray paths in the ionosphere..." (Haselgrove, 1954). And then, in 1960, Haselgrove and Haselgrove implemented a ray tracing program to calculate "twisted ray paths" through a model ionosphere using Cartesian coordinates (Haselgrove and Haselgrove, 1960). Further notable work in the

field includes Radio Waves in the Ionosphere by K. G. Budden, in which the author shows Hamilton's equations correspond to the path of stationary phase of a propagating EM wave (Budden, 1961). Building upon these foundations, Michael Jones and Judith J. Stephenson, in 1975, documented "an accurate, versatile FORTRAN computer program for tracing rays through an anisotropic medium whose index of refraction varies continuously in three dimensions," (Jones and Stephenson, 1975). For this thesis, a significantly improved and updated implementation of the Jones-Stephenson ray tracing algorithm is used, as provided by Mark A. Hausman and L. J. Nickisch.

There are many derivations in the literature leading to Hamiltonian systems of equations for ray tracing, with varying motivations. For example, several papers have derived computationally efficient two-dimensional and three-dimensional ionospheric ray tracing equations and algorithms for use in OTHR applications (Coleman, 1998; and McDonnell, 2000). The Jones-Stephenson paper references other papers for the derivation of the equations it implements. A full derivation may also be found in L. J. Nickisch's "Focusing in the Stationary Phase Approximation," (Nickisch, 1987). The Jones-Stephenson algorithm numerically integrates the Hamiltonian system of equations given in equations 2.6-2.11, to calculate the location and propagation vector of an electromagnetic signal wavefront approximated as a ray point in three-dimensional space using the spherical-polar coordinate system. The ray-tracing equation symbols are defined in Table 1 and the spherical-polar coordinate system is shown with respect to the Cartesian coordinate system in figure 2.8.

**Table 1. Ray-Tracing Equation Symbols**

$f$	Frequency of electromagnetic wave
$H$	Hamiltonian
$k_r, k_\theta, k_\phi$	Components of the propagation vector in $r, \theta, \phi$ spherical polar coordinates -- a vector perpendicular to the wave front having magnitude $2\pi / \lambda = \omega / u$
$P'$	Group path, $P' = ct$
$r, \theta, \phi$	Spherical polar spatial coordinates
$\pi$	3.14159265
$\omega$	Angular wave frequency, $2\pi f$

$$\frac{dr}{dP'} = -\frac{1}{c} \frac{\partial H / \partial k_r}{\partial H / \partial \omega} \quad (2.6)$$

$$\frac{d\theta}{dP'} = -\frac{1}{rc} \frac{\partial H / \partial k_\theta}{\partial H / \partial \omega} \quad (2.7)$$

$$\frac{d\phi}{dP'} = -\frac{1}{rc \sin \theta} \frac{\partial H / \partial k_\phi}{\partial H / \partial \omega} \quad (2.8)$$

$$\frac{dk_r}{dP'} = -\frac{1}{c} \frac{\partial H / \partial r}{\partial H / \partial \omega} + k_\theta \frac{d\theta}{dP'} + k_\phi \sin \theta \frac{d\phi}{dP'} \quad (2.9)$$

$$\frac{dk_\theta}{dP'} = \frac{1}{r} \left( \frac{1}{c} \frac{\partial H / \partial \theta}{\partial H / \partial \omega} - k_\phi \frac{dr}{dP'} + k_\phi r \cos \theta \frac{d\phi}{dP'} \right) \quad (2.10)$$

$$\frac{dk_\phi}{dP'} = \frac{1}{r \sin \theta} \left( \frac{1}{c} \frac{\partial H / \partial \phi}{\partial H / \partial \omega} - k_\phi \sin \theta \frac{dr}{dP'} - k_\phi r \cos \theta \frac{d\theta}{dP'} \right) \quad (2.11)$$

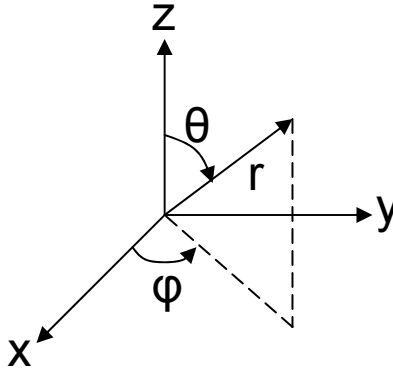


Figure 2.8. Spherical polar coordinates relative to Cartesian coordinates,  $r$  is radial distance from the origin (Earth's center),  $\theta$  is the angle measured in radians down from the  $z$ -axis (North-South Pole axis), and  $\phi$  is the angle measured in radians counter-clockwise from the  $x$ -axis in the  $x$ - $y$  plane (around the Earth eastward from the Prime Meridian).

Equations 2.6-2.11 provide the mathematical relationship between the Hamiltonian, which is a function requiring a specification of the ionospheric index of refraction, and an EM wave propagating through the ionosphere. The selection of the most appropriate Hamiltonian is very complex and will not be introduced here, but it is discussed in detail in the Jones-Stephenson paper. Integrating equations 2.6-2.11 with respect to the group path,  $P'$ , provides a ray's  $r$ -,  $\theta$ -, and  $\phi$ -coordinate position, and the components of the propagation vector,  $k_r$ ,  $k_\theta$ , and  $k_\phi$  at points throughout its path. The propagation vector provides the normalized wave normal direction, such that in free space:

$$k_r^2 + k_\theta^2 + k_\phi^2 = \frac{\omega^2}{c^2} \quad (2.12)$$

where  $\omega = 2\pi f$ , is the angular frequency of the wave, and  $c$  is the speed of light in free space.

The Hamiltonian system of equations is useless without a sufficient specification of the ionosphere's refractive index as a function of position. For this, equation 2.2 provides the

connection between electron density, which can be measured at various points over the Earth, and the index of refraction. However, to objectively estimate a signal path using ray tracing, it is desirable to minimize assumptions about the limits of the signal path. In order to provide as much room as possible for the ray tracing estimate to “maneuver,” it is desirable to be able to specify an extensive region of the ionosphere’s electron density. The next section explains it is not yet and may never be possible to sufficiently measure the ionosphere at any given instant to perform effective ray tracing, which leads to the use of ionospheric electron density models.

## **Ionospheric Models**

Accurate ray tracing through the ionosphere requires an accurate three-dimensional specification of the ionospheric refractive index as an input. As noted previously, this provides the index of refraction component of the Hamiltonian, essential to calculating a signal path through the ionosphere. A true specification of the ionosphere’s refractive index in three dimensions requires near constant measurements of the ionosphere’s electron content and distribution. Updated specifications would be required about every fifteen to thirty minutes due to solar, weather-related, and geomagnetic-field impacts on the ionosphere. This presents a challenge beyond current technological capabilities. For instance, this thesis examines paths between a point on the ground and geosynchronous orbits (approximately 35,800 km altitude). To ensure ray tracing is able to trace a signal anywhere within the ground site’s field of view, a horizon-to-horizon (close to hemispherical) ionospheric specification is warranted. This results in a specification of ionospheric volume on the order of  $10^{14}$  cubic kilometers. Currently,



computer-generated ionospheric specifications, or models, are the best alternative meeting this challenge.

One website maintained by the National Aeronautics and Space Administration (NASA) contains a list of 30 different ionospheric models (NASA/STP, 2005). Discussing and comparing the numerous ionospheric models in and of itself would easily consume an entire thesis, much less attempting to compare signal propagation through each. Two models are chosen for ray tracing comparison in this thesis. The first, the 2001 update of the International Reference Ionosphere (IRI-2001) model was selected because it is the primary model used by the ray tracing algorithm implementation examined in this thesis. The second is the Utah State University (USU) Global Assimilation of Ionospheric Measurements (GAIM) model, selected because it represents the state of the art in ionospheric modeling, and it is currently transitioning to operational employment by the Air Force Weather Agency (AFWA). The following paragraphs will discuss these two models.

The IRI model is an empirical standard ionospheric model internationally sponsored by the Committee on Space Research (COSPAR) and the International Union of Radio Science (URSI). It was initially introduced in 1978 and updated periodically; the latest version was released in 2001. Given inputs of location, time and date, the model predicts electron density, electron content, ion and electron temperatures, and ion composition from about 50 km up to 2000 km. Predictions are based on historical databases of experimental evidence from “all available ground and space data sources,” which are used to establish the non-auroral, monthly average for each ionospheric quantity under magnetically quiet conditions. The averages are

updated each year during IRI Workshops, during which the reliability of new data is discussed and established. Currently, the primary data sources contributing to IRI are the worldwide network of ionosondes, the incoherent scatter RADARs at Jicamarca, Arecibo, Millstone Hill, Malvern, and St. Santin, the International Satellites for Ionospheric Studies and Alouette topside sounders, and in situ instruments on various satellites and rockets (Bilitza, 1990; Bilitza, 2000; Bilitza, 2005). The next update to IRI is expected to extend to higher altitudes and possibly to geosynchronous orbit (Bilitza, 2006).

The USU GAIM model was commissioned by the U.S. Department of Defense as a Multi-Disciplinary University Research Initiative (MURI) with the goal of creating a global, ionospheric data assimilation model capable of specifying and forecasting the ionosphere in real-time. The consortium of universities involved in its development includes USU, the University of Colorado, the University of Texas at Dallas, and the University of Washington (CIRES, 2004).

USU GAIM Version 2.1, delivered to AFWA by USU on 15 July 2004, is used for this thesis. It is a Gauss-Markov Kalman Filter (GMKF) model based on the Ionosphere Forecast Model (IFM) covering the E, F, and *topside ionosphere* regions up to 1500 km, taking into account six ion species: NO<sup>+</sup>, O<sub>2</sub><sup>+</sup>, N<sub>2</sub><sup>+</sup>, O<sup>+</sup>, He<sup>+</sup>, and H<sup>+</sup> (Schunk, 2005). According to USU GAIM 2.1 User's Guide, this model assimilates slant TEC measurements from up to 400 Global Positioning System (GPS) sites, electron density measurements from the Defense Meteorological Satellites Program (DMSP) satellites, ionograms, and nighttime 1356 Å radiances from the Air Force's Advanced Research and Global Observation Satellite (ARGOS) Low Resolution

Airglow and Aurora Spectrograph (LORASS) instrument. The primary output is a time-dependent, three-dimensional electron density distribution (User's Guide, 2004). This release of GAIM is the most mature implementation, having undergone extensive testing and validation efforts to ensure its stability. Additionally, although it is possible to optimize the configuration of GAIM for specific scientific research (Thompson, 2006), the default operational configuration is used for this effort.

A future update of GAIM is known as the Full-Physics Kalman Filter model and is currently undergoing testing and development by USU. This version is composed of two sub-models, an Ionosphere-Plasmasphere Model (IPM) for low and mid-latitudes, and an Ionosphere-Polar Wind Model (IPWM) for high latitudes. The resulting model is much more rigorous in its approach and is expected to be useful in regions where measurements are sparse or during severe conditions (Schunk, 2005). Additionally, this updated version will be able to extend ionospheric specifications to geosynchronous orbits (Thompson, 2006). This new version should definitely be taken into consideration for future research efforts.

It would seem from the standpoint of military applications, GAIM has the advantage. The major difference between the two models is their real-time employment. While IRI is founded on historical databases of the monthly averages of data to predict the conditions expected during magnetically quiet conditions, GAIM predicts conditions using the most current data available. IRI's tables are only updated annually, while GAIM specifications and forecasts require input measurements taken no greater than 3 hours in the past for real-time ionospheric specification. IRI was created when real-time measurements were not as readily available nor as

numerous as they now are, while GAIM was created to take advantage of real-time measurements using the techniques validated by modern weather forecast models. However, IRI has international acceptance; it is recommended by COSPAR and recognized by URSI as “the standard for the ionosphere.” It has an established track record of reliability, whereas GAIM does not (Schunk, 2005; Bilitza, 2000). It is hoped the results of this thesis will help guide future researchers in their determination of which model may be more appropriate to use for ray-tracing predictions in order to improve national defense applications.

### **III. Methodology**

#### **Overview**

The objectives of this thesis are 1) to illustrate how the ionosphere distorts signal propagation in terms of refraction and group path versus the ideal case of free space propagation, as a function of varying frequency and time of day, and 2) to compare results obtained using plasma frequency specifications from two ionospheric models, IRI-2001 and USU GAIM Version 2.1. These models are extended using a diffusive equilibrium model beyond GEO. The results for the comparison include the following:

- 1) Predicted TEC maps from extended and un-extended versions of each model
- 2) Predicted signal refraction versus frequency and elevation angle
- 3) Predicted signal angle to target versus LOS versus time of day and frequency
- 4) Signal group delay versus time of day and frequency

Accomplishing each of these results requires the integration of various components and the establishment of a process, discussed in the next paragraph.

The major components for this research effort are software-implemented applications enabling the computational burden of determining three-dimensional signal paths over distances passing through the ionosphere (tens of thousands of kilometers). These components include ionospheric modeling programs, IRI-2001 and USU GAIM Version 2.1, the Hausman-Nickisch

update of the Jones-Stephenson ray tracing code, and MATLAB® to process inputs and display outputs of these components. For this research, these applications are run on a Pentium Xeon computer with Microsoft Windows 2000 Professional as the operating system. Figure 3.1 illustrates a simplified version of the flow of data between the user and the components. The user provides inputs to all components to ensure desired outputs. IRI specifications are immediately ready for ray tracing, while GAIM specifications require MATLAB® processing before ray tracing. The ray tracing algorithm reads the specifications, and calculates and outputs signal path descriptions. MATLAB® processes ray tracing outputs and display results. The next few sections provide a more complete description of the process components.

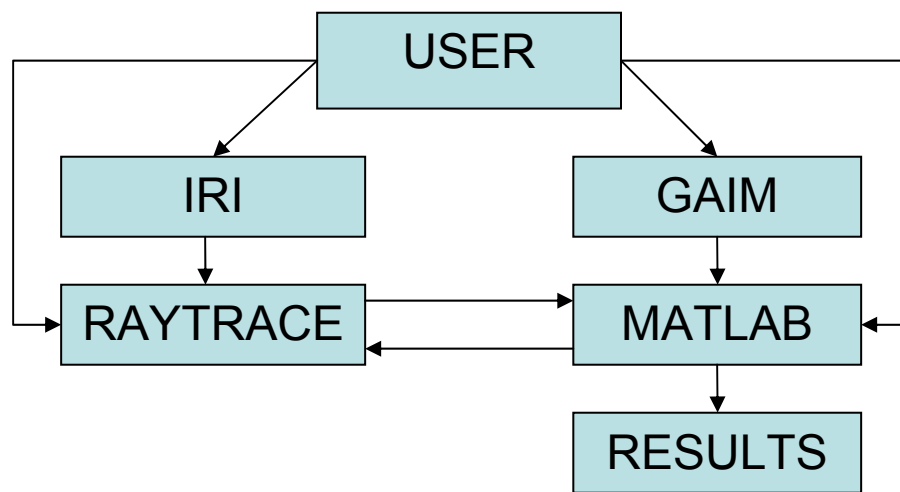


Figure 3.1 shows a simplified version of the process necessary to accomplish the research objectives. The user directs all components to read inputs, process data, and output results in required formats, with the end goal being to display the ionospheric ray tracing results in an easy-to-understand format, showing comparisons and impacts of varying inputs.

## The Models

The first two components of the process consist of ionospheric modeling software based on IRI-2001 and USU GAIM 2.1, hereafter IRI and GAIM respectively. As mentioned throughout this thesis, neither of these models alone is sufficient for this research effort. This research investigates ionospheric impacts on signals between the ground site, Goldstone Deep Space Observatory in southern California, and GEO. However, IRI only models the ionosphere up to 2000 km altitude, and GAIM only up to 1380 km altitude. Therefore, it is necessary to extend each model to estimate ionospheric content out to geosynchronous orbit. The following paragraphs will discuss how each model is extended and describe each model's interface, inputs, and outputs.

The IRI implementation used for this thesis is provided, in addition to the ray tracing algorithm, by Mark A. Hausman and L. J. Nickisch. They implemented this ionospheric model for ease of use with their code, such that its output plasma frequency specification is immediately ready for use by their ray tracing program. (Note: A grid of plasma frequency is required as input for the ray tracing algorithm. Plasma frequency is calculated as the square root of electron density multiplied by a constant.) This model comes as a Microsoft Windows executable file, based on FORTRAN source code. Upon execution, it requires four lines of input: Line 1, minimum and maximum of geographic latitude range, and number of latitude grid divisions; Line 2, minimum and maximum of geographic longitude range, and number of longitude grid divisions; Line 3, the 12-month-running-mean sunspot number (Rz12), specific to the month and year of interest; and Line 4, the date and coordinated uniform time (UTC) of

interest. IRI then accesses its records of historical data to determine the average ionospheric profile expected for the given date, time, and Rz12 inputs, and outputs an ionospheric plasma frequency grid with the specified number of divisions over the geographic region specified by the latitude and longitude inputs. Hausman and Nickisch's IRI model also automatically provides an altitude dimension of 221 nodes, covering from 80 km to 36540 km.

As noted previously, the actual IRI-2001 model is only capable of providing specifications up to 2000 km. Further, Hausman and Nickisch find that on average, the IRI model's electron density predictions above approximately 1500 km are higher than what is actually encountered in the ionosphere. Therefore, their IRI implementation only uses IRI-2001 for the lower portion of their ionospheric specification up to 1500 km, and then extends it by interpolating to a diffusive equilibrium ionospheric model, devised by Sergey Fridman, which begins at 2000 km (Nickisch, 2006). The diffusive equilibrium extension (DEE) model is based upon the simplifying assumption that the ionosphere's electron content, which is approximately equivalent to the ion content, drops off exponentially as a function of plasma temperature and ion-specific scale height. (A full explanation of diffusive equilibrium can be found in Schunk and Nagy, 2000.) To provide the DEE IRI specification above 2000 km, Fridman's model relies on IRI-2001's outputs of ionospheric ion species content and ion temperature at 2000 km. The resulting extended plasma frequency grid is output in the format required by the ray-tracing algorithm. Figure 3.2 provides an DEE IRI specification altitude profile over a single location. Examples of the input and output used to create Hausman and Nickisch's DEE IRI specifications are provided in Appendix A.



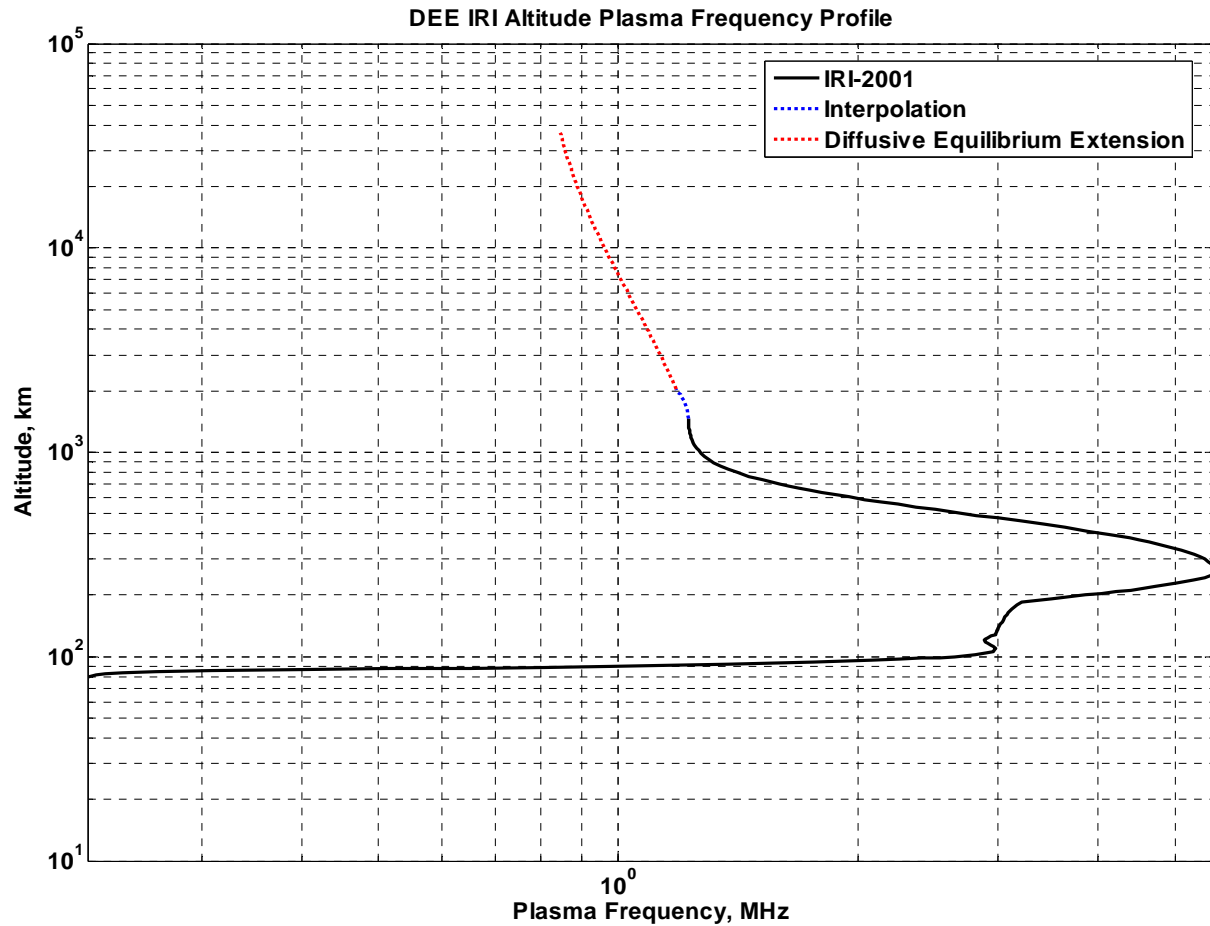


Figure 3.2 shows a log-log plot of IRI ionospheric plasma frequency (MHz) versus altitude (km). The lower black portion represents the IRI-2001 portion of the model, the blue represents interpolation between models, and the red represents the diffusive equilibrium model portion.

GAIM ionospheric specifications are provided for this thesis by the Air Force Weather Agency (AFWA). To create the specifications, AFWA requires minimum and maximum latitudes and longitudes, and date/UTC inputs the same as for IRI. However, unlike IRI, GAIM does not just use a single measure of solar activity, such as Rz12. Instead, it bases its ionospheric specifications on a multitude of ionospheric activity measurements for a given date and time. Because the measurements come from a wide array of resources available to AFWA, and they maintain the GAIM expertise, AFWA establishes the appropriate data for assimilation

into GAIM. For this research, the assimilated data includes measurements of TEC from GPS, ionograms from Digital Ionospheric Sounding System (DISS), and from the Topside Ionospheric Plasma Monitor (SSIIES) on DMSP. Additionally, unlike IRI, GAIM does not allow the user to specify the geographic grid spacing. It automatically assumes an effective grid spacing determined by the extent of the region modeled (Keyser, 2006). Appendix D demonstrates that, at least in IRI's case, ray-tracing results are affected by varying the model's grid spacing, and therefore the grid spacing is an important subject for future research efforts.

Two critical issues encountered in using GAIM for this research are: 1) its output must be reformatted for ray tracing, and 2) similar to IRI, its specification must be extended to reach GEO. First, none of GAIM's available output formats are the specific format required by the Hausman-Nickisch ray tracing code. This issue is solved using MATLAB® processing via the NetCDF toolbox, found at: [http://mexcdf.sourceforge.net/netcdf\\_toolbox.html](http://mexcdf.sourceforge.net/netcdf_toolbox.html). A MATLAB® script is attached (Appendix B, GAIM4mat\_xtend.m), which imports GAIM outputs and reformats them as required for ray tracing. To address the second issue, extending GAIM specifications, the MATLAB® script includes code to extend the specifications from 1,380 km (USU GAIM 2.1's limit) to 36,540 km using the same DEE model as for IRI, but with one significant difference versus IRI. GAIM does not provide outputs of plasma temperature nor ion composition of the ionosphere. Therefore, a scaled version of DEE IRI's upper specification is used for DEE GAIM, at the same date and time, over the same region, and with the same grid spacing for both. The extension is scaled proportional to the output plasma frequency of GAIM at 1,380 km, divided by the output of IRI at the same altitude. Figure 3.3 illustrates a resulting DEE GAIM profile expanded using diffusive equilibrium and figure 3.4 shows the DEE GAIM

profile and the corresponding DEE IRI profile in the same plot. Although both model expansions show notable discontinuities in terms of the rate of change of the plasma frequency, for this research it is deemed more appropriate to leave these discontinuities versus continuing to alter the model (attempt to smooth the discontinuities), which has as much likelihood of reducing accuracy as it does of improving accuracy with respect to the unknown, true ionosphere. These assumptions were necessary for creating ionospheric specifications enabling ray tracing to GEO.

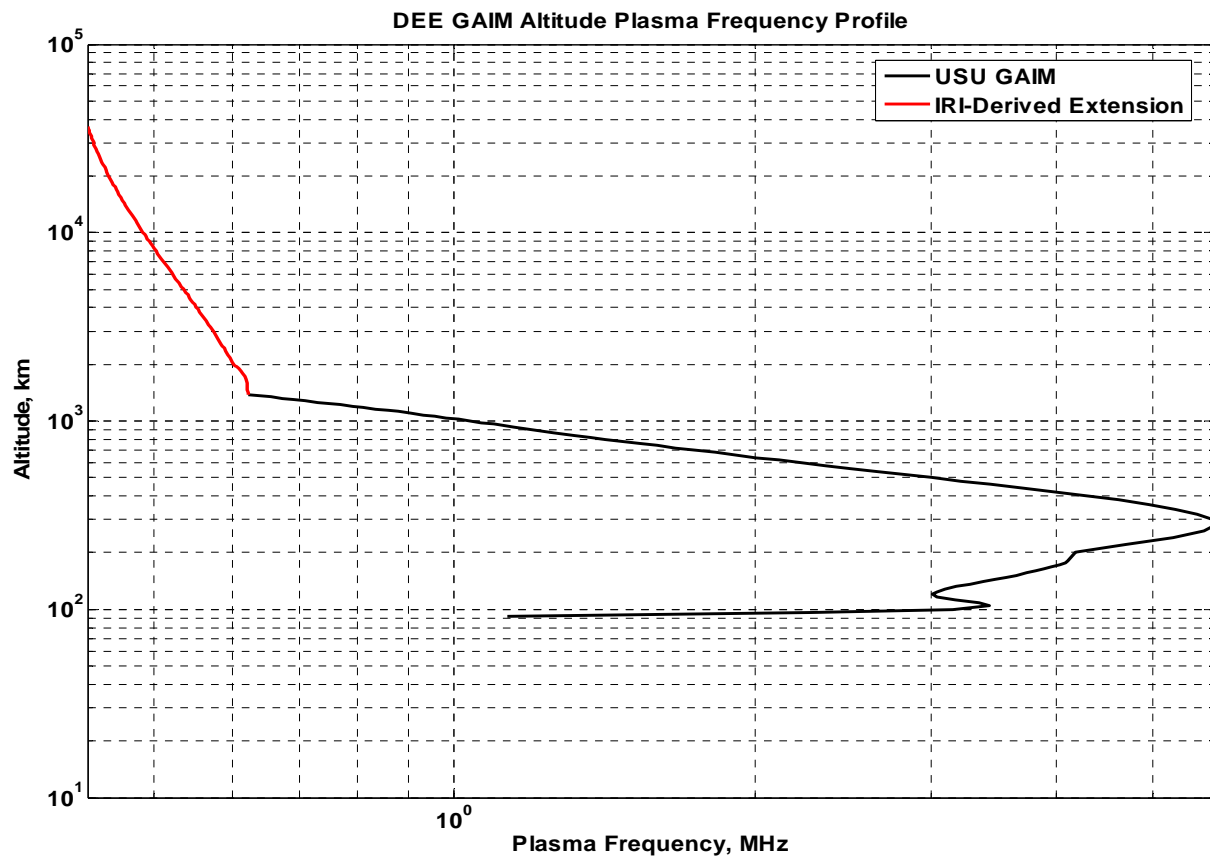


Figure 3.3 shows a log-log plot of GAIM ionospheric plasma frequency (MHz) versus altitude (km). The lower black portion represents the USU GAIM 2.1 portion, and the upper red represents IRI-derived diffusive equilibrium model extension.

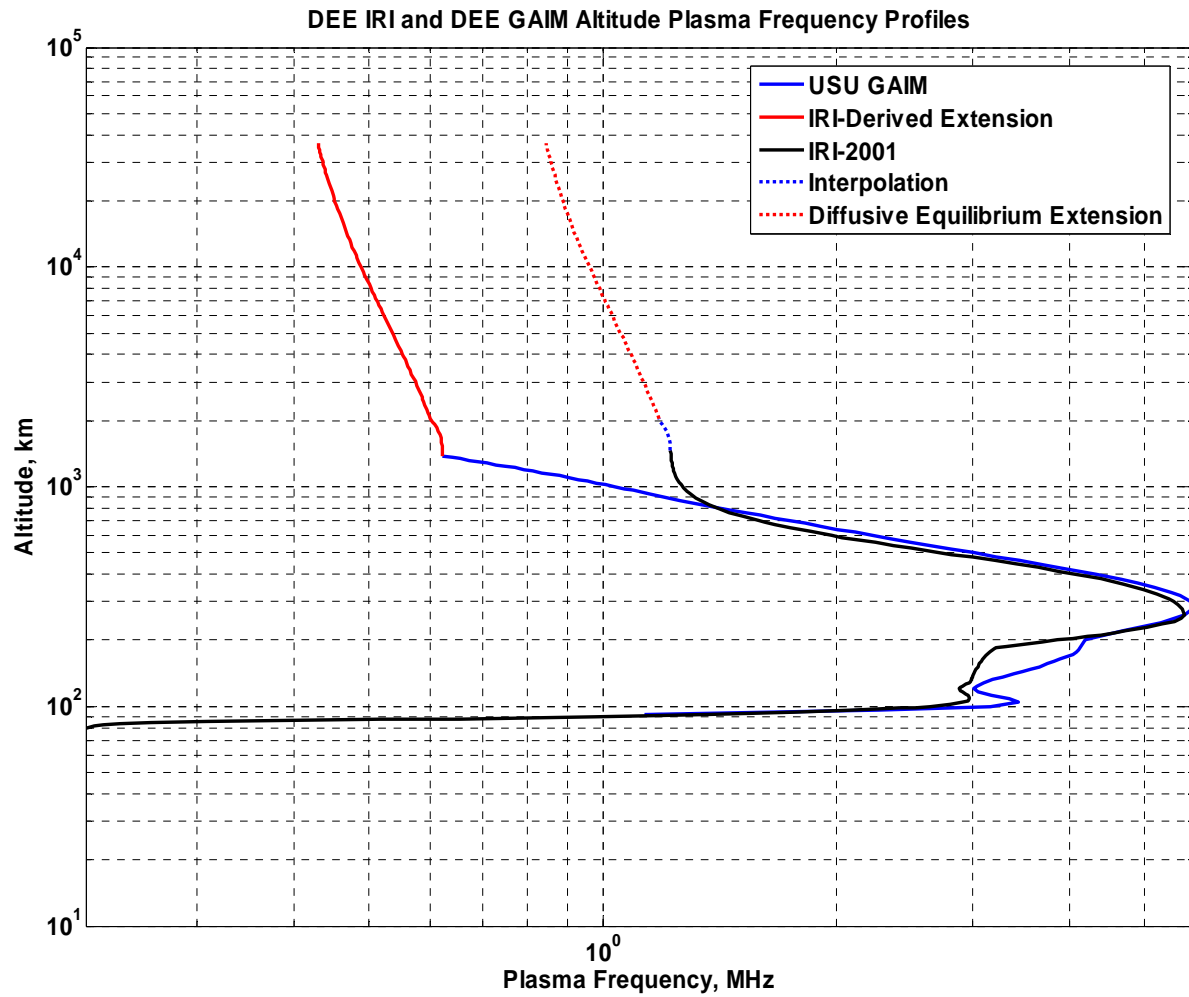


Figure 3.4 shows a log-log plot comparing the DEE IRI and DEE GAIM ionospheric plasma frequency (MHz) profiles versus altitude (km).

## **The Ray-Tracing Algorithm**

The Hausman-Nickisch ray-tracing algorithm chosen for this thesis is a vastly updated, executable version of the Jones-Stephenson ray-tracing algorithm. This executable provides the capability to adjust a wide range of ray properties and other parameters including all those discussed in the original Jones-Stephenson paper (1975). The code requires two specifically formatted files: 1) a parameter specification file and 2) the ionospheric model specification file discussed in the previous section. The parameters set by the parameter file include the signal frequency (or frequency range), geographic locations of transmitter and receiver in latitude, longitude, and altitude, signal homing selection, ray plotting options, and the name of the ionospheric specification file. A more complete description of the parameter specification file and an example are included in Appendix C. The code is executed via a MS Windows command prompt using the command, “runrt <filename.dat>,” where <filename> is the name of the parameter specification file. The ray tracing code outputs binary and ascii files similar to those found in Appendix C. These output files provide the data of primary interest to this research: azimuth, elevation, and group path of the signal. They also make possible plotting the projection of the completed three-dimensional signal raytrace in various two-dimensional and three-dimensional plots using a MATLAB® script provided by Hausman and Nickisch. As discussed in the next section, MATLAB® is also used to extract the data of interest from many ray tracing output files quickly in order to explore a sufficient range of variation in the inputs and achieve greater value in the final results.

## **MATLAB®**

MATLAB® Version 7.0.0.19920, Release 14, provides all inter-component data processing and display capabilities necessary for implementing the ray tracing and ionospheric model comparison in this research. Some of the MATLAB® tools used for this thesis are proprietary and not available for public release. For instance, results in Chapter 4 illustrating ray refraction through the ionospheric plasma background and cross-range ray refraction are made possible using the Rayplot2D.m routine provided by Hausman and Nickisch. They additionally provided another m-file that allowed MATLAB® to read model plasma frequency specifications, transform them to electron density specifications, and enabled the plotting of the TEC maps in the results. However, the m-files found in Appendix B represent the majority of the code created by the thesis author necessary to achieve the desired results. The GAIM4mat\_extend.m subroutine reformats GAIM data, and adds the geosynchronous Fridman diffusive equilibrium extension to the GAIM model specifications. The FullTECPlot.m is the main routine that calls the Hausman-Nickisch routine to read in the model specifications for plotting TEC maps. The RayOut.m subroutine extracts data from the ray tracing output files from the Hausman-Nickisch ray tracing code. Both of the subroutines or “functions,” as written in MATLAB®, GAIM4mat\_extend.m and RayOut.m, are called by main routines, such as RaytraceOut.m to quickly modify and extract data from numerous files. The main routines specify the file paths for files each subroutine must access. The main routines then perform any needed calculations on the data provided by the subroutines, and direct MATLAB® to plot the results, which are discussed next.

## **IV. Results**

### **Overview**

The desired results of this thesis are: 1) to illustrate how the ionosphere distorts signal propagation in terms of signal refraction and group delay versus the ideal case of free space propagation, as a function of varying frequency, time of day, and signal launch angle, and 2) to compare results obtained using plasma frequency specifications of IRI-2001 and USU GAIM 2.1, extended to GEO using Fridman's diffusive equilibrium model. The results for the comparison include the following:

- 1) Predicted TEC maps from extended and un-extended versions for each model
- 2) Predicted vertical and crossrange ray refraction versus frequency and elevation angle
- 3) Predicted ray angle deviation from LOS to target versus time of day and frequency
- 4) Predicted signal group delay versus time of day and frequency

These results are presented and discussed in the following sections, beginning with TEC maps.

## TEC Maps

Ionospheric vertical total electron content, referred to as TEC in the following results, is one of the primary characteristics predicted by ionospheric models such as IRI and GAIM. It is reasonable to expect the predicted TEC from these two models to be different because IRI makes predictions based on historical average, magnetically-quiet ionospheric conditions, while GAIM makes predictions based on actual conditions. These TEC ( $1 \text{ TEC} = 10^{16}$  electrons per square meter) maps are calculated from model plasma frequency specifications by first converting them to electron density specifications, then obtaining the TEC within each latitude-longitude (Lat/Lon) grid by finding the mean electron density between adjacent vertical altitude grids, multiplying the mean by the vertical altitude distance (step size), and summing up the results through all the altitude steps. The specification grids are centered due south of the ground site chosen for this thesis, Goldstone Deep Space Observatory (Goldstone), in southern California, and consists of 30 divisions between  $-52.8333$  and  $72.8333$  degrees North Lat, and 24 divisions between  $157.75$  and  $330.25$  degrees East Lon. The white line is the LOS from the Goldstone to the PanAmSat Galaxy 1R GEO satellite at  $227$  East Lon. TEC maps are given for 1 November 2004 at 0600 Pacific Standard Time (PST), near sunrise at Goldstone; and at 1400 PST, the approximate time the ionosphere's peak density is expected over Goldstone. Figures 4.1 through 4.4 are TEC maps of IRI-2001 and USU GAIM specifications without the diffusive equilibrium extension (DEE) model (TEC summed across altitudes 90 km to 1340 km). Figures 4.6 and 4.7 show TEC for DEE IRI and DEE GAIM, and figures 4.5 and 4.8 provide difference TEC maps to help compare corresponding results. Each is discussed in the following paragraphs.



Figures 4.1 and 4.2 show TEC values predicted by IRI-2001 and USU GAIM at 0600 local Goldstone time (Pacific Standard Time, PST). The most immediately notable difference is the distribution of the electron content predicted by each model, illustrated by the varying colors (dark blue corresponding to the minimum TEC and dark red to the maximum TEC). According to IRI at this time, the densest region is already extending over South America, past its west coast, and well into the Pacific Ocean, with two separate peaks of approximately 48 TEC between 10 and -20 degrees Lat. GAIM predicts lesser densities over most of South America, with the densest ionospheric region still off the east coast. GAIM predicts higher peak densities than IRI, at nearly 60 TEC, north of the Equator, while IRI's peaks are in the south. However, both models predict the peaks are within 20 degrees of the equatorial region as expected given the Sun's energy is directed just south of the equator at this time of year. Both models predict higher densities to the east in the figures, as one would expect given the sun's position over the Earth. Neither model predicts high electron densities affecting the ground-satellite LOS, which would suggest less frequency-dependent refraction will occur at this time. It is reasonable to expect that as the sun progresses westward, the higher densities will enter the signal path resulting in increased refraction. And, if the current trend holds, GAIM's higher densities suggest its model will result in more signal refraction and greater signal delay, at least to the altitude these TEC maps include (1,340 km). The next figures show the progression of the ionosphere into the peak time of day, 1400 PST, when the maximum densities are expected over the ground site, affecting signal propagation.

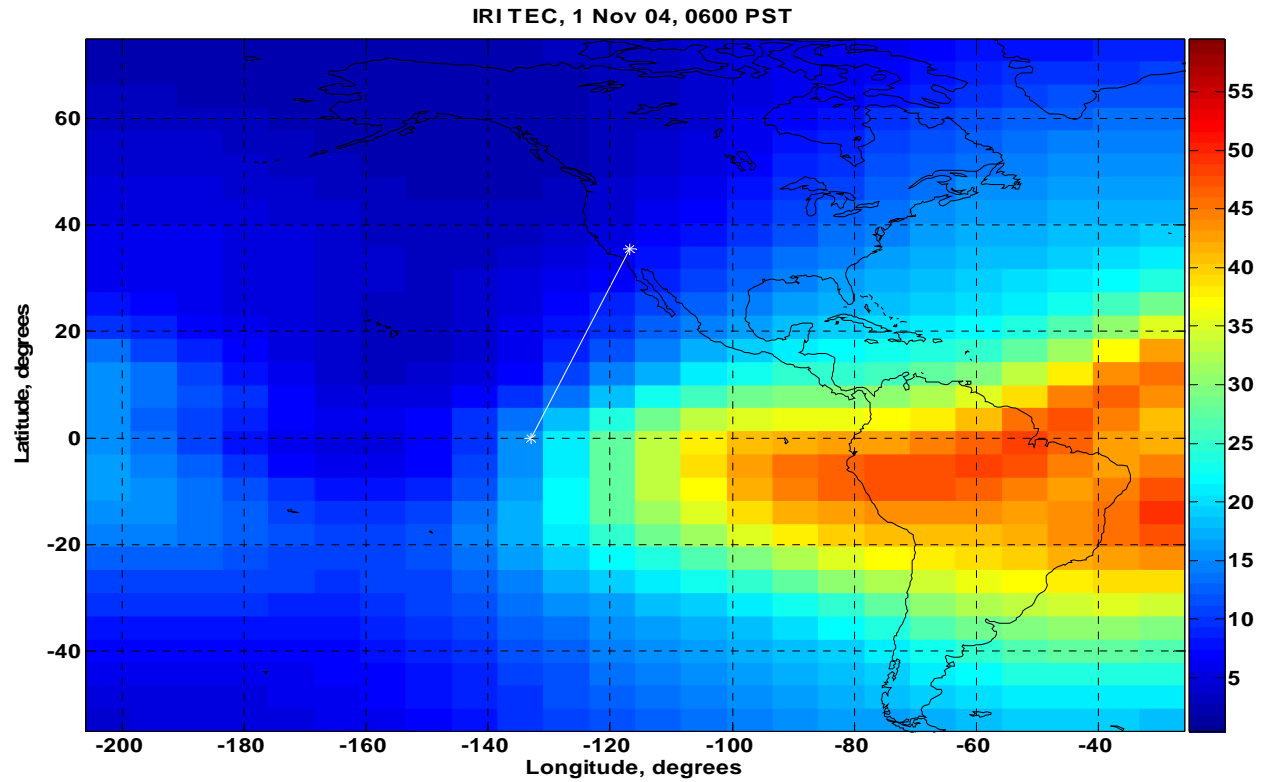


Figure 4.1 illustrates IRI-predicted TEC at 0600 Pacific Standard Time (PST) on 1 Nov 04.

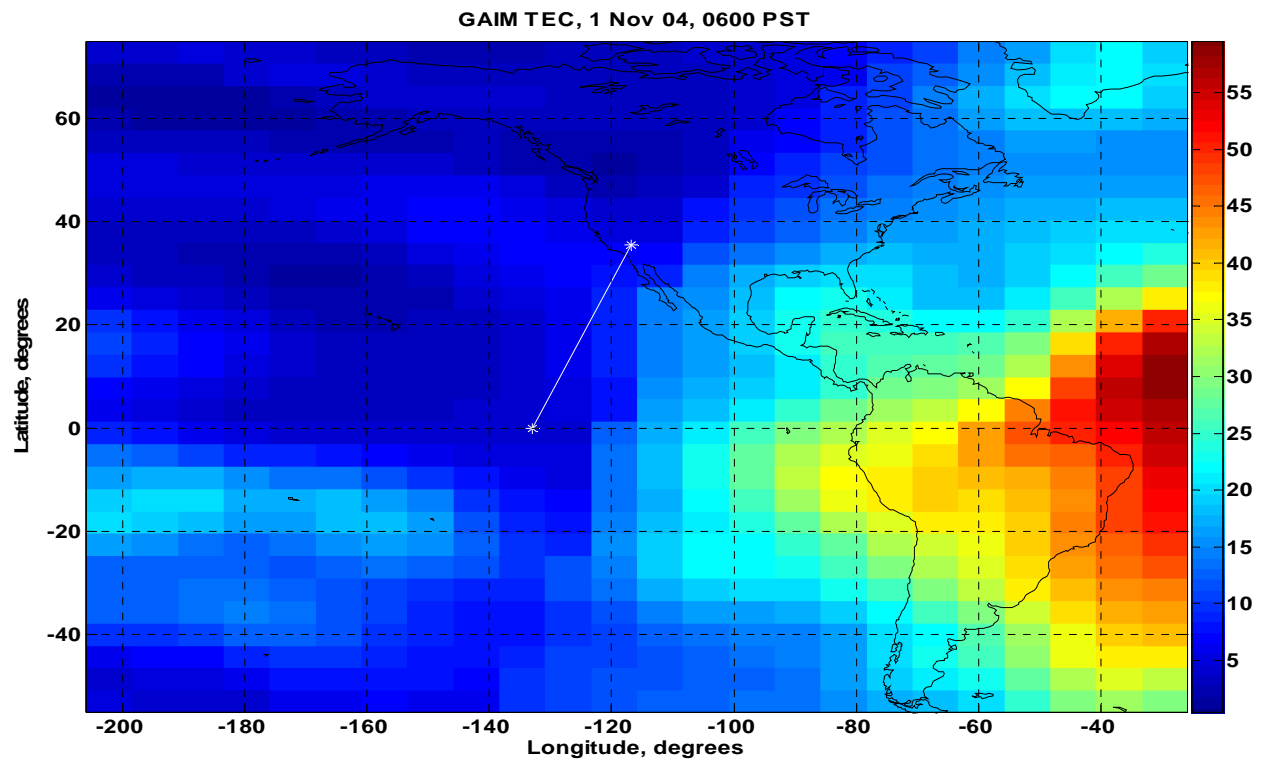


Figure 4.2 illustrates USU GAIM-predicted TEC at 0600 PST on 1 Nov 04.

Figures 4.3 and 4.4 show TEC values predicted by IRI-2001 and USU GAIM 2.1 at 1400 PST. Similar to figures 4.1 and 4.2, the most immediately notable difference again is the distribution of the ionospheric electron content predicted by each model. According to IRI at this time, the densest region of more than 35 TEC, is well-spread on both sides of the Equator between approximately -25 and 20 degrees Lon, and running the length of the figure. The two peak-density regions predicted by IRI of over 50 TEC run nearly parallel, one peak close to the equator and the other near the -20 degree Lat line. GAIM, on the other hand, predicts two much more focused high density peaks up to nearly 70 TEC. The separation between the high density regions is more defined in the GAIM result in which the differential between the highest peak and the “valley” between the peak densities is approximately 25 TEC, whereas IRI’s peak-valley differential is closer to 10 TEC. The densest regions predicted by GAIM also cover a smaller area of the map than IRI’s predictions, such that densities above 40 TEC extend from approximately -20 to -180 degrees Lon, and sharply drop off above 20 Lat and below -26 Lat. Common to model results is the appearance of density tails which stretch back to the approximate location of the higher densities seen in the previous TEC plots at 0600. The following map, figure 4.5, shows the TEC difference between the IRI and GAIM TEC maps at 1400. It is created by subtracting the GAIM TEC from the IRI TEC at each Lat-Lon grid point.

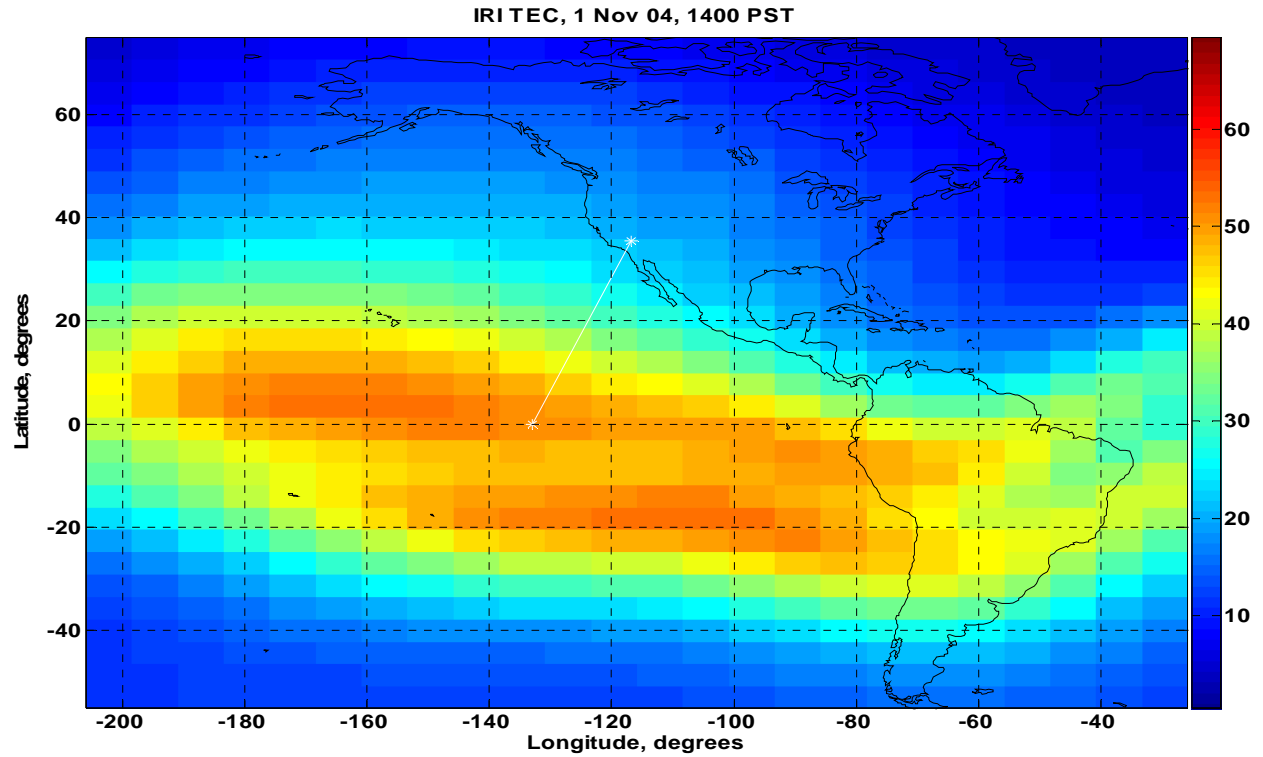


Figure 4.3 illustrates IRI-predicted TEC at 1400 PST on 1 Nov 04.

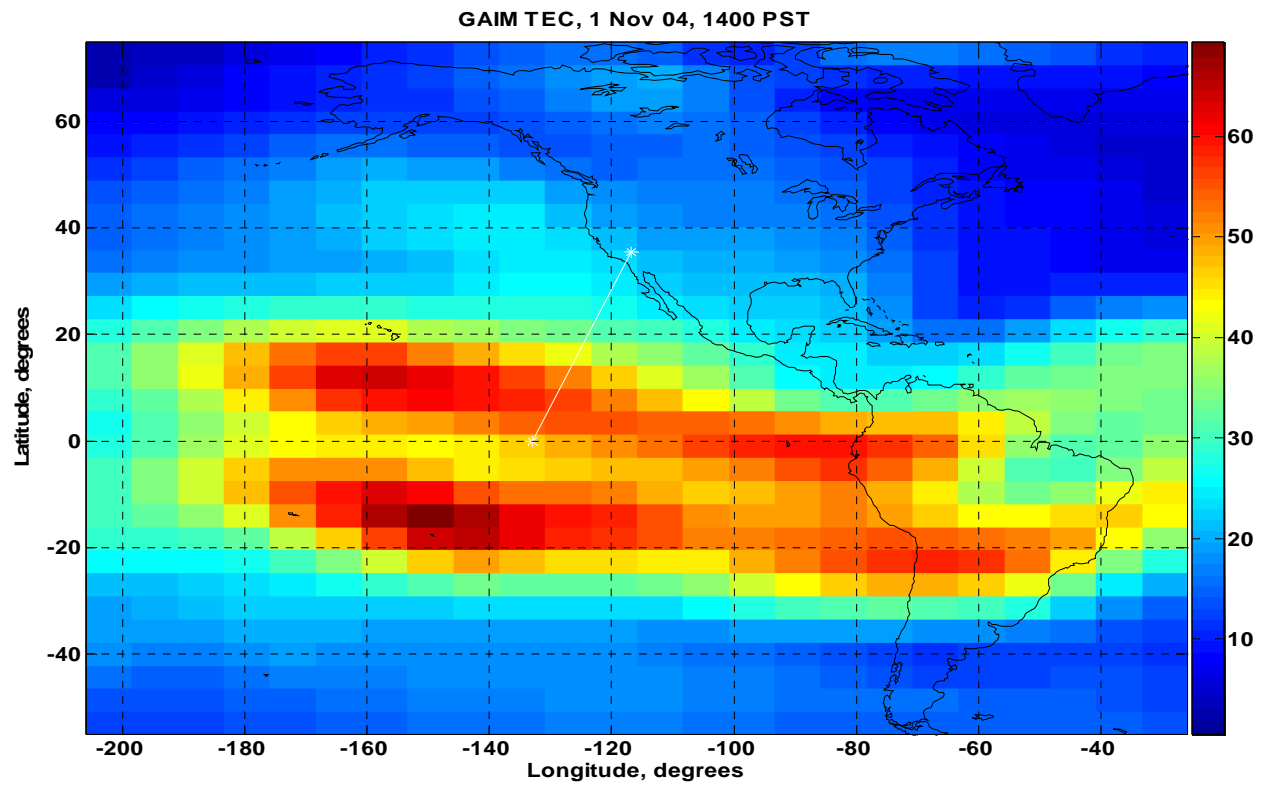


Figure 4.4 illustrates GAIM-predicted TEC at 1400 PST on 1 Nov 04.

Figure 4.5 assists in highlighting the major differences between the GAIM and IRI predictions at 1400 PST. Overall, the magnitude of the average difference between the models is just under 1 TEC at 0.91. However, the dark red indicates the regions where IRI predicts about 15 TEC more than GAIM, and the dark blue regions show GAIM at 20 TEC more than IRI. These greatest differences correspond to different properties of each model's TEC output. Whereas GAIM's peak differences clearly correlate to the peak TEC locations it predicts and the tails stretching back across the map, IRI's greatest differences correlate to its TEC concentrations being spread over a larger area than GAIM. The final figures of this section will explore if these differences translate to the DEE model specifications used for ray tracing.

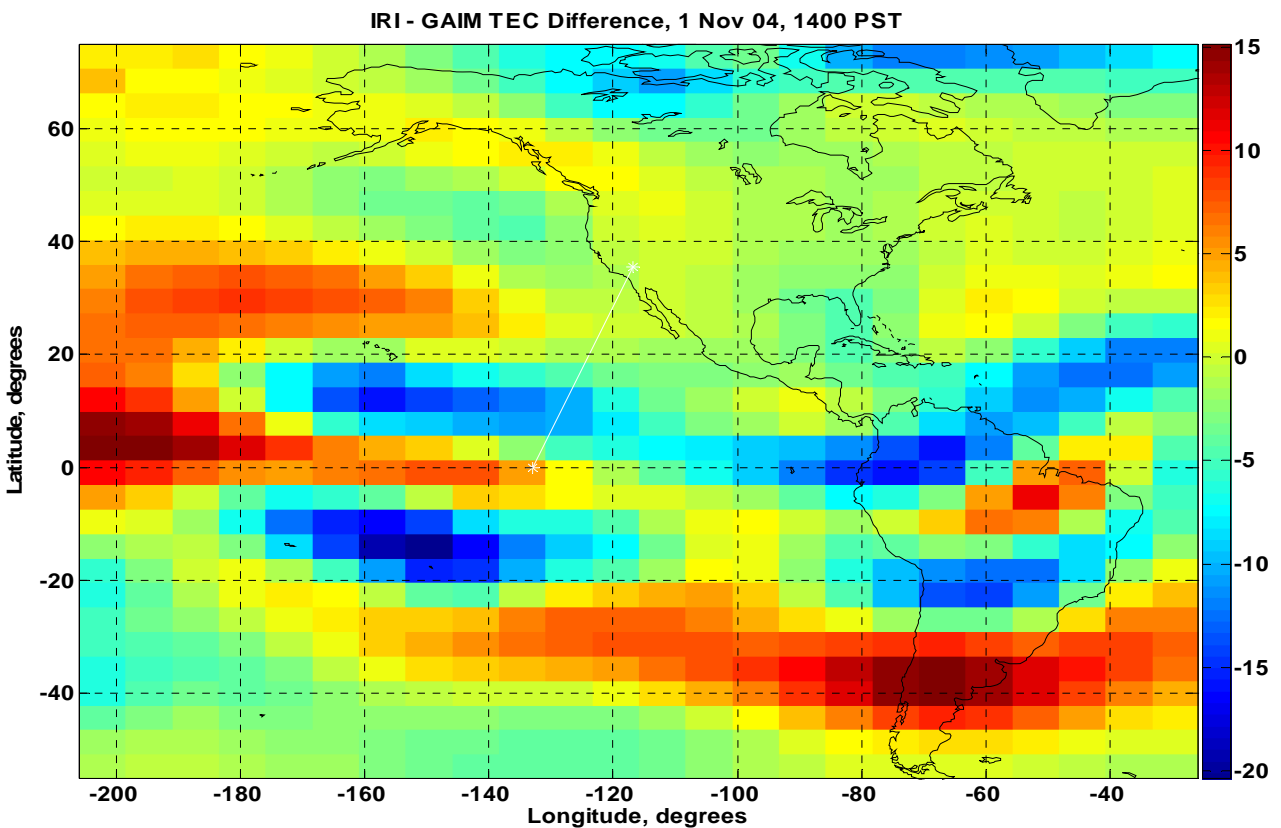


Figure 4.5 illustrates the predicted TEC difference between IRI and GAIM at 1400 PST on 1 Nov 04. This map is created by subtracting GAIM TEC from IRI TEC at every lat/lon grid point.

Figures 4.6 and 4.7 show TEC maps for DEE IRI and DEE GAIM at 1400 PST on 1 Nov 04, the same time as for figures 4.3-4.4. The difference plot in figure 4.8 of DEE IRI minus DEE GAIM highlights the high DEE IRI bias in these results; the DEE IRI-predicted TEC map is hundreds of TEC units greater than that of DEE GAIM. Although the magnitude of the difference is surprising, this outcome is not completely unexpected considering the DEE IRI profile versus the DEE GAIM profile seen in chapter three, figure 3.4, shows IRI plasma frequencies (proportional to electron densities) are significantly higher than GAIM's in both models' upper altitudes (at approximately 1380 km). Because the IRI-derived extension added to GAIM is simply the portion of DEE IRI above 1380 km, scaled by the ratio of the upper altitude plasma frequencies of GAIM versus IRI, and because IRI plasma frequency is apparently greater than GAIM plasma frequency at 1380 km in figure 3.4, DEE IRI remains greater than DEE GAIM above 1380 km for this single case. However, there is wide acceptance in the ionospheric community that IRI's topside ionospheric predictions for electron density are higher than truth (Nickisch, 2006). Therefore, if USU GAIM's upper altitude electron densities are closer to truth than IRI's, or if they are at least always less than IRI's, it can be expected that DEE IRI-predicted TEC maps will typically dominate the corresponding DEE GAIM-predicted TEC maps. Moreover, given the basic relationships found in equations 2.1 through 2.5 explaining how signal refraction and group path rely on ionospheric electron density and TEC, if large differences between DEE IRI and DEE GAIM TEC maps persist, there should be notable differences in ray-tracing through these specifications. The next section compares some ray-tracing refraction predictions based on un-extended IRI and GAIM specifications, and the last two sections confirm there are significant differences in results based on ray tracing through DEE IRI and DEE GAIM.

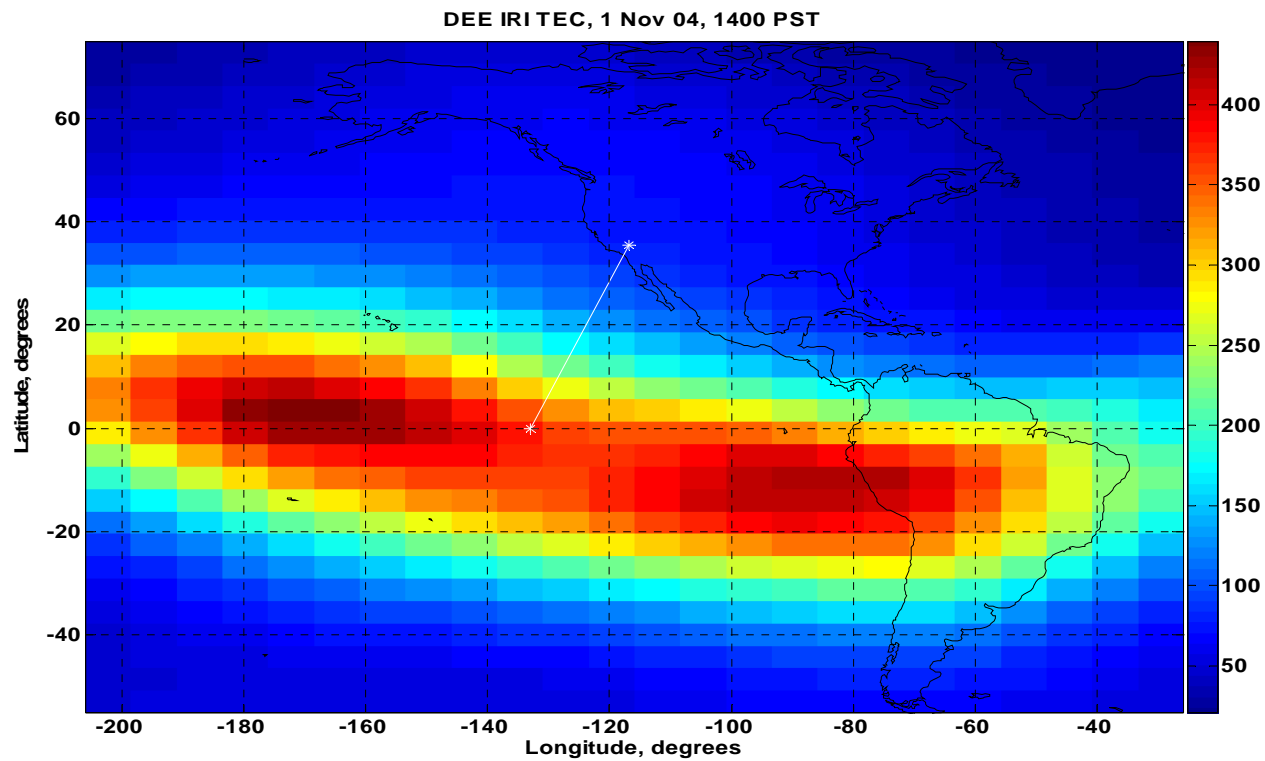


Figure 4.6 illustrates diffusive equilibrium extended IRI at 1400 PST on 1 Nov 04.

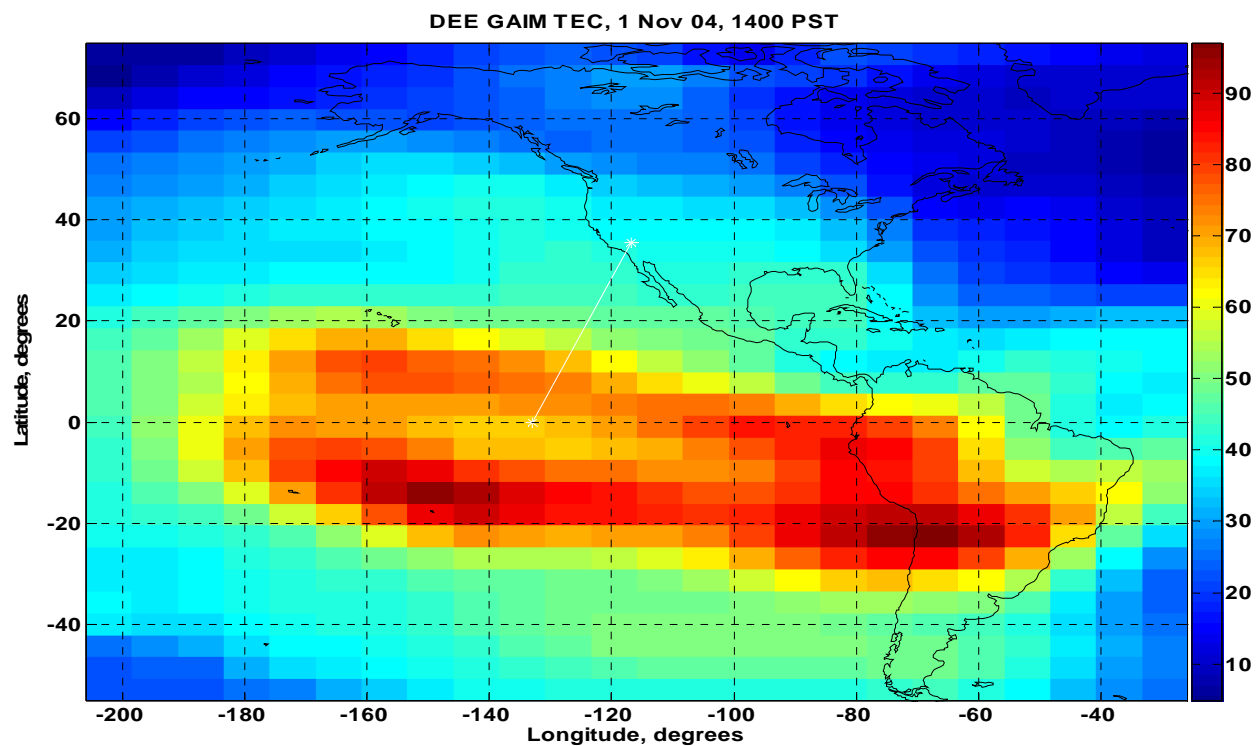


Figure 4.7 illustrates diffusive equilibrium extended GAIM at 1400 PST on 1 Nov 04.

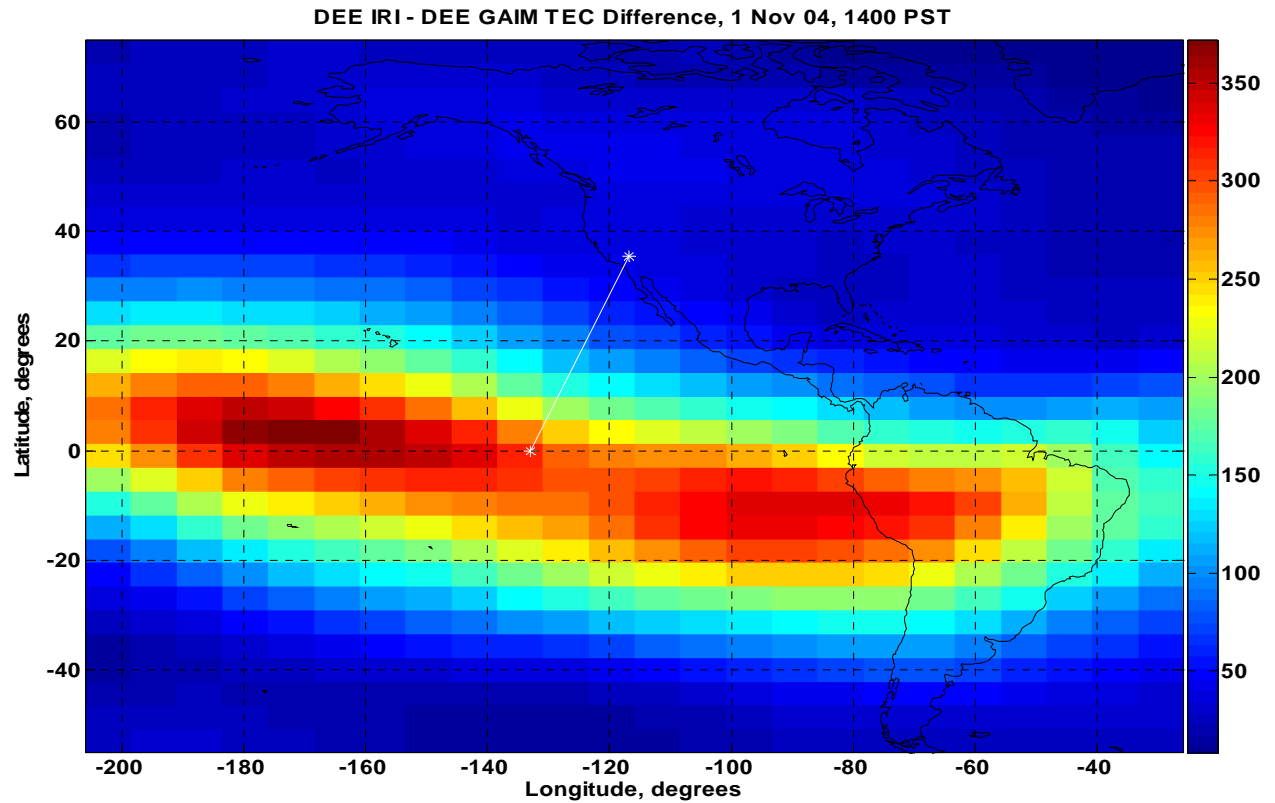


Figure 4.8 illustrates the predicted TEC difference between diffusive equilibrium extended versions of IRI and GAIM at 1400 PST on 1 Nov 04. This map is created by subtracting GAIM TEC from IRI TEC at every lat/lon grid point.



## Ray Refraction

The following figures illustrate how ray tracing through un-extended IRI and GAIM specifications predicts frequencies of 11, 12, 13, and 14 MHz will refract through the ionosphere above Goldstone on 1 Nov 04, at 1400 PST. The results illustrated in figures 4.9 through 4.12 provide insight into how changing the transmitted signals' elevation angles between 20, 45, and 70 degrees causes variation in the amount of refraction below 1,000 km altitude for each model. One major difference found in figures 4.9 and 4.10, and important to applications such as OTHR, HF, and DF is that a 12-MHz ray, launched at 45 degrees, penetrates the ionosphere predicted by IRI but not by GAIM. The explanation, not well illustrated in these figures, is GAIM predicts a higher electron density in the F<sub>2</sub> region (at 250 km altitude) than IRI, resulting in the 12-MHz ray's reflection. Another important difference is each model's cross-sectional peak density thickness. GAIM's peak altitudinal densities are contained in a more compact layer (yellow-to-yellow between approximately 200 and 350 km) than IRI (yellow-to-yellow at less than 200 up to nearly 400 km). These differences in the peak densities and their distributions result in differences in the predicted ray paths. GAIM shows more spread in the 45- and 70-degree rays than IRI, but less spread in the 20-degree rays. Differences in ray spreading for each model are also seen from directly above the ground site looking down at the ray paths projected onto the Earth's surface, herein called the "crossrange." For instance, if the figures shown in figures 4.9 and 4.10 are in the x-z plane of the Cartesian coordinate system the crossrange view is looking straight down the z-axis at the x-y plane. The crossrange results corresponding to figures 4.9 and 4.10 are shown in figures 4.11 and 4.12 and discussed next.

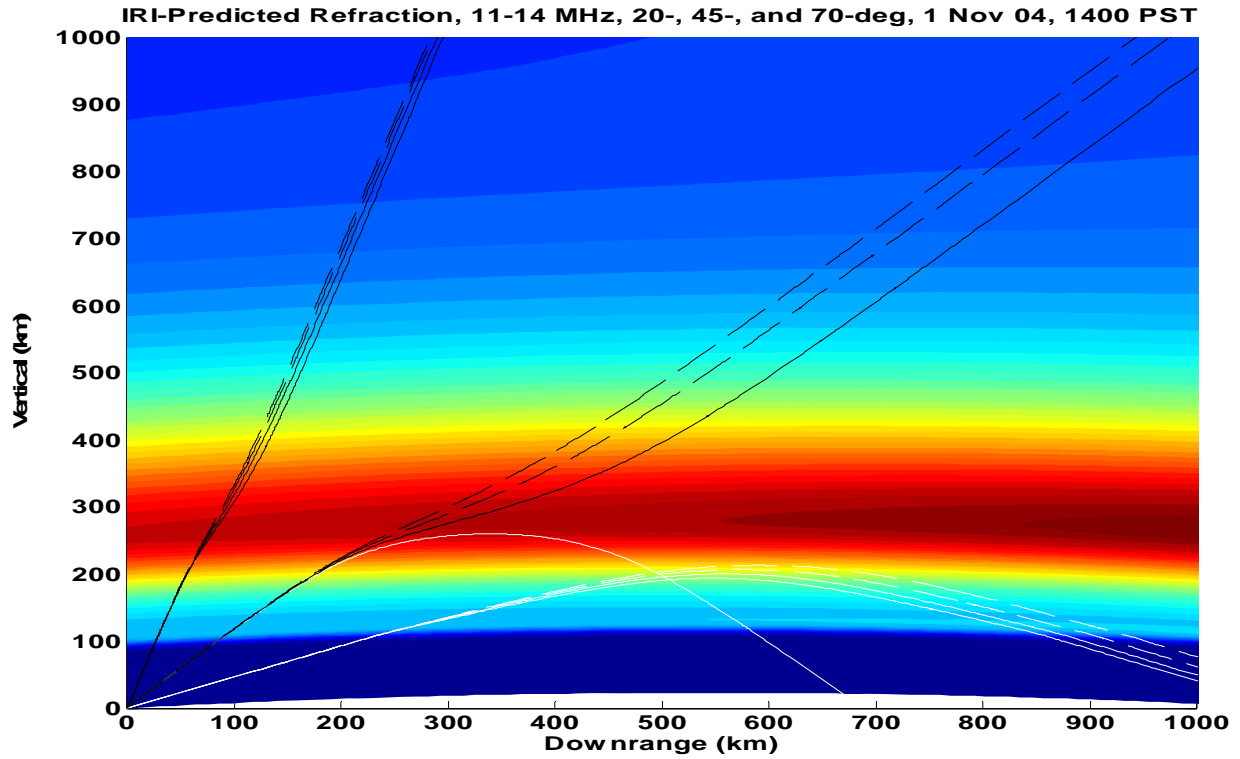


Figure 4.9 illustrates ray refraction for signals at 11, 12, 13, and 14 MHz, launched at 20, 45, and 70 degrees elevation through IRI-2001 at 1400 PST on 1 Nov 04.

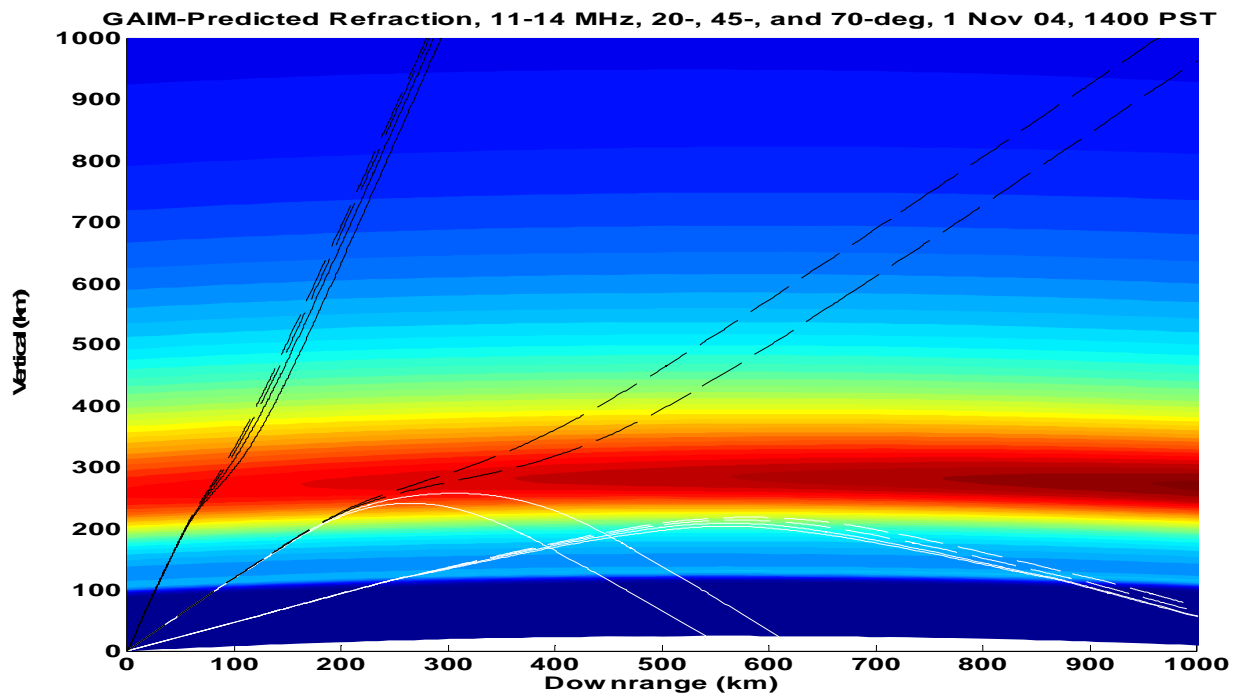


Figure 4.10 illustrates ray refraction for signals at 11, 12, 13, and 14 MHz, launched at 20, 45, and 70 degrees elevation through USU GAIM at 1400 PST on 1 Nov 04.

Figures 4.11 and 4.12 correspond to figures 4.9 and 4.10, this time displaying crossrange ray paths for signal frequencies of 11-14 MHz transmitted at angles of 20, 45, and 70 degrees elevation. The rays diverge more quickly at higher transmission elevation angles. These figures provide a key perspective on why a fully three-dimensional ray tracing algorithm is essential to this research effort versus two-dimensional ray tracing methods, such as that discussed by Coleman for OTHR (Coleman, 1998). Noting the difference in the figures y-axes' scales, GAIM predicts a 13-MHz ray launched at 45 degrees elevation diverges from the same signal launched at 20 degrees elevation by more than 20 km crossrange in its first 1000 km of altitudinal propagation, while IRI only predicts an approximately 8-km divergence for this signal. IRI predicts a maximum divergence for the 12-MHz signal launched at 45 degrees of almost 12 km, while GAIM predicts this signal is reflected. GAIM also predict all rays are initially being refracted more towards the negative crossrange direction, while IRI does not clearly show any initial negative crossrange tendency. Divergence is frequency dependent in both models, wherein lower-frequency, non-reflected rays diverge more and high-frequency rays diverge less for a given elevation angle. Of key interest to OTHR is the difference in IRI- versus GAIM-predicted ray reflection. All frequencies are reflected for 20-degree elevation angles and both models predict a tendency for all frequencies to propagate back towards zero crossrange, which suggests a two-dimensional ray tracing algorithm would be sufficient. However, the 45-degree elevation case shows no return to zero crossrange for the IRI 11-MHz and GAIM 11- and 12-MHz reflections. The next section provides insight into the variation of transionospheric signal elevation and azimuth angles as a function of frequency and time of day, which is of interest to applications such as OTHR, HF, DF, and SATCOMM.

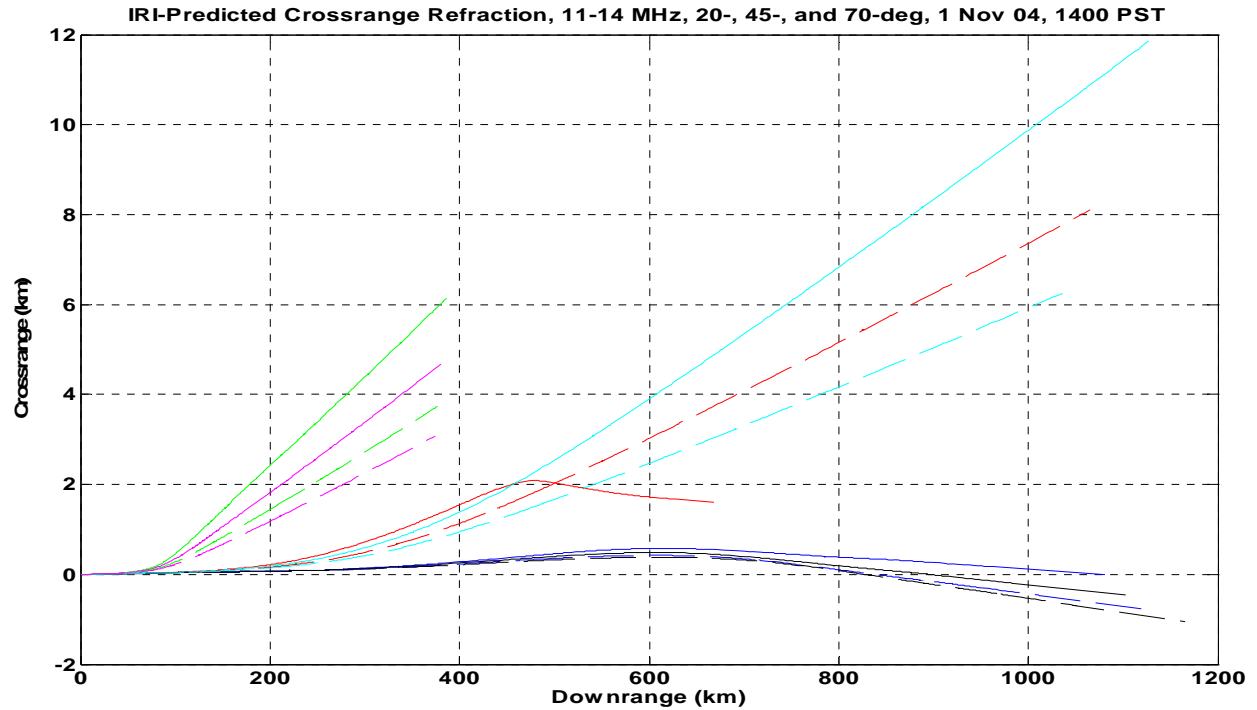


Figure 4.11 shows signal refraction projected on the Earth's surface for 11, 12, 13, and 14 MHz, launched at 20, 45, and 70 degrees elevation through IRI-2001 at 1400 PST on 1 Nov 04.

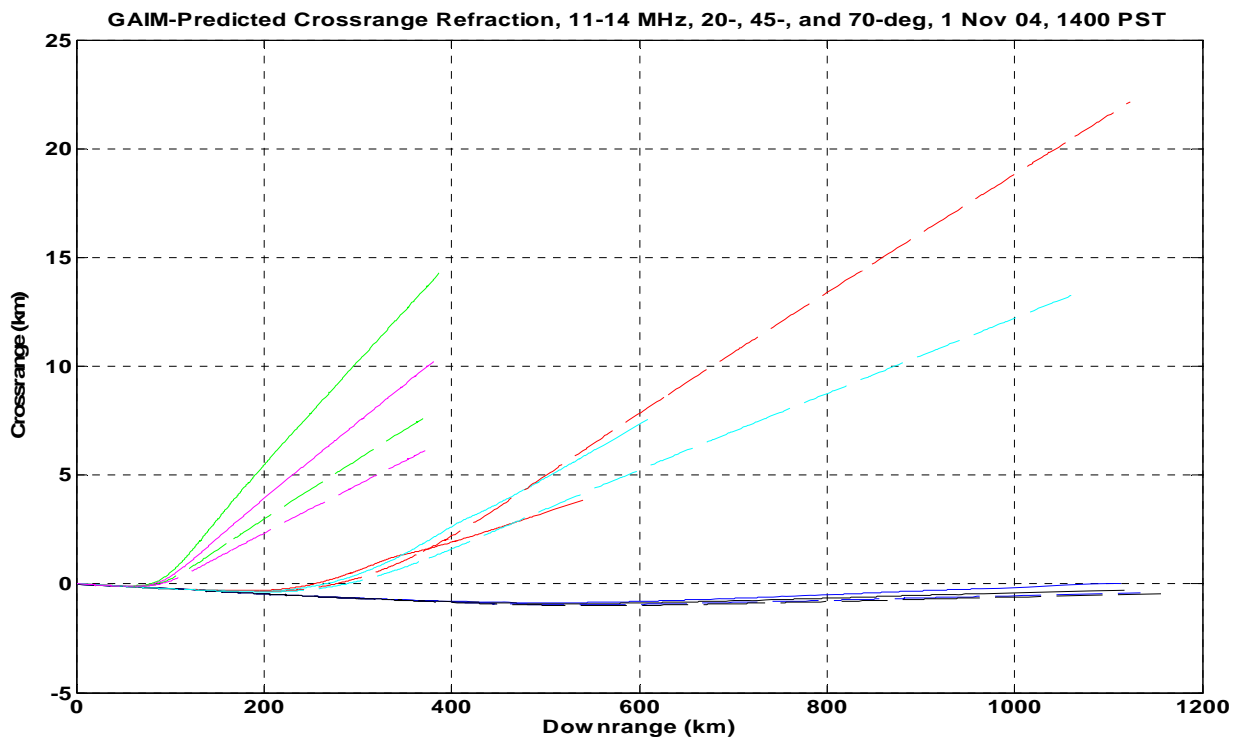


Figure 4.12 shows signal refraction projected on the Earth's surface for 11, 12, 13, and 14 MHz, launched at 20, 45, and 70 degrees elevation through USU GAIM at 1400 PST on 1 Nov 04.

## Angular Deviation

The LOS elevation and azimuth angles to a arbitrarily chosen satellite at geosynchronous orbit (PanAmSat's Galaxy 1R at 0°N Lat, 133°W Lon) from the Goldstone ground site in southern California (35.424707°N Lat, 116.88982°W Lon) are different from the elevation and azimuth at which the ground station antenna should be aimed to ensure the best signal reception at frequencies below 1 GHz. The following ray-tracing results provide predictions for the best signal elevation and azimuth transmission angles for transionospheric communications at frequencies in this range. These angles result from ray tracing through DEE IRI and DEE GAIM as a function of frequency, 15-50 MHz in steps of 5 MHz and 100-1000 MHz in steps of 100 MHz, and time of day, every 30 minutes between 0600 and 1700 PST, on 1 Nov 04. This section specifically seeks to investigate the angular behavior of signals that consistently penetrate the ionosphere as modeled by IRI and GAIM. The lower bound of 15 MHz is chosen because this portion of the studied frequency range increases in increments of 5 MHz and frequencies at or below approximately 11 MHz are already shown to be reflected by IRI and GAIM. The times of this study are chosen somewhat arbitrarily with the intent to characterize the majority of one ionospheric day. However, it should be noted that a full investigation would incorporate multiple days, varying season, and solar cycle, and include nighttime studies as well. This limited study begins with figures 4.13 and 4.14 illustrating elevation angular deviation from LOS predicted by ray tracing through DEE IRI and DEE GAIM specifications.

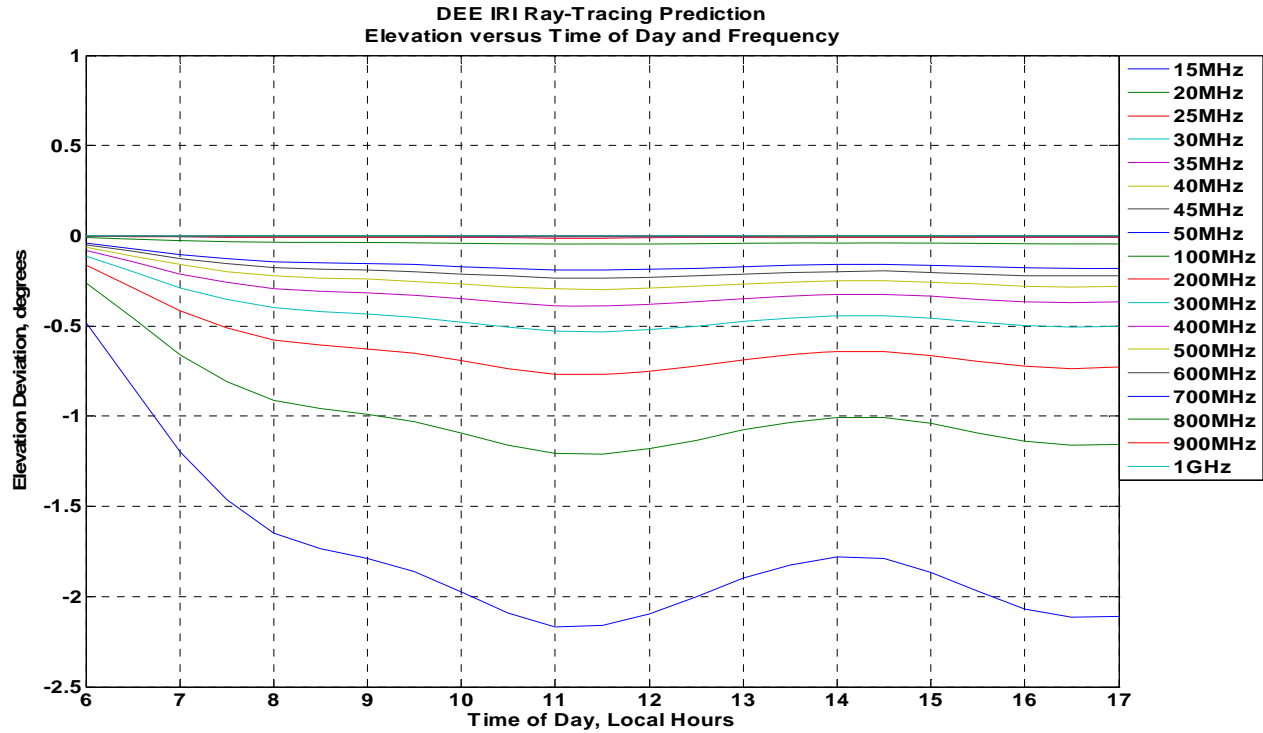


Figure 4.13 illustrates DEE IRI ray-tracing-predicted deviation of elevation angle from LOS for signals from 15 MHz to 1 GHz, and every half hour from 0600 to 1700 PST on 1 Nov 04.

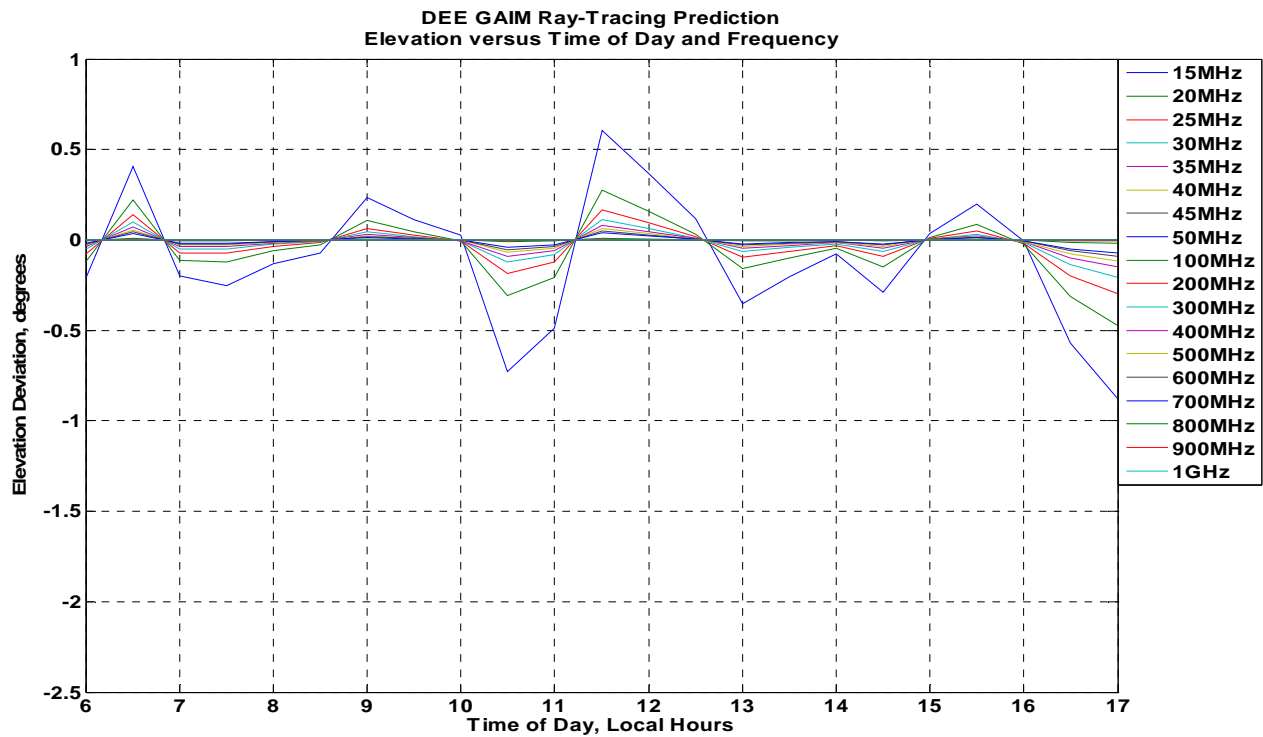


Figure 4.14 illustrates DEE GAIM ray-tracing-predicted deviation of elevation angle from LOS for signals from 15 MHz to 1 GHz, and every half hour from 0600 to 1700 PST on 1 Nov 04.

Figures 4.13 and 4.14 illustrate DEE IRI and DEE GAIM ray-tracing predictions that the best elevation to aim an antenna transmitting through the ionosphere at frequencies below approximately 100 MHz to ensure best reception at the receiver varies over the course of the day. Ray tracing through DEE IRI consistently predicts transmitting at an elevation below LOS is required for optimum communications. However, DEE GAIM ray-tracing predictions are much less consistent, varying elevation angles to slightly higher and lower than the LOS angle over the course of the day. DEE IRI ray-tracing predicts greater deviation from LOS for most of the day, by more than two degrees. This result is extremely significant because referring to the geometry displayed in figure 4.15, a transmitting antenna's boresight aimed at two degrees away from a receiver's actual location over a minimum distance of 35,800 km (ground to GEO) would result in a miss distance of greater than 1,200 km.

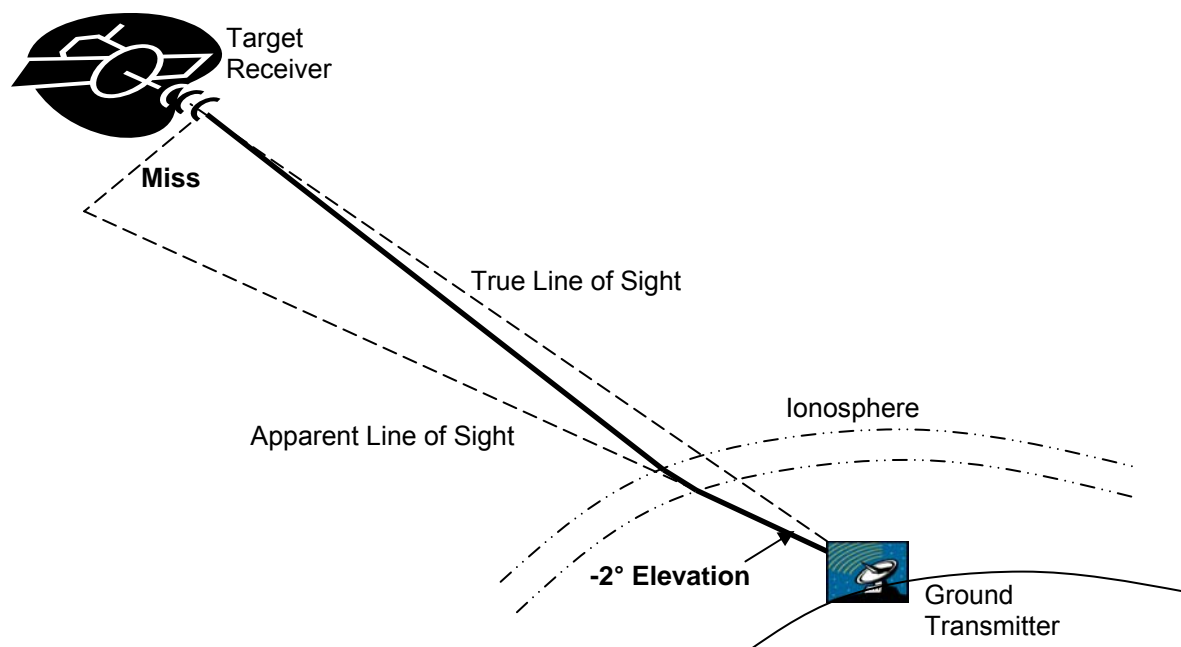


Figure 4.15 illustrates the miss distance associated with an offset elevation angle of  $-2^\circ$ . This translates to a miss of more than 1,200 km at geosynchronous orbit.

The objective of optimizing the transmitting antenna's aim is to ensure the most efficient communications by using the best signal path. If the transmitting antenna is aimed at the LOS to the satellite receiver, there is an associated miss distance similar to that shown in figure 4.15, caused by ionospheric refraction. While DEE IRI ray tracing predicts as much as a two degree adjustment, DEE GAIM results indicate much smaller elevation angle adjustments are necessary. The DEE GAIM ray-tracing predictions also suggest that this adjustment will approach and pass through the LOS elevation angle several times over the course of the day. Both results show that as the frequency increases, the best transmission elevation collapses to the LOS, which agrees with the expectation shown in figure 2.4 where increasing frequency signals are less refracted. Also notable in the predictions from ray tracing through both DEE IRI and DEE GAIM, all higher frequencies are contained under the "envelope" of the lower frequencies, i.e. no higher frequency deviates more from the LOS than a lower frequency for any time of day. Moreover, frequencies above 100 MHz show no visible deviations from LOS during the period of interest. A final difference between these apparent elevation angle predictions is there is no clear correlation between the deviation predictions from ray tracing DEE IRI versus DEE GAIM. It seems impossible to estimate the predictions of one given the predictions of the other. On the other hand, the results shown in figures 4.16 and 4.17 displaying deviation of apparent azimuth angles from LOS are much more similar.

Figures 4.16 and 4.17 show the DEE IRI and DEE GAIM ray-tracing predicted degree of azimuth deviation from LOS as a function of frequency and time of day. As seen in the elevation deviation results, higher frequencies are contained under the "envelopes" of the lower frequencies, and frequencies above approximately 100 MHz do not visibly deviate from the LOS



azimuth. These results again concur with expectations of refraction as a function of frequency. The DEE IRI result again predicts a maximum angular deviation for 15 MHz of approximately negative two degrees from LOS. However, this is where the similarities between these results and the previous elevations results end. The DEE GAIM result is much more similar to the DEE IRI result. Before 1130 PST, DEE GAIM ray tracing predicts negative peak deviations from LOS within one half hour and within 0.5 degrees of those predicted by ray tracing DEE IRI. Both results predict a single zero deviation crossing of the LOS azimuth axis and both models progress from negative to positive deviation in the afternoon. However, the DEE GAIM result again appears jagged versus the DEE IRI result's smooth progression during the day and DEE GAIM's result crosses the zero at 1330, while DEE IRI's does so just before 1600. Further, after the zero crossing, DEE GAIM shows higher deviation than DEE IRI. Figure 4.18 helps clarify why these zero crossing predictions occur. As the ionosphere's peak electron density passes from east to west with the sun's progression, through the signal path, the best antenna azimuth for optimal communications passes through the LOS azimuth, such that the antenna always tends to point into higher electron densities to compensate for ionospheric refraction of the signal to the target receiver. In concluding this section, referring back to figure 4.15, it is clear that compensating for transionospheric signal azimuth and elevation deviations is vital to improving satellite communications. Failure to compensate may cause signals transmitted from the ground to be refracted by the ionosphere to thousands of kilometers off target. The next section provides another important consequence of the ionosphere's impact on the signal path: varying group path length.

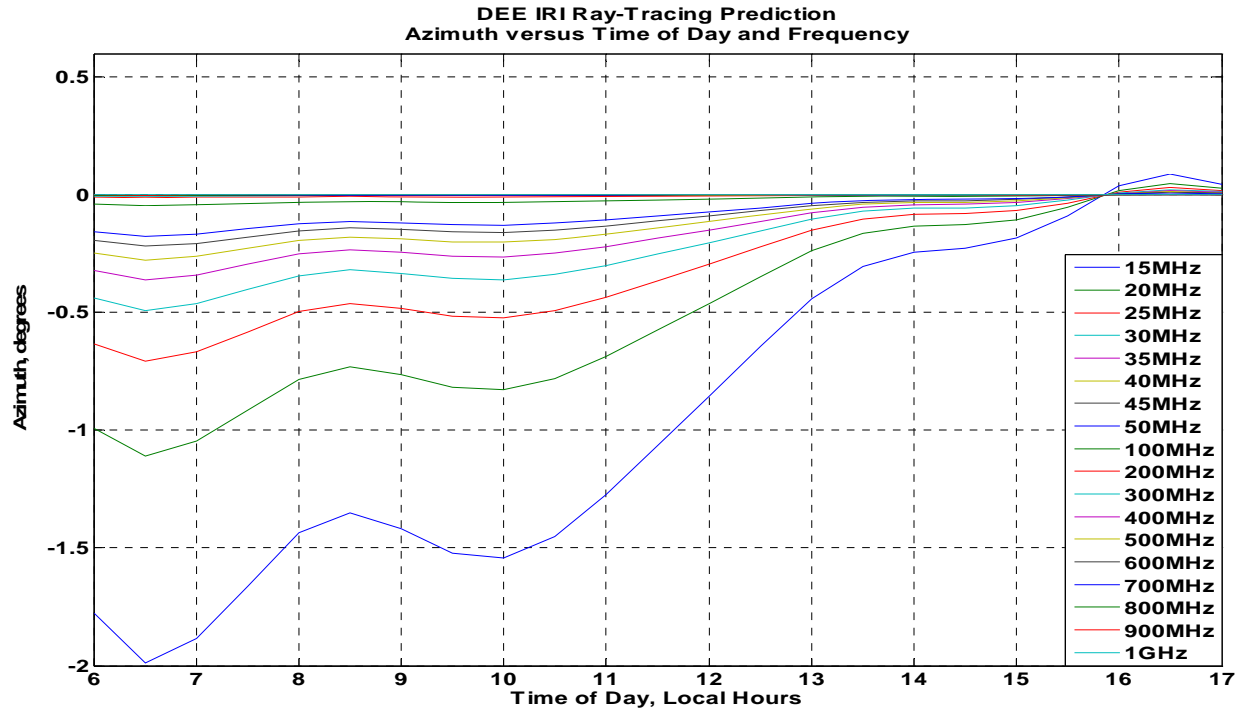


Figure 4.16 illustrates DEE IRI ray-tracing-predicted deviation of azimuth angle from LOS for signals from 15 MHz to 1 GHz, and every half hour from 0600 to 1700 PST on 1 Nov 04.

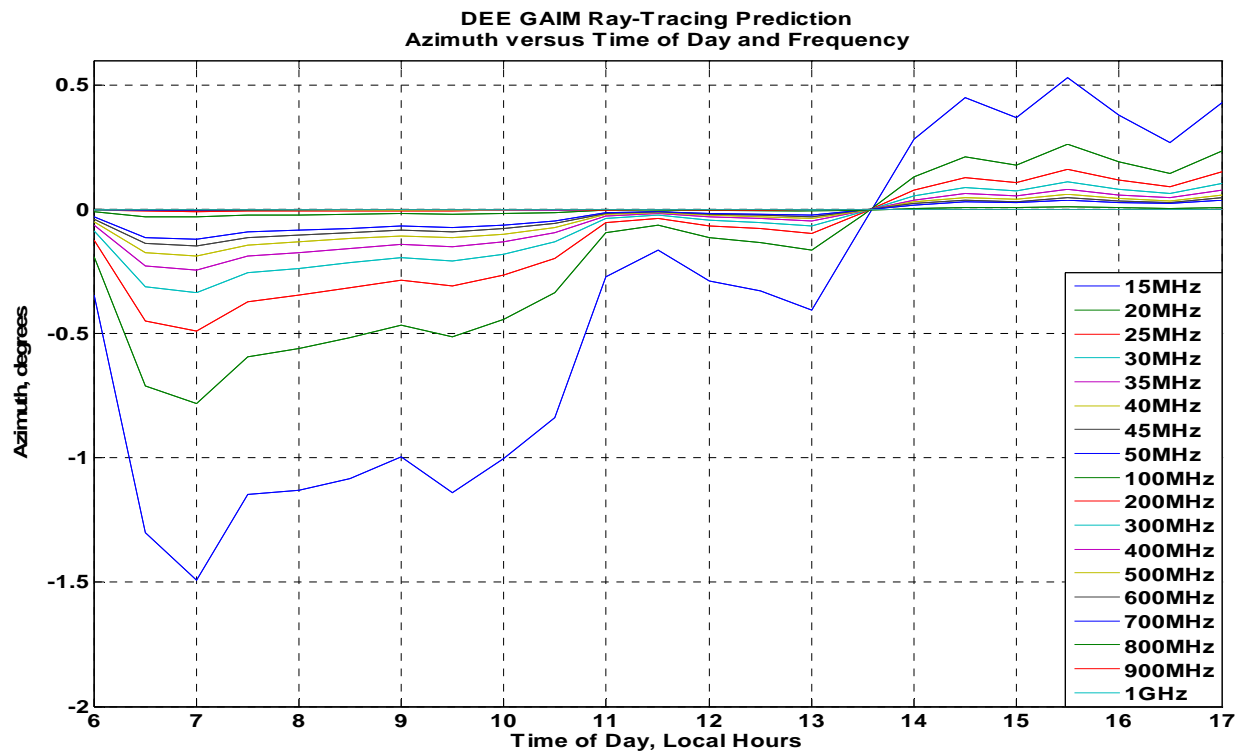


Figure 4.17 illustrates DEE GAIM ray-tracing-predicted deviation of azimuth angle from LOS for signals from 15 MHz to 1 GHz, and every half hour from 0600 to 1700 PST on 1 Nov 04.

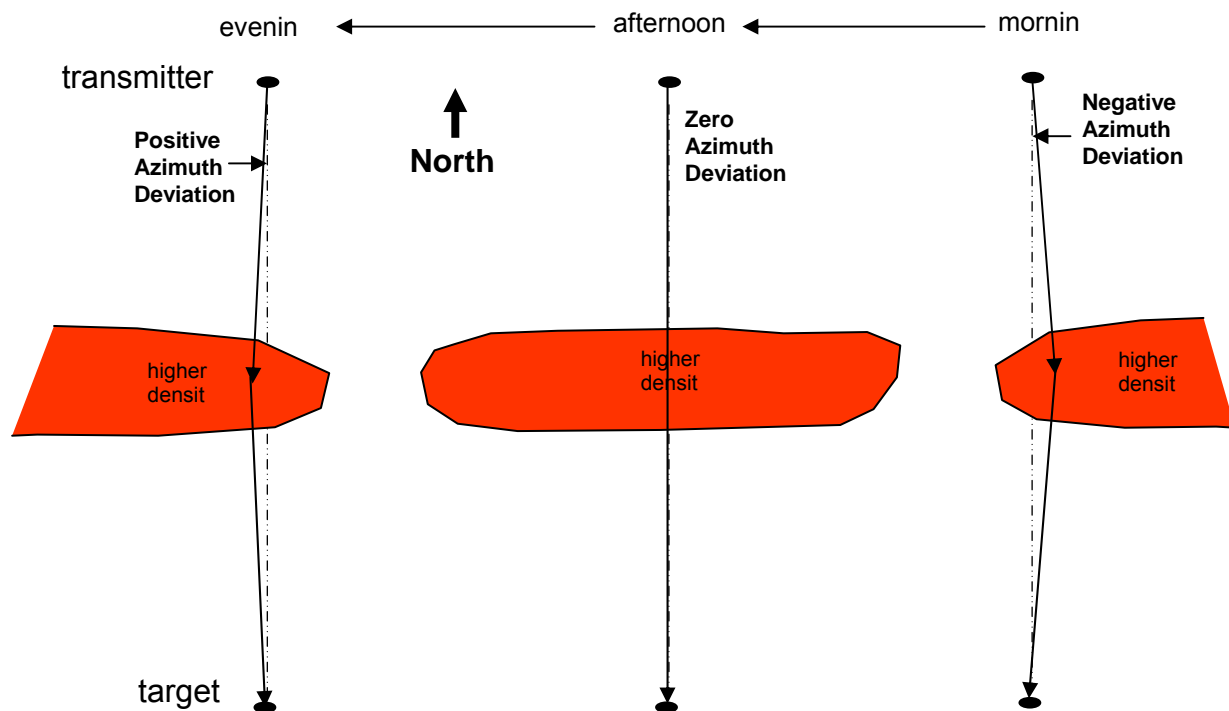


Figure 4.18 illustrates why the signal path azimuth deviation from LOS passes through the LOS azimuth (deviation passes through zero from negative to positive) as the ionospheric peak density (red) progresses from east to west over the course of the day. In order to maintain optimal communications between a transmitter and target receiver, the transmitter must aim into the higher density region to account for refraction of the signal.

## Signal Group Path

The length of signal propagation paths between the Galaxy 1R satellite and Goldstone are a function of the ionospheric index of refraction and TEC. The varying refractive index non-uniformly alters the phase velocity of signals causing their associated EM wavefront or phase group to change direction as it propagates through the medium. In effect, the signal phase group travels longer paths and takes more time to propagate between the transmitter and receiver than would be the case in free space, where the refractive index equals one. Additionally, equation 2.5 provides the approximate relationship between TEC and group path length. The difference between the free space path length and the actual signal path length is critical to applications that rely on signals to calculate distance to targets, such as various methods of DF and OTHR do for target coordinate registration.

Figures 4.19 and 4.20 illustrate the signal group path lengths predicted by ray tracing through DEE IRI and DEE GAIM respectively, as a function of frequency and Goldstone local time of day. Again, as seen in the angular deviation section, higher-frequency ray-tracing predictions are contained within the envelopes provided by the lower frequencies. Frequencies above approximately 100MHz again show almost no deviation from a minimum group path, which is the LOS, or free space path distance between the Goldstone and the Galaxy 1R, approximately equal to 37,394.029 km (determined by ray tracing through both models with a frequency of 1000 GHz). The most notable differences include the deviation of the DEE IRI ray-tracing-predicted ground path length from the LOS path length is typically on the order of hundreds of kilometers higher than the DEE GAIM ray-tracing-predicted group paths for

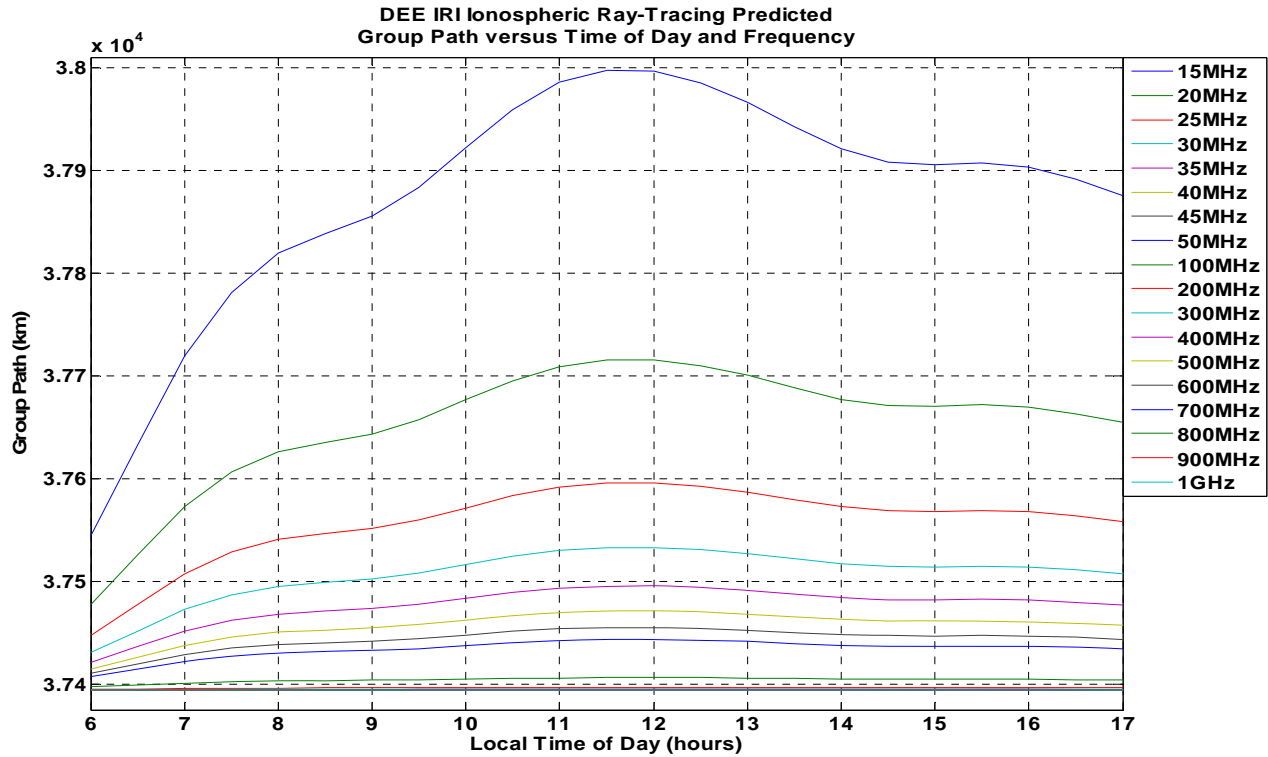


Figure 4.19 illustrates DEE IRI ray-tracing-predicted group path length for signals from 15 MHz to 1 GHz, and every half hour from 0600 to 1700 PST on 1 Nov 04.

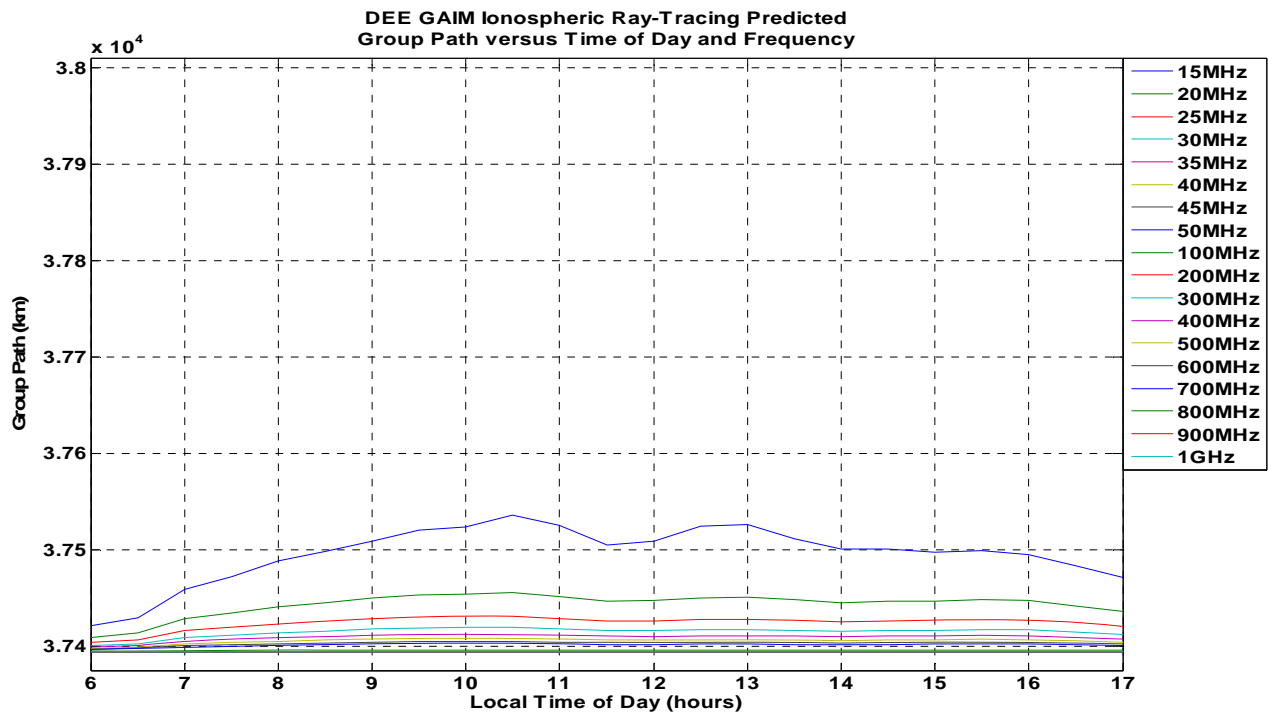


Figure 4.20 illustrates DEE GAIM ray-tracing-predicted group path length for signals from 15 MHz to 1 GHz, and every half hour from 0600 to 1700 PST on 1 Nov 04.

frequencies less than approximately 35MHz. Further, the DEE IRI result appears to have one true maximum while the DEE GAIM result displays a dual-peak structure over the course of the day. It is interesting to note that the peak group paths through each model arise hours before the time peak electron densities are expected to be over the ground site (1400 Local). The predicted peak group paths occur close to local noon. What makes this result even more unexpected is that the LOS, shown in figures 4.1-4.8, points to the southwest from the ground site up through the ionosphere. This would seem to suggest higher electron densities should not cause peak group paths until sometime after the expected 1400 peak overhead electron density time. This odd timing of peak group path lengths certainly demands future research, but is beyond the scope of this thesis. The next chapter summarizes and concludes the findings of this thesis. It will include suggested alternatives for future research to provide better insight into oddities such as the timing of the peak group path.

## V. Conclusion

### Summary

The results of this thesis provided basic insights into the predictions of transionospheric signal refraction and group paths obtained using ray-tracing theory interfacing with ionospheric model specifications. Of the primary two models compared, IRI is a well-established, climatological model considered by many in the international ionospheric community as the standard of ionospheric models, and USU GAIM is a data assimilation model just recently becoming operational through the Air Force Weather Agency for use by U.S. national defense activities. The Hausman-Nickisch updated Jones-Stephenson Ray-Tracing Algorithm was used to ray trace through un-extended IRI and GAIM ionospheric specifications, and to ray trace through the same specifications extended to above geosynchronous orbits using Fridman's diffusive equilibrium ionospheric model. The results included the following outputs from the two primary models and from ray tracing through the various ionospheric specifications:

- 1) Predicted total electron content ionospheric maps
- 2) Predictions of ionospheric signal refraction versus frequency versus signal launch angle
- 3) Predictions of ionospheric signal refraction leading to angular deviation from the line of sight to a target versus frequency and time of day
- 4) Predictions of signal group path length versus frequency and time of day

This thesis included ray-tracing predictions of ionospheric refraction and group delay effects on signals in the frequency range of 11 MHz to 1 GHz; the range in which applications such as OTHR, DF, HF, and SATCOMM depend on transionospheric signals. The results contained herein were intended to help users of applications such as the above to determine if ray-tracing predictions might assist them in reducing errors caused by ionospheric effects. Users may be able to compare errors they are seeing in their applications to the results shown in this thesis or they may wish to fund their own studies and provide “ground truth” data to compare to further ray-tracing predictions. These results might also help application users determine which ionospheric model, IRI or GAIM, might be more appropriate to their needs depending on which set of results more closely match any recorded signal angular deviations or path delays they are able to compare against. Additionally, these results provide insight into the frequencies for which there is a need to compensate for ionospheric refraction and path distortion; depending on the amount of error an application can tolerate, ionospheric affects on signals at frequencies above approximately 100 MHz are much less significant than the effects seen in signals whose frequencies are below 100 MHz. Finally, the results from this thesis certainly raise more than a few interesting questions for future research. Some of the questions raised and ideas for future research are discussed in the following, final section of this thesis: Future Research.



## **Future Research**

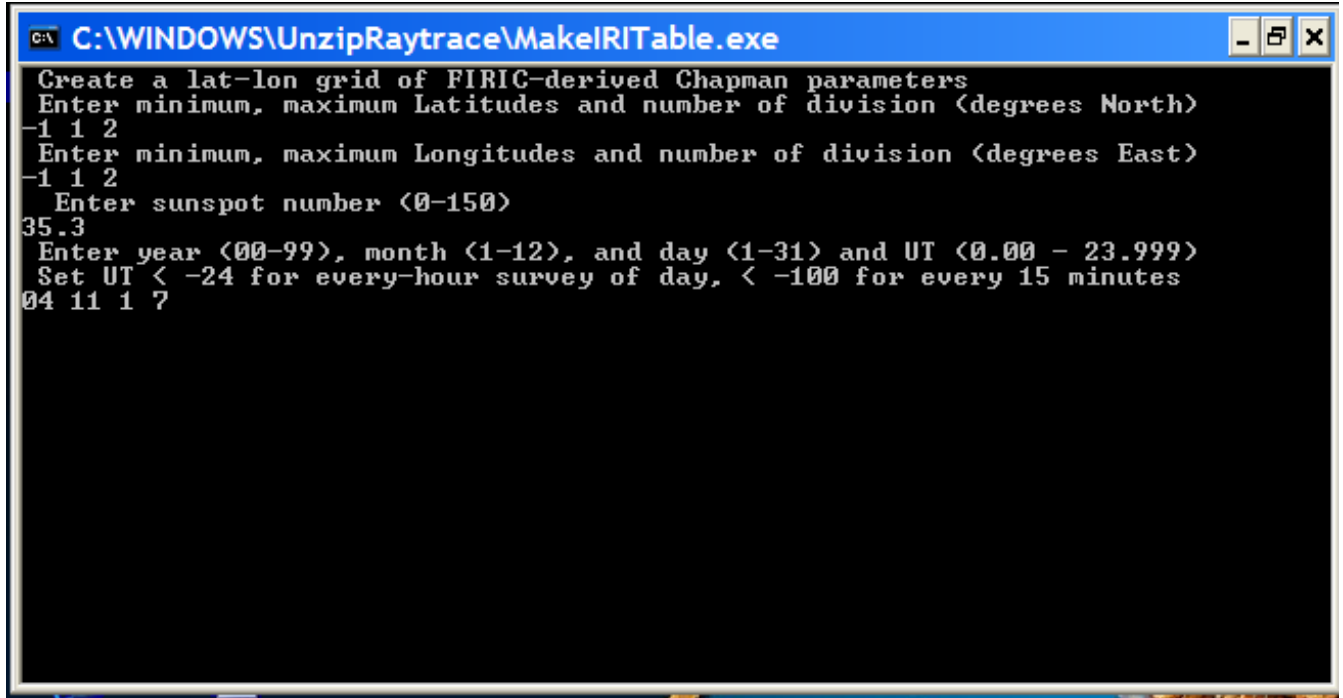
Some of the more interesting results and areas recommended for further research include:

- 1) Determining more accurate methods versus using a diffusive equilibrium model to extend ionospheric specifications to GEO from lower altitude models such as IRI and GAIM in order to provide better ray-tracing predictions to assist in optimizing applications such as SATCOMM. Appendix E discusses an attempt to extend GAIM specifications using an extrapolation method.
- 2) A study on why the elevation angle ray-tracing predictions through DEE IRI were so dissimilar from the predictions through DEE GAIM, while the azimuth predictions from the two models were much more similar.
- 3) A comparison study of IRI, USU GAIM, and other models' TEC map predictions (or other predictions from models) for a similar range of altitudes, which includes plots of the locations and types of measurements included in the GAIM and other model specifications.
- 4) A study of ionospheric model ray-tracing predictions signal refraction and group path delays over a longer period of time (days and nights), for varying season and/or solar cycle, or comparing geomagnetic storm-time predictions versus non-storm-time results.
- 5) A study on why the group path distortions seen included peak distortion hours before the expected time of peak ionospheric densities. This study could be accomplished beginning with the relationship between signal group path length and the TEC in the signal group path given in equation 2.5. The Hausman-Nickisch ray-tracing algorithm provides estimates of the signal path TEC. A good thesis topic would be a comparison of ray-tracing signal path TEC predictions versus TEC measured by GPS.

All of the future research ideas discussed here are graduate research opportunities and could be easily accomplished using the various process components already used in this thesis. Continuing research in this area has the potential to provide highly valuable results to the ionospheric community and to national defense activities. As the technology driving ionospheric modeling accuracy advances allowing for more accurate ray-tracing predictions of various ionospheric signal effects, applications such as OTHR, HF, DF, and SATCOMM could benefit by significant improvements to their operational accuracy. All that is needed is a voice to keep the effort moving forward by highlighting the results being achieved and by demonstrating the future potential ray-tracing through ionospheric models holds for critical national defense applications.

## Appendix A: IRI Model Specification Input and Output Example

MakeIRITable.exe provided by L. J. Nickisch and Mark A. Hausman; example of inputs used for creating Diffusive Equilibrium Extended (DEE) IRI specifications:



```
C:\WINDOWS\UnzipRaytrace\MakeIRITable.exe
Create a lat-lon grid of FIRIC-derived Chapman parameters
Enter minimum, maximum Latitudes and number of division (degrees North)
-1 1 2
Enter minimum, maximum Longitudes and number of division (degrees East)
-1 1 2
Enter sunspot number (0-150)
35.3
Enter year (00-99), month (1-12), and day (1-31) and UT (0.00 - 23.999)
Set UT < -24 for every-hour survey of day, < -100 for every 15 minutes
04 11 1 7
```

MakeIRITable.exe outputs a DEE IRI specification as a .TBL file that begins as follows, best viewed in Microsoft Wordpad:

```
221 nodes of altitudinal grid
 80.000  81.000  82.000  ... 36540.000
    3 nodes of latitudinal grid
-1.0000  0.0000  1.0000
    3 nodes of longitudinal grid
-1.0000  0.0000  1.0000
 0.1707  0.1746  0.1779  ...
```

The last line shown here are the plasma frequencies (MHz) corresponding to the first altitude, first latitude, and first three longitudes specified (alt = 80.000; Lat = -1.0000; Lon = -1.0000, 0.0000, 1.0000). This DEE IRI specification continues with one plasma frequency output per altitude, latitude, and longitude, taking up hundreds of pages. USU GAIM 2.1 specifications of electron density are also hundreds of pages long, but are output in a very different format than this IRI .TBL file. A MATLAB m-file (GAIM4mat\_xtend.m contained in Appendix B) was written to reformat the USU GAIM 2.1 specifications so they are in the same format (.TBL file and plasma frequencies) as the above DEE IRI specification, which is required for use by Nickisch-Hausman ray tracing algorithm. Additionally, the MATLAB file creates DEE GAIM specifications by combining the reformatted USU GAIM 2.1 specification with a scaled version of the high altitudes plasma frequencies from the DEE IRI specification for the same time, date, latitudes and longitudes.

## Appendix B: MATLAB m-Files

```
%%%%%%%%%%%%%%%%%%%%%%%%%%%%%%%%%%%%%%%%%%%%%%%%%%%%%%%%%%%%%%%%%%%%%%%% FullTECPlot.m %%%%%%%%%%
%%%%%%%%%%%%%%%%%%%%%%%%%%%%%%%%%%%%%%%%%%%%%%%%%%%%%%%%%%%%%%%%%%%%%%%%
%
% Title: FullTECPlot.m
% Description: Program to plot TEC maps from provided electron density
% grids, and a TEC difference map for an IRI TEC map vs a GAIM TEC map.
% Outputs: (file_name).TBL
% Authors: Dr. Mark A. Hausman and Lt Shayne Aune
% Organization/Office: AFIT/ENG
% Last Updated: 18 Feb 06
% IMPORTANT NOTES:
% (1) Requires another MATLAB script (I used a proprietary file
% owned by NorthWest Research Associates) to read in electron density grids
% (Negrids), altitudes, and latitudes and longitudes for the grid into
% the MATLAB workspace prior to being able to plot any desired TEC maps.
% (2) Requires geoshow toolbox for plots.
%
%%%%%%%%%%%%%%%%%%%%%%%%%%%%%%%%%%%%%%%%%%%%%%%%%%%%%%%%%%%%%%%%%%%%%%%%
% Create first TEC grid

% Find mean Ne between alt grid locations (cm^-3)
Nemean1 = (Negrid1(2:end,:) + Negrid1(1:end-1,:))/2;

dalt1 = (altgrid1(2:end) - altgrid1(1:end-1)); % altitude separation (km)
Nemean1 = reshape(Nemean1, naltgrid1-1, nlatgrid1*nlonggrid1);
TEC1 = (Nemean1 * dalt1) * 1.e5; % 1.e5 converts km to cm
TEC1 = reshape(TEC1, nlatgrid1, nlonggrid1)./(10^12);
% vertical in TEC units (10^16 electrons/m^-2)

% Create second TEC grid

% Repeat above process for second model density grid
Nemean2 = (Negrid2(2:end,:) + Negrid2(1:end-1,:))/2;
dalt2 = (altgrid2(2:end) - altgrid2(1:end-1));
Nemean2 = reshape(Nemean2, naltgrid2-1, nlatgrid2*nlonggrid2);
TEC2 = (Nemean2 * dalt2) * 1.e5;
TEC2 = reshape(TEC2, nlatgrid2, nlonggrid2)./(10^12);

%Plots

% Difference TEC Map
figure(1), imagesc(longgrid1-360, latgrid1, (TEC1-TEC2))
colorbar
hold on
grid on
load coast
```

```

geoshow(lat,long)
xlabel('Longitude, degrees','FontSize',16,'FontWeight','bold')
ylabel('Latitude, degrees','FontSize',16,'FontWeight','bold')
title({'Diffusive Equilibrium GAIM1 - GAIM2 TEC Difference'; '1 Nov 04, 1400
PST'},'FontSize',16,'FontWeight','bold')
set(gca,'FontSize',16,'FontWeight','bold')
set(gca,'YDir','normal')
xpts=[-116.88982; -133.0];
ypts=[35.424707; 0.0];
geoshow(ypts(1),xpts(1),'DisplayType','point','Marker','*','Color','w','MarkerSize',10)
geoshow(ypts(2),xpts(2),'DisplayType','point','Marker','*','Color','w','MarkerSize',10)
geoshow(ypts,xpts,'Color','w')

% First model TEC map
figure(2),imagesc(longrid1-360,latgrid1,TEC1)
colorbar
hold on
grid on
load coast
geoshow(lat,long)
xlabel('Longitude, degrees','FontSize',16,'FontWeight','bold')
ylabel('Latitude, degrees','FontSize',16,'FontWeight','bold')
title('Diffusive Equilibrium GAIM TEC, 1 Nov 04, 1400 PST','FontSize',16,'FontWeight','bold')
set(gca,'FontSize',16,'FontWeight','bold')
set(gca,'YDir','normal')
xpts=[-116.88982; -133.0];
ypts=[35.424707; 0.0];
geoshow(ypts(1),xpts(1),'DisplayType','point','Marker','*','Color','w','MarkerSize',10)
geoshow(ypts(2),xpts(2),'DisplayType','point','Marker','*','Color','w','MarkerSize',10)
geoshow(ypts,xpts,'Color','w')

% Second model TEC map
figure(3),imagesc(longrid1-360,latgrid1,TEC2)
colorbar
hold on
grid on
load coast
geoshow(lat,long)
xlabel('Longitude, degrees','FontSize',16,'FontWeight','bold')
ylabel('Latitude, degrees','FontSize',16,'FontWeight','bold')
title('Extrapolated GAIM TEC, 1 Nov 04, 1400 PST','FontSize',16,'FontWeight','bold')
set(gca,'FontSize',16,'FontWeight','bold')
set(gca,'YDir','normal')
xpts=[-116.88982; -133.0];
ypts=[35.424707; 0.0];
geoshow(ypts(1),xpts(1),'DisplayType','point','Marker','*','Color','w','MarkerSize',10)
geoshow(ypts(2),xpts(2),'DisplayType','point','Marker','*','Color','w','MarkerSize',10)
geoshow(ypts,xpts,'Color','w')

%%%%%%%%%%%%%%%%%%%%%%%%%%%%%%%%%%%%%%%%%%%%%%%%%%%%%%%%%%%%%%%%%%%%%%%%
%%%%%%%%%%%%%%%%%%%%%%%%%%%%%%%%%%%%%%%%%%%%%%%%%%%%%%%%%%%%%%%%%%%%%%%% End of FullTECPlot.m %%%%%%%%%%%%%%%%%%%%%%%%%%%%%%%%%%%%%%%%%%%%%%%%%%%%%%%%%%%%%%%%%%%%%%%%%
%%%%%%%%%%%%%%%%%%%%%%%%%%%%%%%%%%%%%%%%%%%%%%%%%%%%%%%%%%%%%%%%%%%%%%%%

```

```

%%%%%%%%%%%%%%%%%%%%%%%%%%%%%%%%%%%%%%%%%%%%%%%%%%%%%%%%%%%%%%%%%%%%%%%% GAIM4mat_xtend.m %%%%%%%%%%%%%%%%%%%%%%%%%%%%%%%%%%%%%%%%%%%%%%%%%%%%%%%%%%%%%%%%%%%%%%%%%
%%%%%%%%%%%%%%%%%%%%%%%%%%%%%%%%%%%%%%%%%%%%%%%%%%%%%%%%%%%%%%%%%%%%%%%%
function gaim_table = GAIM4mat_xtend(GAIM_file, IRI_file, new_GAIM)
%%%%%%%%%%%%%%%%%%%%%%%%%%%%%%%%%%%%%%%%%%%%%%%%%%%%%%%%%%%%%%%%%%%%%%%%
%
% Title: GAIM4mat_xtend.m
% Description: Reformat GAIM netcdf file to .tbl file in format required
% for raytrace and extend using IRI based diffusive equilibrium model
% Inputs: GAIM_file and IRI_file are the file paths and new_GAIM is the
% desired output file name
% Outputs: (file_name).TBL
% Authors: Lt Col Matthew Goda and Lt Shayne Aune
% Organization/Office: AFIT/ENG
% Last Updated: 18 Feb 06
% Notes: Requires GAIM ionospheric model as a .nc file and MATLAB netCDF toolbox.
%
%%%%%%%%%%%%%%%%%%%%%%%%%%%%%%%%%%%%%%%%%%%%%%%%%%%%%%%%%%%%%%%%%%%%%%%%
%%%%%%%%%%%%%%%%%%%%%%%%%%%%%%%%%%%%%%%%%%%%%%%%%%%%%%%%%%%%%%%%%%%%%%%%

% Read in IRI extension Diffusive Equilibrium data
disp('Read Diffusive Equilibrium Extension')
% IRI_file = 'IRI3dLL_25Oct04-1400.TBL';
fid=fopen(IRI_file);
d=fscanf(fid,'%c');
fclose(fid);

% Set data for inclusion in .TBL file
DE_alt=str2num(d(1251:2250));
indx = 1;
DE_EC = zeros(720,100);
for i = 4088:999+1213:length(d),
    EC=str2num(d(i:i+999));
    DE_EC(indx,:)=EC;
    indx = indx+1;
end

% Extract GAIM data using MATLAB netCDF toolbox
disp('Read GAIM netCDF file')
% GAIM_file = 'GMF20042991400.NC';
gaim = netcdf(GAIM_file);
alt = gaim{'Altitudes'};
lat = gaim{'Latitudes'};
lon = gaim{'Longitudes'};
den = gaim{'Edensity'};
alts = alt(:);
alt2 = [alts' DE_alt];
lats = lat(:);
lons = lon(:);
dens = den(:);
dens = sqrt(dens).*8.9785282*10^-3;

% Assemble GAIM into 2D matrix
plsm = [];

```

```

for indx1 = 1:length(lons)
    tmp(1:length(lats),1:length(alts)) = dens(indx1,:,:), %lon/lat/alt;
    plsm = [plsm; tmp];
end

% Scale Upper Ionospheric Specification
for i = 1:720,
    DE_EC(i,:) = DE_EC(i,:).*plsm(i,83)./DE_EC(i,1);
end

plasmaF = [plsm DE_EC];

% Write GAIM data to .TBL file for raytracing algorithm
% NOTE: The following format is required for input to raytracing!

disp('Write new GAIM file')

alt_str = [num2str(length(alt2)) 'alts'];
lat_str = [num2str(length(lats)) 'lats'];
lon_str = [num2str(length(lons)) 'lons'];

% new_GAIM = 'GAIM_25Oct1400';
file_out = '.TBL';
fid2=fopen([new_GAIM file_out], 'w');
fprintf(fid2, '%12d nodes of altitudinal grid \n', length(alt2));
fprintf(fid2, '%10.3f', alt2);
fprintf(fid2, '\n');
fprintf(fid2, '%12d nodes of latitudinal grid \n', length(lats));
fprintf(fid2, '%10.4f', lats);
fprintf(fid2, '\n');
fprintf(fid2, '%12d nodes of longitudinal grid \n', length(lons));
fprintf(fid2, '%10.4f', lons);
fprintf(fid2, '\n');
for indx2 = 1:720,
    fprintf(fid2, '%10.4f', plasmaF(indx2,:));
    fprintf(fid2, '\n');
end
fprintf(fid2, '\n');

fclose(fid2);

return

%%%%%%%%%%%%%%%%%%%%%%%%%%%%%%%%%%%%%%%%%%%%%%%%%%%%%%%%%%%%%%%%%%%%%%%%
%%%%%%%%%%%%%%%%%%%%%%%%%%%%%%%%%%%%%%%%%%%%%%%%%%%%%%%%%%%%%%%%%%%%%%%%
%%%%%%%%%%%%%%%%%%%%%%%%%%%%%%%%%%%%%%%%%%%%%%%%%%%%%%%%%%%%%%%%%%%%%%%% End of GAIM4mat_xtend.m %%%%%%%%%
%%%%%%%%%%%%%%%%%%%%%%%%%%%%%%%%%%%%%%%%%%%%%%%%%%%%%%%%%%%%%%%%%%%%%%%%

```

```

%%%%%%%%%%%%%%%%%%%%%%%%%%%%%%%%%%%%%%%%%%%%%%%%%%%%%%%%%%%%%%%%%%%%%%%% RayOutput.m %%%%%%%%%%%%%%%%%%%%%%%%%%%%%%%%%%%%%%%%%%%%%%%%%%%%%%%%%%%%%%%%%%%%%%%%%
%%%%%%%%%%%%%%%%%%%%%%%%%%%%%%%%%%%%%%%%%%%%%%%%%%%%%%%%%%%%%%%%%%%%%%%%
%
% Title: RayOutput.m
% Description: Program to get data from several raytracing .OUT files using the
% RaytraceOut function and plot desired results.
% Author: Lt Shayne Aune
% Organization/Office: AFIT/ENG
% Date Last Updated: 18 Feb 06
%
%%%%%%%%%%%%%%%%%%%%%%%%%%%%%%%%%%%%%%%%%%%%%%%%%%%%%%%%%%%%%%%%%%%%%%%%
%%%%%%%%%%%%%%%%%%%%%%%%%%%%%%%%%%%%%%%%%%%%%%%%%%%%%%%%%%%%%%%%%%%%%%%%

clear;

% Specify file path(s) to be concatenated with file path in function RaytraceOut.m

filea(1,:) = 'IRI\Time_of_Day\1400_15_50.out';
filea(2,:) = 'IRI\Time_of_Day\1430_15_50.out';

fileb(1,:) = 'IRI\Time_of_Day\1400_100_1000.out';
fileb(2,:) = 'IRI\Time_of_Day\1430_100_1000.out';

% Get data from files

Data = [];

for i = 1:2,
    Data = [Data RaytraceOut(filea(i,:))];
    Data = [Data RaytraceOut(fileb(i,:))];
end

% Calculations and Plots

c = 299792.458; % Speed of free space signal propagation in km/sec
TruRng = 37394.029; % Range in km estimated by raytracing 1000 GHz signal
TruAzi = -153.513186; % Azimuth in degrees estimated by raytracing 1000 GHz signal
TruElev = 45.439650; % Elevation in degrees estimated by raytracing 1000 GHz signal

% Get Time of Day Data
Times = Data(1,:)-800;

% Get Frequencies
Freqs = Data(2,:);

% Create Group Path Surface
for i = 1:2
    GP(i,:) = Data(5,18*i-17:18*i);
end

% Calculate group delays
Delays = (GP-TruRng)/c;

```



```
% Plot 3D Delays versus Frequency versus Time of Day
```

```
surf(Freqs,Times',Delays)
```

```
hold on
```

```
grid on
```

```
xlabel('Frequency, MHz')
```

```
ylabel('Time of Day, Local Hours')
```

```
zlabel('Delays, seconds')
```

```
title({'IRI Predicted'; 'Ionospheric Signal Delays versus Time of Day and Frequency'})
```

```
%%%%%%%%%%  
%%%%%%%%%  
%%%%%%%%% End of RayOutput.m %%%%%%%%%%
```

```

%%%%%%%%%%%%%%%%%%%%%%%%%%%%%%%%%%%%%%%%%%%%%%%%%%%%%%%%%%%%%%%%%%%%%%%% RaytraceOut.m %%%%%%%%%
%%%%%%%%%%%%%%%%%%%%%%%%%%%%%%%%%%%%%%%%%%%%%%%%%%%%%%%%%%%%%%%%%%%%%%%%
function data_out = RaytraceOut(file_str)
%%%%%%%%%%%%%%%%%%%%%%%%%%%%%%%%%%%%%%%%%%%%%%%%%%%%%%%%%%%%%%%%%%%%%%%%
%
% Title: RaytraceOut.m
% Description: Function to read time, frequency, azimuth, elevation, Group
% Path, Geometric Path, and LOG TEC from ray tracing .OUT file.
% Authors: Lt Col Matthew Goda and Lt Shayne Aune
% Organization/Office: AFIT/ENG
% Last Updated: 22 Jan 06
% Note: This file specifically reads outputs from the Nickisch-Hausman
% ray-tracing algorithm and is unlikely to be compatible with any other
% .OUT files. Additionally, it depends on the type of ray tracing being done,
% i.e. this program may not work for non-homing ray trace output files.
%
%%%%%%%%%%%%%%%%%%%%%%%%%%%%%%%%%%%%%%%%%%%%%%%%%%%%%%%%%%%%%%%%%%%%%%%%
%%%%%%%%%%%%%%%%%%%%%%%%%%%%%%%%%%%%%%%%%%%%%%%%%%%%%%%%%%%%%%%%%%%%%%%%

disp('Read Raytrace Output File')

% Open Output File
path_dir = 'C:\WINDOWS\UnzipRaytrace\Results\';
file_str = 'IRI\Baseline5\Baseline5_11_15.out';
fid=fopen([path_dir file_str]);

% Read Data
d = fscanf(fid, '%c');
fclose(fid);

% Find and return Time, Frequency, Azimuth, Elevation, Group Path, Geometric Path
indx = 1;

tt = strfind(d, '@IRI3dLL_');
tim = str2num(d(tt+17:tt+21));
if tim<0200,
    tim = tim+2400;
end

k = strfind(d, '*** USING HOMER: RAY HOMING ALGORITHM ***');
k(end+1)=length(d);
data_out = zeros(7,length(k)-1);
for ii = 2:length(k)

    rng = k(ii-1):k(ii);

    d2 = d(rng);
    k2 = strfind(d2, 'ITERATION');
    klast = k2(length(k2));
    d3 = d2(klast:end);
    frqf = strfind(d3, 'FREQUENCY =');
    freq = str2num(d3(frqf+12:frqf+18));
    flg = strfind(d3, 'PENETRATION FAILURE:');

```

```

bad = length(flag); % There is no output if penetration failure occurs
flag2 = strfind(d3,'Off Grid');
bad2 = length(flag2);

if(bad2)
    disp('OFF GRID')
end

if (bad)
    az = NaN;
    elev = NaN;
    gpPath = inf;
    gePath = inf;
    LOGTEC = NaN;
else
    az = str2num(d3(freq+61:freq+71));
    elef = strfind(d3,'ELEVATION ANGLE OF TRANSMISSION =');
    elev = str2num(d3(elef+35:elef+45));
    pathf = strfind(d3,'RCVR');
    gpPath = str2num(d3(pathf+81:pathf+90));
    gePath = str2num(d3(pathf+101:pathf+110));
    LOGTEC = str2num(d3(pathf+113:pathf+120));
end

data_out(:,indx) = [tim freq az elev gpPath gePath LOGTEC]';
indx = indx+1;

end

return
%%%%%%%%%%%%%%%%%%%%%%%%%%%%%%%%%%%%%%%%%%%%%%%%%%%%%%%%%%%%%%%%%%%%%%%%
%%%%%%%%%%%%%%%%%%%%%%%%%%%%%%%%%%%%%%%%%%%%%%%%%%%%%%%%%%%%%%%%%%%%%%%%
%%%%%%%%%%%%%%%%%%%%%%%%%%%%%%%%%%%%%%%%%%%%%%%%%%%%%%%%%%%%%%%%%%%%%%%% End of RaytraceOut.m %%%%%%%%%
%%%%%%%%%%%%%%%%%%%%%%%%%%%%%%%%%%%%%%%%%%%%%%%%%%%%%%%%%%%%%%%%%%%%%%%%

```

## Appendix C: Nickisch-Hausman Ray Tracing Algorithm Input and Output Examples

Example Input .DAT File for Nickisch-Hausman Ray Tracing Algorithm:

```
'AHWFNC' 'T3DLLLOG' 'NOELECT1' 'HARMONY' 'NOCOLFRZ'
!-----
Homing Rays of a 11-14 MHz / Description of ray trace
1          1 / ORDINARY RAY
4          35.424707 'DEG' / NORTH GEOGRAPHIC LATITUDE OF TRANSMITTER
5          -116.88982 'DEG' / EAST GEOGRAPHIC LONGITUDE OF TRANSMITTER
7          11.0 / INITIAL FREQUENCY (MHZ)
8          14.0 / FINAL FREQUENCY (MHZ)
9          1.0 / STEP IN FREQUENCY (MHZ)
11         207.0 'DEG' / INITIAL AZIMUTH ANGLE
12         207.0 'DEG' / FINAL AZIMUTH ANGLE
13          0. 'DEG' / STEP IN AZIMUTH ANGLE
15         15. 'DEG' / INITIAL ELEVATION ANGLE
16         15. 'DEG' / FINAL ELEVATION ANGLE
17          0. 'DEG' / STEP IN ELEVATION ANGLE
19          0. / 3=HOMER one freq, 7=HOMER multiple freq
20         35800. / Receiver altitude (km)
22          1 / NUMBER OF HOPS
23          1.E4 / MAXIMUM NUMBER OF STEPS PER HOP
24         89.9999 'DEG' / LATITUDE OF GEOMAGNETIC POLE (RAD)
25          0.00 'DEG' / LONGITUDE OF GEOMAGNETIC POLE (RAD)
26          1 / Number of ground reflections
29          1 / STOPRAY (use STOPCHK routine)
30         50000. / Stop at group path of 50000 km
42          1.E-9 / MAXIMUM RELATIVE SINGLE STEP ERROR
45         100. / MAXIMUM INTEGRATION STEP LENGTH (KM)
57          2. / PHASE PATH ! =1 TO INTEGRATE
60          2. / PATH LENGTH ! =2 TO INTEGRATE AND PRINT
62          2. / TEC
63          1. / TEC**2
71          0 / NUMBER OF STEPS BETWEEN PERIODIC PRINTOUTS
72          1 / GENERATE PUNCHED OUTPUT FILE
81          5 / PLOT FLAG
83         -52. 'DEG' / LATITUDE OF BOTTOM EDGE OF PLOT
84        -205. 'DEG' / LONGITUDE OF LEFT EDGE OF PLOT
85          72. 'DEG' / LATITUDE OF TOP EDGE OF PLOT
86         -27. 'DEG' / LONGITUDE OF RIGHT EDGE OF PLOT
100         1 / READ TABLEX DATA
320         0. / POWER FLAG (1 = on, REQUIRED for ray homing)
321         1. / Do not use REACH
330         0.0 / Latitude for HOMING
331        -133. / Longitude for HOMING
332         0.001 / Accuracy
// / End of input parameters
!*****
@IRI3dLL_01Nov04-2200.tbl / The .TBL model specification file used for trace
!-----
```

# Example Output .OUT File from Nickisch-Hausman Ray Tracing Algorithm:

C:\WINDOWS\UnzipRaytrace\fort.9

```
'AHWFNC' 'T3DLLLOG' 'NOELECT1' 'HARMONY' 'NOCOLFRZ'
!-----
Rays of a varying frequency
1      1      / ORDINARY RAY
4      35.424707 'DEG' / NORTH GEOGRAPHIC LATITUDE OF TRANSMITTER
5      -116.88982 'DEG' / EAST GEOGRAPHIC LONGITUDE OF TRANSMITTER
7      11.0      / INITIAL FREQUENCY (MHZ)
8      14.0      / FINAL FREQUENCY (MHZ)
9      1.0      / STEP IN FREQUENCY (MHZ)
11     207.0     'DEG' / INITIAL AZIMUTH ANGLE
12     207.0     'DEG' / FINAL AZIMUTH ANGLE
13     0.        'DEG' / STEP IN AZIMUTH ANGLE
15     15.       'DEG' / INITIAL ELEVATION ANGLE
16     15.       'DEG' / FINAL ELEVATION ANGLE
17     0.        'DEG' / STEP IN ELEVATION ANGLE
19     0.        / 3=HOMER at one freq, 7=HOMER at multipl
20     35800.    / receiver altitude (km)
22     1         / NUMBER OF HOPS
23     1.E4      / MAXIMUM NUMBER OF STEPS PER HOP
24     89.9999   'DEG' / LATITUDE OF GEOMAGNETIC POLE (RAD) (use
25     0.00      'DEG' / LONGITUDE OF GEOMAGNETIC POLE (RAD)
26     1         / number of ground reflections
29     1         / STOPRAY (use STOPCHK routine)
30     50000.    / Stop at group path of 5000 km
42     1.E-9     / MAXIMUM RELATIVE SINGLE STEP ERROR
45     100.      / MAXIMUM INTEGRATION STEP LENGTH (KM)
57     2.        / PHASE PATH ! =1 TO INTEGRATE
60     2.        / PATH LENGTH ! =2 TO INTEGRATE
62     2.        / TEC !
63     1.        / TEC**2 !
71     0         / NUMBER OF STEPS BETWEEN PERIODIC PRINTOUTS
72     1         / GENERATE PUNCHED OUTPUT FILE
81     5         / PLOT FLAG
83     -52.      'DEG' / LATITUDE OF BOTTOM EDGE OF PLOT
84     -205.     'DEG' / LONGITUDE OF LEFT EDGE OF PLOT
85     72.       'DEG' / LATITUDE OF TOP EDGE OF PLOT
86     -27.      'DEG' / LONGITUDE OF RIGHT EDGE OF PLOT
100    1         / READ TABLEX DATA
320    0.        / POWER FLAG (1 to turn on - REQUIRED for
321    1.        / do not use REACH
330    0.0       /
331    -133.     /
332    0.001     /
//
!*****
@IRI3dLL_01Nov04-2200.tbl
*      221 nodes of altitudinal grid
*      80.000    81.000    82.000    83.000    84.000    85.000    86.000
```

```

*          30 nodes of latitudinal grid
*   -52.8333 -48.5000 -44.1666 -39.8333 -35.5000 -31.1666 -26.8333
*          24 nodes of longitudinal grid
*   157.7500 165.2500 172.7500 180.2500 187.7500 195.2500 202.7500
*    0.2156  0.2211  0.2271  0.2383  0.2618  0.3086  0.3975
File too long to echo every line...
!-----
1Rays of a varying frequency launched at approximately 45 degrees
T3DLLLOG NOELECT1 HARMONY NOCOLFRZ APPLETON-HARTREE FORMULA ORDINARY
02/07/ 6
NO COLLISIONS

INITIAL VALUES FOR THE W ARRAY -- ALL ANGLES IN RADIANS, ONLY NONZERO VALUES PRINTED

1  1.000000000000E+00
2  6.371200000000E+03
4  6.18277773704E-01
5 -2.04011222106E+00
7  1.100000000000E+01
8  1.400000000000E+01
9  1.000000000000E+00
11 3.61283155163E+00
12 3.61283155163E+00
15 2.61799387799E-01
16 2.61799387799E-01
20 1.000000000000E+03
22 1.000000000000E+00
23 1.000000000000E+04
24 1.57079458147E+00
26 1.000000000000E+00
29 1.000000000000E+00
30 5.000000000000E+04
41 3.000000000000E+00
42 1.000000000000E-09
43 5.000000000000E+01
44 1.000000000000E+00
45 1.000000000000E+02
46 1.000000000000E-08
47 5.000000000000E-01
48 1.000000000000E+02
57 2.000000000000E+00
60 2.000000000000E+00
62 2.000000000000E+00
63 1.000000000000E+00
71 1.000000000000E+04
72 -1.000000000000E+00
81 5.000000000000E+00
83 -9.07571211037E-01
84 -3.57792496659E+00
85 1.25663706144E+00
86 -4.71238898038E-01
100 1.000000000000E+00
321 1.000000000000E+00
331 -1.330000000000E+02
332 1.000000000000E-03
Beginning one-time computation of SJ coefficients

```

Finished computation of SJ coefficients

1	0	1	2	3	4	5	6
	G	G	G	G	G	G	G
	N	N	N	N	N	N	N
	0.000000	0.000000	0.000000	0.000000	0.000000	0.000000	0.000000
	0.296194	0.017282	0.000000	0.000000	0.000000	0.000000	0.000000
	0.034016	-0.053146	-0.014470	0.000000	0.000000	0.000000	0.000000
	-0.033490	0.070055	-0.024247	-0.005649	0.000000	0.000000	0.000000
	-0.040788	-0.043541	-0.009783	0.008429	-0.000823	0.000000	0.000000
	0.017231	-0.035725	-0.017084	0.006137	0.003740	0.000091	0.000000
	-0.010438	-0.012892	-0.011089	0.016030	0.000322	-0.000393	0.000607

	0	1	2	3	4	5	6
	H	H	H	H	H	H	H
	N	N	N	N	N	N	N
	0.000000	0.000000	0.000000	0.000000	0.000000	0.000000	0.000000
	0.000000	-0.051861	0.000000	0.000000	0.000000	0.000000	0.000000
	0.000000	0.042983	0.003966	0.000000	0.000000	0.000000	0.000000
	0.000000	0.006969	-0.005682	0.003882	0.000000	0.000000	0.000000
	0.000000	-0.015086	0.009075	-0.002506	0.002247	0.000000	0.000000
	0.000000	-0.004453	-0.013211	0.006264	0.000872	-0.000746	0.000000
	0.000000	0.003289	-0.009519	-0.006486	0.003340	-0.000016	-0.000294

1Rays of a varying frequency launched at approximately 45 degrees

02/07/ 6

T3DLLLOG NOELECT1 HARMONY NOCOLFRZ

APPLETON-HARTREE FORMULA ORDINARY

NO COLLISIONS

FREQUENCY = 11.000000 MHZ, AZIMUTH ANGLE OF TRANSMISSION = 207.000000 DEG  
ELEVATION ANGLE OF TRANSMISSION = 15.000000 DEG

	HEIGHT KM	RANGE KM	AZIMUTH DEVIATION		ELEVATION		POLARIZATION		GROUP KM	PATH KM	PHAS KM	PATH KM	GEOM KM	PATH KM	LOG TEC CM-2
			XMTR DEG	LOCAL DEG	XMTR DEG	LOCAL DEG	REAL	IMAG							
-2.E-16 XMTR	0.0000	0.0000				15.000	0.000	-0.951	0.000	0.000	0.000	0.000	0.000	-10.000	

#### Appendix D: Variable DEE IRI Grid-Spacing Effects on Ray-Tracing Predictions

Due to the use of USU GAIM in this thesis, the grid spacing used was 30 latitude divisions by 24 longitude divisions over the area during the day of interest, 1 Nov 04. USU GAIM version 2.1 does not allow for varying the number of grid divisions in order to ensure the model's stability. To determine if grid spacing might have significant impacts on ray-tracing results, the following plots were accomplished by ray tracing through variable DEE IRI grid spacing. The DEE IRI grid spacings used are:

- 1) IRI 1 = 130 lat x 180 lon
- 2) IRI 2 = 65 lat x 60 lon
- 3) IRI 3 = 65 lat x 90 lon
- 4) IRI 4 = 260 lat x 360 lon
- 5) IRI 5 = 30 lat x 24 lon (the one used throughout this thesis)

These grids were generated by the DEE IRI specification executable file provided as part of the ray-tracing algorithm by Hausman and Nickisch. The ray tracing results are for the line of sight between the Goldstone ground station and the Galaxy 1R geosynchronous satellite on 1 Nov 04 at 1200 PST.

The resulting figures, D.1-D.3, show variable grid spacing impacts ray-tracing predictions of signal azimuth and elevation, and signal group path delay. Further study is recommended to determine the extent of the impact and whether or not a recommendation should be made to USU GAIM's creators to include the ability to specify USU GAIM's output specification grid spacing in future versions.

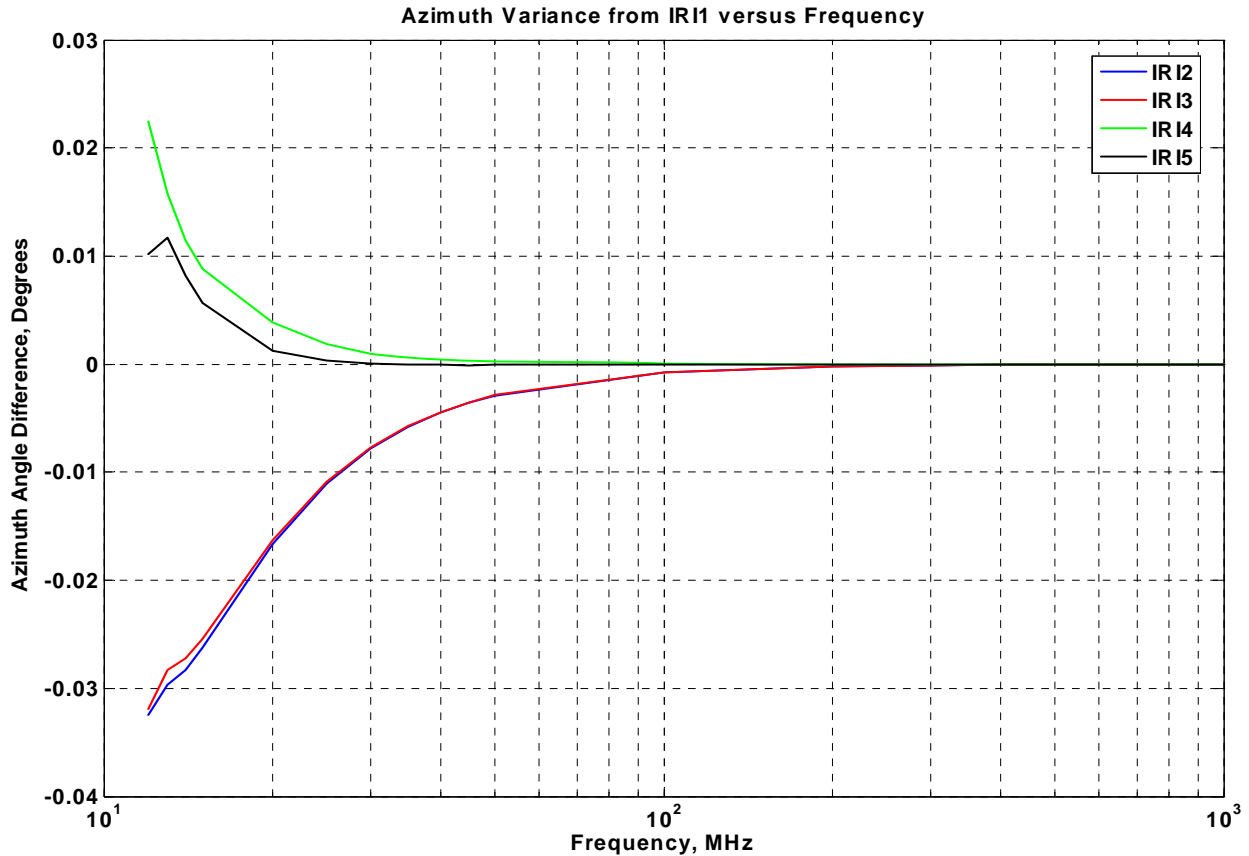


Figure D.1 shows the ray-tracing predicted azimuth variance from IRI 1 versus frequency due to varying grid spacing in DEE IRI specifications. The grid spacings used are as follows: IRI 1 = 130 lat x 180 lon, IRI 2 = 65 lat x 60 lon, IRI 3 = 65 lat x 90 lon, IRI 4 = 260 lat x 360 lon, IRI 5 = 30 lat x 24 lon.



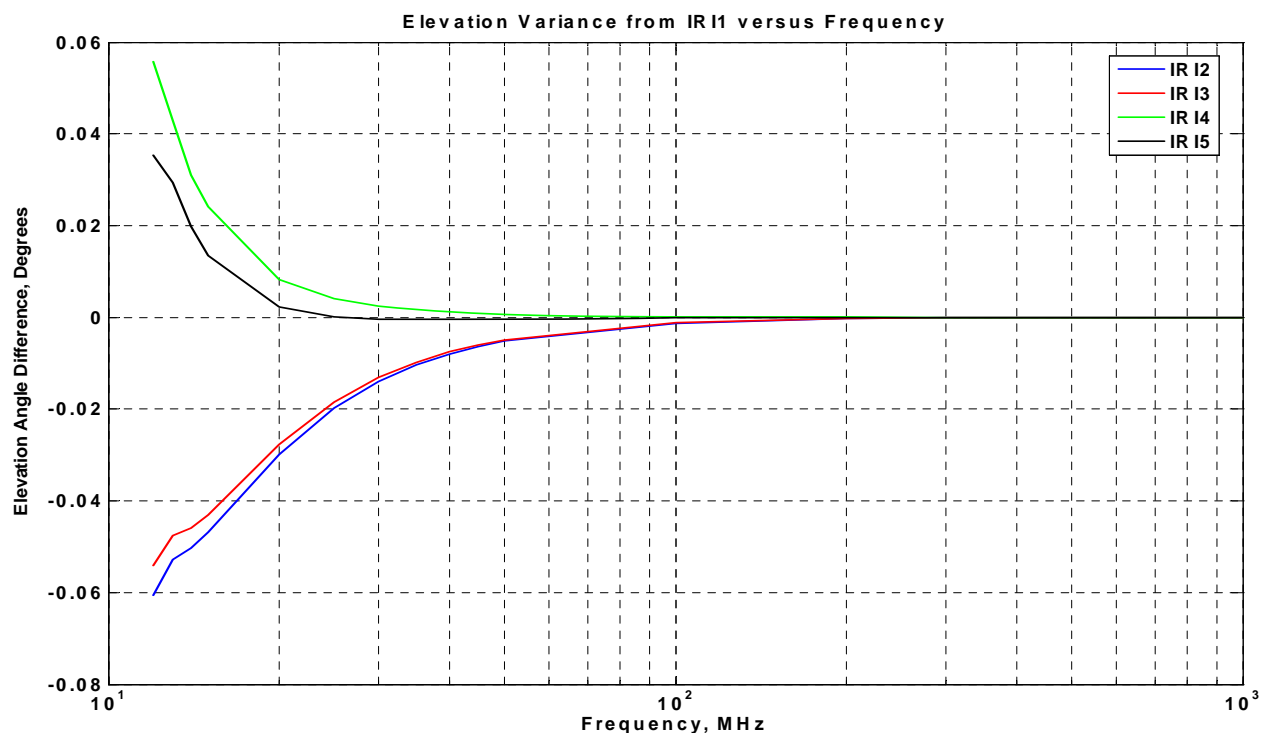


Figure D.2 shows the ray-tracing predicted elevation variance from IRI 1 versus frequency due to varying grid spacing in DEE IRI specifications. The grid spacings used are as follows: IRI 1 = 130 lat x 180 lon, IRI 2 = 65 lat x 60 lon, IRI 3 = 65 lat x 90 lon, IRI 4 = 260 lat x 360 lon, IRI 5 = 30 lat x 24 lon.

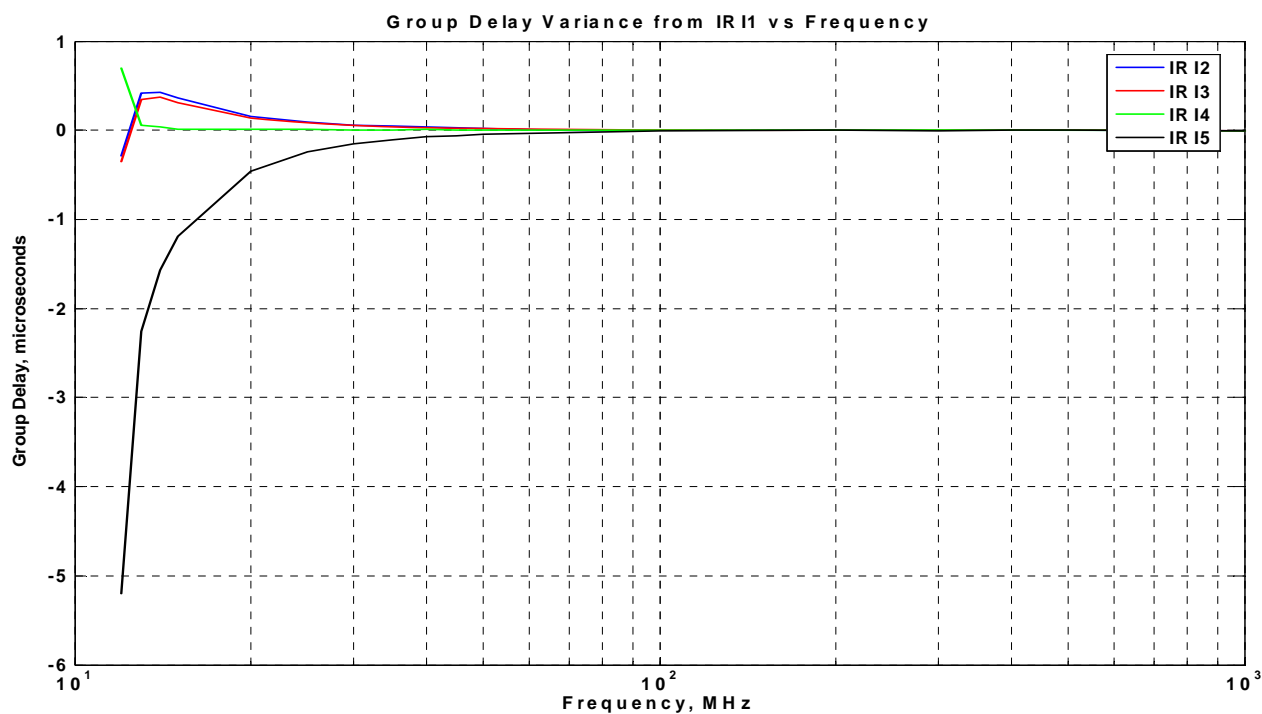


Figure D.3 shows the ray-tracing predicted group delay variance from IRI 1 versus frequency due to varying grid spacing in DEE IRI specifications. The grid spacings used are as follows: IRI 1 = 130 lat x 180 lon, IRI 2 = 65 lat x 60 lon, IRI 3 = 65 lat x 90 lon, IRI 4 = 260 lat x 360 lon, IRI 5 = 30 lat x 24 lon.

## Appendix E: Attempted USU GAIM Model Specification Extrapolation

Figure E.1 illustrates an alternate attempt to provide USU GAIM ionospheric specifications up to geosynchronous orbits versus the diffusive equilibrium model extension method used in this thesis (resulting in DEE GAIM). Essentially, this extrapolation method intended to extrapolate GAIM specifications using a linear fit of the logarithm of the electron densities at GAIM highest three altitudes for each latitude-longitude grid point. It was assumed that the electron densities would be decreasing exponentially at the high altitudes of GAIM. However, the resulting extrapolated GAIM specifications were thrown out as an alternative due to results such as that shown in figure E.1, in which one of GAIM's grid points had a positive slope for its highest three altitudes resulting in a logarithmically increasing electron density with altitude. This leads to an inordinately high relative TEC value for the corresponding grid location. Note that the grid points close to the specific "bad" grid location have a similar tendency, although not as "bad," and one of the affected grid points appears in the signal path. Therefore ray-tracing predictions along this path could be subject to the inaccuracies of the extrapolated specification. All of the ionospheric experts consulted for this research agreed this method was not appropriate for use in this thesis.

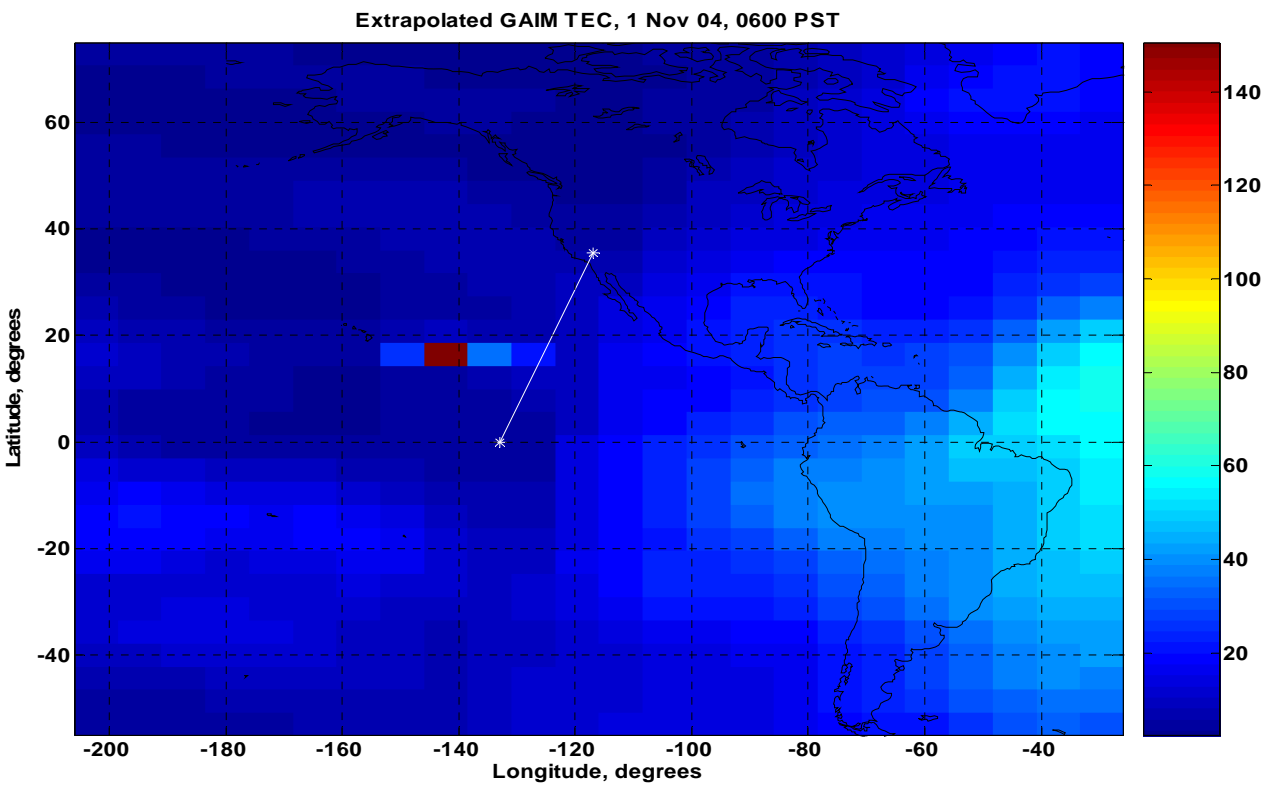


Figure E.1 illustrates extrapolated GAIM at 0600 PST on 1 Nov 04.

## Bibliography

- Bilitza, Dieter. *International Reference Ionosphere 1990*. National Space Science Data Center / World Data Center A for Rockets and Satellites. Lanham: Science Applications Research, 1990.
- Bilitza, Dieter K. "International Reference Ionosphere 2000." *Radio Science*, Vol. 36, Num 2 (2001): 261-275.
- Bilitza, Dieter K. "International Reference Ionosphere." *International Reference Ionosphere*. 2005. National Aeronautics and Space Administration, Goddard Space Flight Center, National Space Science Data Center. 14 Feb 2006 <http://modelweb.gsfc.nasa.gov/ionos/iri.html>.
- Bilitza, Dieter K. Various e-mails to author. NASA/GSFC, NSSDC. 2006.
- Borer, William S. Presentations, personal interview, and by various e-mails to author. Air Force Research Lab Space Vehicles Directorate. 2005-2006.
- Budden, K. G. *Radio Waves in the Ionosphere; the Mathematical Theory of the Reflection of Radio Waves from Stratified Ionised Layers*. Cambridge: Cambridge UP, 1961.
- CIRES, Webpage: <http://cires.colorado.edu/science/projects/aoms-andersonD03.html>. 2004.
- Coleman, C. J. "A Ray Tracing Formulation and its Application to Some Problems in Over-The-Horizon RADAR." *Radio Science*. Vol. 33, Num 4 (1994): 1187-1197.
- Hamilton, W.R. Third Supplement to treatise on geometrical optics. 1931.
- Hausman, Mark A. Various e-mails to author. NorthWest Research Associates. 2005-2006.
- Haselgrove, Jenifer. "Ray Theory and a New Method for Ray Tracing." *Report of Conference on the Physics of the Ionosphere*. London: London Physical Society, 355-364, 1954.
- Haselgrove, C. B., and Jenifer Haselgrove. "Twisted Ray Paths in the Ionosphere." The University, Manchester. *Proc. Phys. Soc. London*, Vol. 75, 357-361, 1960.
- Jones, R. Michael, and Judith J. Stephenson. *A Versatile Three-Dimensional Ray Tracing Computer Program for Radio Waves in the Ionosphere*. Institute for Telecommunication Sciences, Office of Telecommunications, US Dept. of Commerce. Springfield: National Technical Information Service, 1975.

- Keyser, Herbert L. Various e-mails to author. Air Force Weather Agency. 2006.
- McDonnell, M. D. "A Fast Three-Dimensional Ray Tracing Formulation, with Applications to HF Communications and RADAR Prediction." 27 Apr. 2000. Dept. of Electrical and Electronic Eng., The Univ. of Adelaide, South Australia. 14 Feb. 2006  
<http://www.ips.gov.au/IPSHosted/NCRS/wars/wars2000/commg/mcdonnell.pdf>.
- Misra. *Global Positioning System, Signals, Measurements, and Performance*. Lincoln: Ganga-Jamuna P, 2001. 137-138.
- NASA, Ionospheric Modeling Webpage: [http://modelweb.gsfc.nasa.gov/models\\_home.html](http://modelweb.gsfc.nasa.gov/models_home.html). 2006.
- NASA/JPL/California Institute of Technology, Deep Space Network Webpage: <http://deepspace.jpl.nasa.gov/dsn/>. 2006.
- NGDC/STP. Webpage: <http://www.ngdc.noaa.gov/stp/IONO/grams.html>. 2006.
- NetCDF Toolbox, MATLAB®, Webpage: [http://mexcdf.sourceforge.net/netcdf\\_toolbox.html](http://mexcdf.sourceforge.net/netcdf_toolbox.html). 2006.
- Nickisch, L. J. "Focusing in the Stationary Phase Approximation." *Radio Science*. Vol. 23, Num 2 (1988): 171-182.
- Nickisch, L. J. Various e-mails to author. NorthWest Research Associates. 2005-2006.
- Schunk, Robert W., and Andrew F. Nagy. *Ionospheres, Physics, Plasma Physics, and Chemistry*. New York: Cambridge UP, 2000. 25-31.
- Schunk, Robert W., L. Scherliess, J. J. Sojka, and Don C. Thompson. Global Assimilation of Ionospheric Measurements (GAIM): An Operational Space Weather Model. Second Symposium on Space Weather, 11 Jan. 2005, American Meteorological Society (AMS). 14 Feb 2006  
[http://ams.confex.com/ams/Annual2005/techprogram/paper\\_86412.htm](http://ams.confex.com/ams/Annual2005/techprogram/paper_86412.htm).
- Tascione, Thomas F. *Introduction to the Space Environment*, 2<sup>nd</sup> Ed. Malabar: Krieger Company, 1994. 113-114.
- Thompson, Don C. Various e-mails to author. Utah State University Center for Atmospheric and Space Sciences. 2006.
- User's Guide Version 2.1, Global Assimilation of Ionospheric Measurements model. 2004.

## **Vita**

Second Lieutenant Shayne C. Aune graduated from Northwest High School in Clarksville, Tennessee; however, as a youth he attended schools across the country and abroad as part of a military family. He completed undergraduate studies at Virginia Polytechnic Institute and State University (Virginia Tech) and graduated with a Bachelor of Science degree in Electrical Engineering in May 2004. He was commissioned through the Airman's Education and Commission Program (AECPP) through Detachment 875, AFROTC at Virginia Tech. He received the Society of American Military Engineer's Outstanding Senior ROTC Engineering Student award, and he was recognized as the AFROTC Blue Chip recipient, third in his class.

Lieutenant Aune has had an extensive Air Force career since his enlistment in December 1993. His first tour was to the Defense Language Institute-Foreign Language Center at the Presidio of Monterey, California, with follow-on training at Goodfellow AFB in San Angelo, Texas, to complete initial career training as a Spanish Cryptologic Linguist. His second tour was to the Medina Regional Signals Intelligence (SIGINT) Operations Center (MRSOC) on Kelly AFB in San Antonio, Texas, initially assigned to the 93<sup>rd</sup> Intelligence Squadron. In 1996, he was selected for promotion to senior airman below-the-zone and moved to the 543<sup>rd</sup> Intelligence Group Commander's office as a protocol specialist. He returned to Goodfellow AFB in 1997 for cross-training into the Electronic Intelligence (ELINT) career field, from which he graduated as the Top Graduate. He was then assigned to the Air Force Information Warfare Center (AFIWC), Kelly AFB, and performed routine duties maintaining the Constant Web intelligence database, while also serving as a squad leader on the Air Intelligence Agency's all-volunteer Honor Guard. In 1998, he completed Airman Leadership School receiving the John L. Levitow award for leadership. He was then selected as the AFIWC Junior Enlisted Member of the Year for 1998. His next tour was to Osan AB, Republic of South Korea, where he performed duties as a Foreign Instrumentation Signals Intelligence (FISINT) analyst. There he was selected for AECPP, promoted to SSgt, selected for promotion to TSgt, and named his unit's NCO of the Year for 2000. In May 2004, he entered the Air Force Institute of Technology (AFIT). At AFIT he finished the online Basic Acquisitions Officer course (ACQ101) and received a graduate certificate in Measurements and Signatures Intelligence (MASINT). His follow-on assignment is to the National Reconnaissance Office.

<b>REPORT DOCUMENTATION PAGE</b>				Form Approved OMB No. 074-0188	
<p>The public reporting burden for this collection of information is estimated to average 1 hour per response, including the time for reviewing instructions, searching existing data sources, gathering and maintaining the data needed, and completing and reviewing the collection of information. Send comments regarding this burden estimate or any other aspect of the collection of information, including suggestions for reducing this burden to Department of Defense, Washington Headquarters Services, Directorate for Information Operations and Reports (0704-0188), 1215 Jefferson Davis Highway, Suite 1204, Arlington, VA 22202-4302. Respondents should be aware that notwithstanding any other provision of law, no person shall be subject to a penalty for failing to comply with a collection of information if it does not display a currently valid OMB control number.</p> <p><b>PLEASE DO NOT RETURN YOUR FORM TO THE ABOVE ADDRESS.</b></p>					
<b>1. REPORT DATE (DD-MM-YYYY)</b> 23-03-2006		<b>2. REPORT TYPE</b> Master's Thesis		<b>3. DATES COVERED (From – To)</b> Aug 04 – Mar 06	
<b>4. TITLE AND SUBTITLE</b>  Comparison of Ray Tracing through Ionospheric Models				<b>5a. CONTRACT NUMBER</b>	
				<b>5b. GRANT NUMBER</b>	
				<b>5c. PROGRAM ELEMENT NUMBER</b>	
<b>6. AUTHOR(S)</b>  Aune, Shayne C., 2d Lt, USAF				<b>5d. PROJECT NUMBER</b>	
				<b>5e. TASK NUMBER</b>	
				<b>5f. WORK UNIT NUMBER</b>	
<b>7. PERFORMING ORGANIZATION NAMES(S) AND ADDRESS(S)</b> Air Force Institute of Technology Graduate School of Engineering and Management (AFIT/EN) 2950 Hobson Way WPAFB OH 45433-7765				<b>8. PERFORMING ORGANIZATION REPORT NUMBER</b>  AFIT/GE/ENG/06-04	
<b>9. SPONSORING/MONITORING AGENCY NAME(S) AND ADDRESS(ES)</b> AFRL/VSBXP Attn: Dr. William Borer, GS-15 29 Randolph RD Hanscom AFB, MA 01731 DSN: 478-3039				<b>10. SPONSOR/MONITOR'S ACRONYM(S)</b>	
				<b>11. SPONSOR/MONITOR'S REPORT NUMBER(S)</b>	
<b>12. DISTRIBUTION/AVAILABILITY STATEMENT</b> APPROVED FOR PUBLIC RELEASE; DISTRIBUTION UNLIMITED.					
<b>13. SUPPLEMENTARY NOTES</b>					
<b>14. ABSTRACT</b>  A comparison of ray tracing predictions for transionospheric electromagnetic wave refraction and group delays through ionospheric models is presented. Impacted applications include over-the-horizon RADAR, high frequency communications, direction finding, and satellite communications. The ionospheric models used are version 2.1 of Utah State University's Global Assimilation of Ionospheric Measurements (USU GAIM) model and the 2001 version of the International Reference Ionosphere (IRI) model. In order to provide ray tracing results applicable to satellite communications for satellites at geosynchronous orbit (GEO), a third ionospheric model is used to extend the sub-2000-km USU GAIM and IRI ionospheric specifications to 36540 km in altitude. The third model is based on an assumption of diffusive equilibrium for ion species above 2000 km. The ray-tracing code used is an updated implementation of the Jones-Stephenson ray tracing algorithm provided by L. J. Nickisch and Mark A. Hausman. Ray tracing predictions of signal refraction and group delay are given for paths between Goldstone Deep Space Observatory near Barstow, California, and the PanAmSat Galaxy 1R satellite. Results are given for varying frequency between 11MHz to 1GHz, varying time of day between 0600 and 1700 Pacific Standard Time on 1 November 2004, and varying signal transmission elevation angle.  Ray tracing predicts minimal ionospheric effects on signals at or above approximately 100 MHz. Signals below 100 MHz are predicted to refract on different paths by each model. Ray tracing in diffusive equilibrium extended (DEE) specifications of USU GAIM predicts as much as 500 km less group delay than in DEE IRI. This appears to be due to the diffusive equilibrium extension from typically higher electron densities predicted in the upper altitudes of IRI's specifications. USU GAIM also indicates higher frequencies will not penetrate the ionosphere's F <sub>2</sub> region versus IRI-2001 during the period of interest.					
<b>15. SUBJECT TERMS</b> ray tracing, raytracing, ionospheric models, Global Assimilation of Ionospheric Measurements model, USU GAIM, GAIM, International Reference Ionosphere model, IRI, ionospheric ray tracing, ionospheric raytracing					
<b>16. SECURITY CLASSIFICATION OF:</b>		<b>17. LIMITATION OF ABSTRACT</b>  UU	<b>18. NUMBER OF PAGES</b>  94	<b>19a. NAME OF RESPONSIBLE PERSON</b> Matthew E. Goda, Lt Col, USAF	
REPORT U	ABSTRACT U			<b>19b. TELEPHONE NUMBER (Include area code)</b> (937) 255-3636 ext 4614; e-mail: matthew.goda@afit.edu	